AD-A103 538 PENNSYLVANIA STATE UNIV UNIVERSITY PARK IONOSPHERE R--ETC F/G 20/14
NONLINEAR PHENOMENA ARISING FROM RADIO WAVE HEATING OF THE LOWE--ETC(U)
AUG 81 A A TOMKO N00014-81-K-0276
UNCLASSIFIED PSY-TRL-SCI-470 NL

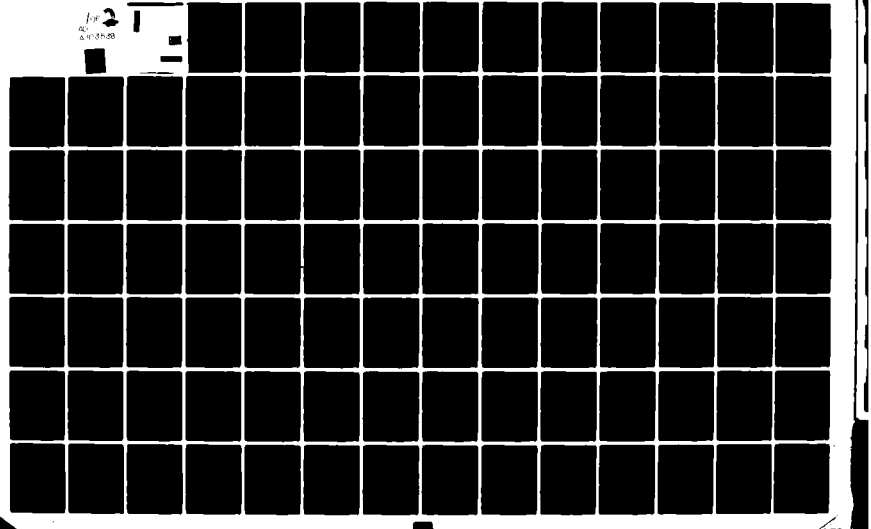

Tomko, Albert Andrew., Nonlinear Phenomena Arising From Radio Wave Heating of the Lower Ionosphere, The Ionosphere Research Laboratory, Department of Electrical Engineering, University Park, PA 16802. 1981.

PSU-IRL-SCI-470

Classification Numbers:

1.5.1 D-Region
1.9.2 Chemical Aeronomy
3.1 Theory of Wave Propagation
3.2.1 Ground-Based Techniques and Measurements

This document describes a theoretical and experimental study of the interaction of high power, high frequency radio waves with the lower ionosphere. The theoretical calculations presented here show that the electron temperature of the ionospheric plasma can be greatly enhanced when the plasma is irradiated by a powerful groundbased HF transmitter with an effective radiated power of the order of 100 MW. If this plasma heating is maintained for times exceeding a few seconds, the composition of the plasma can also be altered. These temperature and composition modifications cause significant changes in the plasma conductivity and wave absorption in the medium.

Two experiments were conducted in order to test for the predicted absorption and conductivity modifications: a vertical incidence pulse absorption experiment and a nonlinear demodulation experiment. Data from the absorption experiment clearly show a large (9 dB) increase in wave absorption at 2.4 MHz due to a high power (60 MW ERP) HF heating of the ionosphere. The nonlinear demodulation experiment generated strong VLF radiation when the ionosphere was irradiated by a powerful modulated HF wave. These VLF signals are believed to be due to HF heating induced conductivity modulation of the dynamo current system.

Tomko, Albert Andrew., Nonlinear Phenomena Arising From Radio Wave Heating of the Lower Ionosphere, The Ionosphere Research Laboratory, Department of Electrical Engineering, University Park, PA 16802. 1981.

PSU-IRL-SCI-470

Classification Numbers:

1.5.1 D-Region
1.9.2 Chemical Aeronomy
3.1 Theory of Wave Propagation
3.2.1 Ground-Based Techniques and Measurements

This document describes a theoretical and experimental study of the interaction of high power, high frequency radio waves with the lower ionosphere. The theoretical calculations presented here show that the electron temperature of the ionospheric plasma can be greatly enhanced when the plasma is irradiated by a powerful groundbased HF transmitter with an effective radiated power of the order of 100 MW. If this plasma heating is maintained for times exceeding a few seconds, the composition of the plasma can also be altered. These temperature and composition modifications cause significant changes in the plasma conductivity and wave absorption in the medium.

Two experiments were conducted in order to test for the predicted absorption and conductivity modifications: a vertical incidence pulse absorption experiment and a nonlinear demodulation experiment. Data from the absorption experiment clearly show a large (9 dB) increase in wave absorption at 2.4 MHz due to a high power (60 MW ERP) HF heating of the ionosphere. The nonlinear demodulation experiment generated strong VLF radiation when the ionosphere was irradiated by a powerful modulated HF wave. These VLF signals are believed to be due to HF heating induced conductivity modulation of the dynamo current system.

Tomko, Albert Andrew., Nonlinear Phenomena Arising From Radio Wave Heating of the Lower Ionosphere, The Ionosphere Research Laboratory, Department of Electrical Engineering, University Park, PA 16802. 1981.

PSU-IRL-SCI-470

Classification Numbers:

1.5.1 D-Region
1.9.2 Chemical Aeronomy
3.1 Theory of Wave Propagation
3.2.1 Ground-Based Techniques and Measurements

This document describes a theoretical and experimental study of the interaction of high power, high frequency radio waves with the lower ionosphere. The theoretical calculations presented here show that the electron temperature of the ionospheric plasma can be greatly enhanced when the plasma is irradiated by a powerful groundbased HF transmitter with an effective radiated power of the order of 100 MW. If this plasma heating is maintained for times exceeding a few seconds, the composition of the plasma can also be altered. These temperature and composition modifications cause significant changes in the plasma conductivity and wave absorption in the medium.

Two experiments were conducted in order to test for the predicted absorption and conductivity modifications: a vertical incidence pulse absorption experiment and a nonlinear demodulation experiment. Data from the absorption experiment clearly show a large (9 dB) increase in wave absorption at 2.4 MHz due to a high power (60 MW ERP) HF heating of the ionosphere. The nonlinear demodulation experiment generated strong VLF radiation when the ionosphere was irradiated by a powerful modulated HF wave. These VLF signals are believed to be due to HF heating induced conductivity modulation of the dynamo current system.

Tomko, Albert Andrew., Nonlinear Phenomena Arising From Radio Wave Heating of the Lower Ionosphere, The Ionosphere Research Laboratory, Department of Electrical Engineering, University Park, PA 16802. 1981.

PSU-IRL-SCI-470

Classification Numbers:

1.5.1 D-Region
1.9.2 Chemical Aeronomy
3.1 Theory of Wave Propagation
3.2.1 Ground-Based Techniques and Measurements

This document describes a theoretical and experimental study of the interaction of high power, high frequency radio waves with the lower ionosphere. The theoretical calculations presented here show that the electron temperature of the ionospheric plasma can be greatly enhanced when the plasma is irradiated by a powerful groundbased HF transmitter with an effective radiated power of the order of 100 MW. If this plasma heating is maintained for times exceeding a few seconds, the composition of the plasma can also be altered. These temperature and composition modifications cause significant changes in the plasma conductivity and wave absorption in the medium.

Two experiments were conducted in order to test for the predicted absorption and conductivity modifications: a vertical incidence pulse absorption experiment and a nonlinear demodulation experiment. Data from the absorption experiment clearly show a large (9 dB) increase in wave absorption at 2.4 MHz due to a high power (60 MW ERP) HF heating of the ionosphere. The nonlinear demodulation experiment generated strong VLF radiation when the ionosphere was irradiated by a powerful modulated HF wave. These VLF signals are believed to be due to HF heating induced conductivity modulation of the dynamo current system.

SECURITY CLASSIFICATION OF THIS PAGE (When Data Entered)

REPORT DOCUMENTATION PAGE

READ INSTRUCTIONS BEFORE COMPLETING FORM

1. REPORT NUMBER: PSU-IRL-SCI-470	2. GOVT ACCESSION NO.: AD-A103 538
3. RECIPIENT'S CATALOG NUMBER	
4. TITLE (and Subtitle): Nonlinear Phenomena Arising From Radio Wave Heating of the Lower Ionosphere	5. TYPE OF REPORT & PERIOD COVERED: Technical Report
6. PERFORMING ORG. REPORT NUMBER: PSU-IRL-SCI-470	
7. AUTHOR(s): Albert Andrew Tomko	8. CONTRACT OR GRANT NUMBER(s): ~~ATM79-10064~~ N00014-81-K-0276
9. PERFORMING ORGANIZATION NAME AND ADDRESS: The Pennsylvania State University, 318 Electrical Engineering East, University Park, Pennsylvania 16802	10. PROGRAM ELEMENT, PROJECT, TASK AREA & WORK UNIT NUMBERS: NR SRO-108
11. CONTROLLING OFFICE NAME AND ADDRESS: Office of Naval Research, Code 464, Arlington, VA 22217; National Science Foundation, Washington, D.C. 20550	12. REPORT DATE: August, 1981
	13. NUMBER OF PAGES: 175
14. MONITORING AGENCY NAME & ADDRESS (if different from Controlling Office)	15. SECURITY CLASS. (of this report): Unclassified
	15a. DECLASSIFICATION/DOWNGRADING SCHEDULE

16. DISTRIBUTION STATEMENT (of this Report)

Distribution Unlimited

17. DISTRIBUTION STATEMENT (of the abstract entered in Block 20, if different from Report)

18. SUPPLEMENTARY NOTES

19. KEY WORDS (Continue on reverse side if necessary and identify by block number)

D-Region
Chemical Aeronomy
Theory of Wave Propagation
Ground-Based Techniques and Measurements

20. ABSTRACT (Continue on reverse side if necessary and identify by block number)

This document describes a theoretical and experimental study of the interaction of high power, high frequency radio waves with the lower ionosphere. The theoretical calculations presented here show that the electron temperature of the ionospheric plasma can be greatly enhanced when the plasma is irradiated by a powerful groundbased HF transmitter with an effective radiated power of the order of 100 MW. If this plasma heating is maintained for times exceeding a few seconds, the composition of the plasma can also be altered. These temperature and composition modifications cause significant

DD FORM 1 JAN 73 1473 EDITION OF 1 NOV 68 IS OBSOLETE
S/N 0102-014-6601

SECURITY CLASSIFICATION OF THIS PAGE (When Data Entered)

changes in the plasma conductivity and wave absorption in the medium.

Two experiments were conducted in order to test for the predicted absorption and conductivity modifications: a vertical incidence plus absorption experiment and a nonlinear demodulation experiment. Data from the absorption experiment clearly show a large (9 dB) increase in wave absorption at 2.4 MHz due to a high power (60 MW ERP) HF heating of the ionosphere. The nonlinear demodulation experiment generated strong VLF radiation when the ionosphere was irradiated by a powerful modulated HF wave. These VLF signals are believed to be due to HF heating induced conductivity modulation of the dynamo current system.

PSU-IRL-SCI-470
Classification Numbers: 1.5.1, 1.9.2, 3.1, 3.2.1

Scientific Report 470

Nonlinear Phenomena Arising From Radio Wave Heating of the Lower Ionosphere

by

Albert Andrew Tomko

August, 1981

The research reported in this document has been supported by the Office of Naval Research under Contract No. N00014-81-K-0276 and by the National Science Foundation under Grant No. ATM 78-19964.

Submitted by: A. J. Ferraro
Professor of Electrical Engineering

Approved by: John S. Nisbet
Director, Ionosphere Research Laboratory

Ionosphere Research Laboratory
Department of Electrical Engineering
The Pennsylvania State University
University Park, Pennsylvania 16802

ACKNOWLEDGEMENTS

The author wishes to thank Professors A. J. Ferraro and H. S. Lee for their invaluable assistance during this study, Professor J. L. Brown, Jr. and Drs. L. A. Carpenter and J. J. Olivero for serving on his doctoral committee, Dr. A. P. Mitra of the National Physical Laboratory, New Delhi, India, for many helpful discussions, and the staff of Arecibo Observatory for their assistance in the experimental phase of this research.

This study was supported in part by the National Science Foundation under Grant No. ATM 78-19964 and the Office of Naval Research under Contract No. N00014-81-K-0276.

Arecibo Observatory is operated by Cornell University under a contract with the National Science Foundation.

TABLE OF CONTENTS

LIST OF TABLES

LIST OF FIGURES

LIST OF SYMBOLS

$\vec{F}$ - a vector quantity

$\hat{a}$ - a unit vector

$\vec{F} \times \vec{G}$ - vector cross product

$\vec{F} \cdot \vec{G}$ - scalar or dot product of two vectors

$d\vec{r}$ - differential volume in position space

$d\vec{v}$ - differential volume in velocity space

$\vec{\nabla}$ - del operator in position space

$\vec{\nabla}_v$ - del operator in velocity space

$\underline{F}$ - a matrix or tensor quantity

$\underline{F}^{-1}$ - inverse of matrix $\underline{F}$

$\dot{F} = \partial F/\partial t$ - partial time derivative of F

$\tilde{F}$ - value of F following a collision

F^* - complex conjugate of F

$Re\{F\}$ - real part of the complex quantity F

$\langle F \rangle$ - average value of F over all velocity space

$\overline{\vec{F} \cdot \vec{G}}$ - time average of $Re\{\vec{F}\} \cdot Re\{\vec{G}\}$

$F \sim G$ - F of the order of G

$[A] = n_A$ - number density of constituent A

$m!$ - m factorial

$j = \sqrt{-1}$

$\delta T_e = T_e - T_n$

ABSTRACT

This document describes a theoretical and experimental study of the interaction of high power, high frequency radio waves with the lower ionosphere. The theoretical calculations presented here show that the electron temperature of the ionospheric plasma can be greatly enhanced when the plasma is irradiated by a powerful groundbased HF transmitter with an effective radiated power of the order of 100 MW. If this plasma heating is maintained for times exceeding a few seconds, the composition of the plasma can also be altered. These temperature and composition modifications cause significant changes in the plasma conductivity and wave absorption in the medium.

Two experiments were conducted in order to test for the predicted absorption and conductivity modifications: a vertical incidence pulse absorption experiment and a nonlinear demodulation experiment. Data from the absorption experiment clearly show a large (9 dB) increase in wave absorption at 2.4 MHz due to a high power (60 MW ERP) HF heating of the ionosphere. The nonlinear demodulation experiment generated strong VLF radiation when the ionosphere was irradiated by a powerful modulated HF wave. These VLF signals are believed to be due to HF heating induced conductivity modulation of the dynamo current system.

CHAPTER I

INTRODUCTION

1.1 The Ionospheric Plasma

The ionospheric plasma is a partially ionized region in the earth's upper atmosphere extending from 50 km to over 1000 km. It consists of a mixture of free electrons, positive and negative ions and neutral particles, and is a transition layer between the non-ionized lower atmosphere and the fully ionized plasma of the magnetosphere. The ionosphere is formed and maintained by the ionization of the neutral atmosphere by solar radiations and energetic particles such as cosmic rays. In the uppermost regions of the atmosphere the neutral particle density is very small; hence there are few particles to ionize. As one moves to lower heights the neutral density increases exponentially, and as a result there is a corresponding increase in the ionization density. However, the increase in neutral density also leads to increased attenuation of the ionizing radiation; consequently, the ionization density eventually reaches a peak, and then decreases as the ionizing radiation is further attenuated with decreasing height.

The ionosphere is usually divided into three regions based on the magnitude and structure of the electron density distribution. These regions are designated in order of increasing height by the letters D (50 to 90 km), E (90 to 130 km) and F (> 130 km), respectively. The normal daytime electron density distribution has a maximum in the F-region near 300 km of about 10^6 cm^{-3} and a secondary maximum in the E-region of about 10^5 cm^{-3}. In the D-region the electron density

decreases by more than three orders of magnitude from 10^4 cm^{-3} at 90 km to less than 10^1 cm^{-3} at 50 km. The ionospheric electron density distribution can vary considerably from day to night and during periods of enhanced solar activity.

In addition to the ionizing radiations, the physical properties of the ionospheric plasma such as its temperature, composition, permeability, and conductivity depend upon the motion of its constituent particles, which, in turn, depend upon the force fields acting on the plasma. In the ionosphere these force fields include gravity, the earth's magnetic field, the Coulomb fields of the charged plasma particles, short range force fields associated with particle interactions and the electromagnetic fields of radio waves which propagate through the ionosphere.

The focus of this study will be on the interaction between radio wave fields and the ionospheric plasma. However, in the development of this topic, it will be necessary to consider the effects of many of the other fields listed above.

The ionosphere is an extremely interesting medium for the purpose of studying electromagnetic wave propagation. The ionosphere, as illustrated by its electron content, is a nonhomogeneous medium; hence its electromagnetic properties have a spatial dependence. Due to the presence of the earth's magnetic field, the plasma exhibits prefered directions for wave propagation and is thus an anisotropic medium. The ionosphere is also both temporally and spatially dispersive. Finally, and of foremost interest, nonlinear electromagnetic effects manifest themselves quite readily in the ionosphere. An outstanding

example of this is the well-known Luxembourg or cross modulation effect (e.g. Fejer, 1955).

When an electromagnetic wave propagates through a plasma, the Lorentz force due to the wave fields alters the motion of the electron component of the plasma and, to a lesser extent, the ion component. If the plasma is nonrelativistic (i.e. one in which the particle velocities are much less than the speed of light), the component of the Lorentz force due to the magnetic field of the wave is much smaller than that due to the electric field. Hence, charged particle motion in the plasma is perturbed primarily by the wave's electric field (Holt and Haskell, 1965). Now the electromagnetic properties of a plasma, such as its permeability, conductivity, refractive index and absorption coefficient are determined by plasma particle motion and therefore can be altered by the wave field.

There are several mechanisms by which the electric field of a radio wave can alter the electromagnetic properties of the ionosphere. Two of the most important of these mechanisms are collisional heating of the plasma electrons (thermal effect), and compression of the plasma (striction effect).

The thermal effect is of principal importance in those regions of the ionosphere where particle collisions are frequent (i.e. the lower ionosphere). If the electron mean free path (i.e. average distance between collisions) is not too small, the plasma electrons can acquire a significant amount of kinetic energy from the wave between collisions as they are accelerated by the electric field. When collisions between

electrons and ions or neutral particles occur, the average energy transferred to these heavier particles is small. The main effect of collisions is to randomize the directed electron motion imparted by the wave field. As a result, the average thermal energy of the electrons (i.e. electron temperature) is increased and the plasma is said to be "heated." The electromagnetic properties of the plasma are directly dependent on the electron energy and thus can be modified by radio wave heating.

In those regions of the ionosphere where particle collisions are less frequent (i.e. the F-region), plasma modifications due to the striction effect become important. In the striction effect, the electric field of a wave exerts pressure on the plasma electrons and thereby compresses the plasma. This results in a local variation in the electron density and, since the electromagnetic properties of the plasma depend on its electron content, there is a corresponding variation in these properties (Gurevich, 1978).

In the study of radio wave propagation in the ionosphere, one often assumes that the electric field of the wave is relatively weak, so that the properties of the plasma are not noticably affected by the passage of the wave. However, as the magnitude of the wave field increases, the electron temperature and density of the plasma can be significantly modified by thermal and striction effects, and consequently, the electromagnetic properties of the medium become dependent on the magnitude of the wave field. The propagation of radio waves in the ionosphere is, of course, directly dependent upon the electromagnetic properties of the plasma and hence a strong wave can alter the

propagation of all other waves whose paths intersect it. The ionosphere thus supports the interaction of radio waves and it is this interaction which is responsible for the nonlinear phenomena which occur in the ionosphere. In particular, wave interaction invalidates the use of the superposition principle which characterizes linear media and leads to a nonlinear relationship between the electric field and the electric displacement and current densities in the plasma.

1.2 Ionospheric Modification

Ionospheric modification, in the broadest sense, is an attempt to modify the physical properties of the ionospheric plasma in a controlled manner. This may be accomplished by the in situ release of chemically reactive gases or plasma clouds, by bombarding the ionosphere with particle beams from accelerators aboard spacecraft, by VLF stimulation of plasma instabilities, or by irradiating the ionosphere with high power radio waves (usually HF or higher frequency) from ground based transmitters (Walker, 1979). This study is concerned with the last of these techniques, radio wave modification, and shall focus on nonlinear electromagnetic effects arising in the lower ionosphere due to plasma heating (i.e. the thermal effect).

Plasma modification experiments employing high power radio waves have been ongoing since the late sixties at Platteville, Colorado (Utlaut, 1970), at Arecibo, Puerto Rico (Gordon et al., 1971) and at several locations in the U.S.S.R. (Gurevich and Shlyuger, 1975). The motivation for these experiments was provided by theoretical studies (Ginzburg and Gurevich, 1960; Farley, 1963; Meltz and LeLevier, 1970)

which showed that the deviative absorption of energy from HF waves propagating through the F-region could substantially modify the local electron temperature and density. The results of F-region heating experiments conducted during the seventies support this theory and have revealed many unanticipated physical phenomena including artificial spread F, field aligned scattering and plasma line enhancements. The heated region also acts as a significant radio scatterer at frequencies as high as the UHF band and is thus potentially useful for telecommunications purposes (Utlaut, 1975).

Before any of the energy radiated by a ground based transmitter can be deposited in the F-region, it must first traverse the lower regions of the ionosphere where the large neutral densities and hence high electron-neutral collision frequency can result in significant nondeviative absorption. If the transmitted wave field is large, the absorbed wave energy can significantly heat the plasma. Theoretical studies by Holway and Meltz (1973) and Meltz et al. (1974) based upon current estimates of electron energy loss due to collisions predict large electron temperature enhancements in the D and E regions when the plasma is irradiated by high power radio waves at frequencies near or above the local electron gyrofrequency (~ 1 MHz). For an effective radiated power (ERP) of 100 MW, a factor of five or more increase in electron temperature is anticipated. A temperature change of this magnitude can significantly alter the electromagnetic properties of the plasma, resulting in a number of interesting nonlinear phenomena.

One of the principal results of plasma heating by a high power radio wave, often called a "heating" wave, is the modification of wave absorption. Wave absorption in a plasma is directly related to the frequency of electron collisions with other plasma particles, and the frequency of these collisions increases as the plasma is heated. A heating wave can therefore vary the amplitude of all other waves that intersect its path by altering the absorption of these waves. In particular, if the heating wave is amplitude modulated, its modulation can be transferred to another wave via the ionosphere (cross modulation). Moreover, if the heating wave is of sufficient duration, it can modify the absorption of itself (self absorption, e.g. Gurevich, 1978).

Another important class of nonlinear phenomena arises from heating induced conductivity modifications. Nonlinear wave interactions via the plasma conductivity can lead to the creation of new waves at frequencies which are a linear combination of those of the interacting waves (nonlinear mixing) or, if the heating wave is amplitude modulated at some frequency, Ω_m, the plasma conductivity may be varied at this frequency and lead to the generation of a wave of frequency Ω_m (nonlinear demodulation, e.g. Ginzburg, 1970).

If the electron temperature in the ionospheric plasma is maintained at an enhanced level by continuous wave (CW) heating, the composition of the plasma may be modified due to the electron temperature dependence of chemical processes involving electrons, such as ion-electron recombination and electron attachment to neutral particles.

An increase in electron temperature is expected to decrease the rate of ion-electron recombination, leading to enhancements of both the electron and positive ion densities in the E and upper D regions (Holway and Meltz, 1973; Meltz et al.,1974), while heating the lower D-region may increase the rate of electron attachment to neutral particles resulting in a decrease in electron density and an enhancement of the negative ion population (Tomko et al.,1980). In a very strong wave field, collisional ionization of neutral particles by the field accelerated electrons may also modify the plasma composition (Gurevich et al.,1977b). The electromagnetic properties of the ionospheric plasma depend directly on the electron content and thus can be modified by the above mechanisms. In particular, heating induced electron density variations could modulate the ionospheric dynamo current by changing the plasma conductivity (Willis and Davis, 1973).

Experimental evidence of heating induced plasma modifications in the lower ionosphere is at present rather limited, due largely to a lack of facilities with adequate heating power. The Platteville facility has the capability of radiating 100 MW ERP (pulsed or CW) over 3 to 10 MHz and is ideally suited for ionospheric modification studies. However, only a small amount of preliminary D-region observations were made at this facility during the early seventies (Utlaut, 1975) and the facility was not operational during much of the later seventies. At Arecibo, Showen (1972) has used the 430 MHz incoherent backscatter radar as a diagnostic in order to observe E-region heating at 40 MHz.

His measurements of backscatter power indicate a factor of two enhancement of the electron temperature at 90 km. More recently, Coco (1979) has used the 430 MHz radar as both a heater and a diagnostic in order to observe temperature modifications near 100 km. D-region HF heating experiments at Arecibo have been attempted using a log periodic antenna mounted at the focus of the Arecibo Observatory's 305 m spherical dish and fed by a 100 kw transmitter (e.g. Sulzer et al., 1976). However, the ERP for this arrangement (about 15 MW at 5 MHz) is inadequate for producing large electron temperature modifications. New facilities for ionospheric modification studies have recently been completed at Arecibo and at Tromsø, Norway (e.g. Kopka et al., 1976), and each has the capability of radiating in excess of 100 MW ERP (pulsed or CW) over the 3 to 12 MHz range. These new facilities together with the reactivated Platteville facility should soon supply a wealth of data on radio wave modification of the lower ionosphere.

Experimental results from previous operations at Platteville have been summarized by Utlaut and Violette (1974). D-region data were obtained from observations of vertical incidence pulse (A1) absorption and cross modulation. The A1 absorption measurements were made on a 2.667 MHz diagnostic wave and showed about a 6 dB increase in attenuation due to heating at 100 MW ERP and 3 to 6 MHz. Attenuation of the diagnostic increased promptly (< 40 ms) after turn on of the heating transmitter, but recovered to its unheated level very slowly ($\sim$ 10 min.) following a long period of CW heating (10 min.). The prompt increase in attenutation can be attributed to a change in collision frequency

as the electron temperature increases, while the long term recovery is most likely due to an electron density modification. Observations of amplitude modulation impressed on signals passing through the region heated by the HF transmitter (Jones et al., 1972; Jones, 1973) show modulation exceeding 8% at 2.5 MHz, 12% at 60 kHz and a few percent at 20 kHz for heating at 5.1 MHz and 50 MW. Jones (1973) has estimated that a 40% increase in electron temperature between 70 and 80 km is necessary to reproduce the observed modulation. Jones (1973) also observed nonlinear mixing effects at Platteville.

Utlaut (1975) has reported that during a solar flare sudden phase anomolies (SPA's) were observed in the normal manner on VLF and LF signals propagating through an unheated D-region, but the SPA was absent on a 60 kHz signal passing through a heated D-region. Mitra (1975a) has suggested that the absence of the SPA at 60 kHz may be due to a change in electron attachment induced by heating, with the increase in electron density in the lower D-region due to the solar flare being cancelled by the decrease in electron density due to increased attachment. Full VLF calculations by Tomko (1978) support this theory.

Much of the theoretical and experimental work on radio wave modification of the lower ionosphere has been pioneered by Soviet scientists. High power self interaction and cross modulation effects have been studied by Gurevich and Shlyuger (1975), Krotova et al. (1977), and Gurevich et al. (1977a), while observations of nonlinear demodulation effects have been reported by Getmantsev et al. (1974), Budilin

et al. (1977) and Kapustin et al. (1977). Radio wave heating theory has been extensively reviewed and developed in works by Gurevich (1970) and Ginzburg (1978).

Very recently, Turunen et al. (1980) and Stubbe (1980) have observed nonlinear demodulation effects in Northern Scandinavia.

1.3 Objectives

The objectives of this study are to develop a theoretical model which describes the interaction of a high power radio wave with the complex, chemically dominated plasma of the lower ionosphere, and to ascertain the validity of this model by experimental observation of nonlinear electromagnetic effects which result from wave-plasma interactions.

The theoretical foundation for this study is given in Chapter II, where Maxwell's equations are combined with plasma kinetic theory in order to obtain a self consistent set of equations which describe wave-plasma interactions in the ionosphere. In Chapter III, a numerical procedure for the simultaneous solution of the electron energy equation and the heating wave energy flux equation is described and implemented in order to study electron temperature modifications arising from the thermal effect, and self-absorption effects due to the action of the modified plasma on the heating wave. In these initial calculations, it is assumed that the composition of the ionospheric plasma, and, in particular, the electron density, are not altered by the heating wave. The validity of this assumption is examined in Chapter IV, and detailed calculations of ion chemistry modifications

arising from radio wave heating are presented.

In Chapter V the electron temperature and density models developed in the previous chapters are used to calculate the change in Al absorption on a diagnostic wave due to plasma modifications induced by a heating wave. The magnitude and time variation of Al absorption predicted by the model is compared with the experimental results of Al absorption measurements made at the HF heating facility of the Arecibo Observatory by the author and his coworkers (Tomko et al., 1981), as well as with the Platteville results which were described earlier.

Chapter VI presents the basic theory of the generation of very low frequency radiation by nonlinear demodulation of high power HF waves in the ionosphere. The electron temperature model developed in Chapter III is used to calculate the change in plasma conductivity due to an amplitude modulated HF wave which, in turn, is used to estimate the strength of ELF and VLF fields radiated by the ionosphere due to the modulation of ionospheric currents. The predicted characteristics of the ELF/VLF radiation are compared with the results of nonlinear demodulation experiments conducted at polar latitudes (e.g. Stubbe, 1980) and with data from a recent experiment at the Arecibo HF facility.

The conclusions of this study are summarized in Chapter VII.

The research study outlined above should prove to be useful in a number of applications. With the increased availability of HF heating facilities, a rapid increase in active experimentation with the ionospheric plasma can be anticipated. The ionospheric model developed in

this study should prove to be a valuable tool in the design and evaluation of these future HF heating experiments. In turn, future observational results will undoubtably lead to improvement of the model and a better understanding of ionospheric processes. For example, the intensity of ionospheric radiation generated by nonlinear demodulation of HF waves is directly dependent upon the magnitude of ionospheric currents and their associated electric fields. These radiations could thus act as a highly sensitive indicator of natural changes in the global current system. VLF and ELF radiation generated by nonlinear demodulation may also have potential applications to submarine communications.

The results of this research study will also be useful in assessing the impact of solar power satellites (SPS) on the lower ionosphere, and on radio wave propagation in this medium. Proposed SPS systems (Glaser, 1977) would convert solar radiations into microwave energy which would be transmitted to earth and converted into electrical power. The SPS microwave beam would have a power density as large as 200 W/m^2 and could thus cause significant electron heating in spite of the relatively low ionospheric absorption at microwave frequencies. The present work extends the results of previous SPS impact studies (e.g. Perkins and Roble, 1978; Duncan and Zinn, 1978; Holway et al., 1978) by taking into account the complex chemistry of the lower ionosphere and its dependence on electron temperature.

CHAPTER II

IONOSPHERIC ELECTRODYNAMICS

2.1 Maxwell's Equations

The objective of this chapter is to develop a self-consistent set of equations to describe the interaction of a strong electromagnetic wave with the ionospheric plasma. The starting point in the description of electromagnetic phenomena in the ionosphere, as in all media, is Maxwell's equations. In the international (MKS) system of units, these equations are of the form (e.g. Yeh and Liu, 1972)

$$\vec{\nabla} \times \vec{H}(\vec{r}, t) = \dot{\vec{D}}(\vec{r}, t) + \vec{J}'(\vec{r}, t) \tag{2.1}$$

$$\vec{\nabla} \times \vec{E}(\vec{r}, t) = - \dot{\vec{B}}(\vec{r}, t) \tag{2.2}$$

$$\vec{\nabla} \cdot \vec{D}(\vec{r}, t) = \rho'(\vec{r}, t) \tag{2.3}$$

$$\vec{\nabla} \cdot \vec{B}(\vec{r}, t) = 0 \tag{2.4}$$

where

$\vec{E}$ - electric field strength

$\vec{H}$ - magnetic field strength,

$\vec{D}$ - displacement density,

$\vec{B}$ - magnetic flux density,

$\vec{J}'$ - current density, and

ρ' - charge density.

The dot above a given quantity denotes partial differentiation with respect to time (i.e. $\partial/\partial t$).

Strictly speaking, the field quantities which appear in Maxwell's equations are average values taken in the statistical sense (i.e.

averaged over an ensemble of equivalent systems). However, in plasma applications, one is concerned with fields whose wavelength is large compared with the mean distance between plasma particles. Statistical averaging is thus equivalent to averaging over a physically infinitesimal volume, $d\vec{r}$ = dxdydz, of dimensions which are much larger than the mean distance between plasma particles (i.e. a volume containing a large number of particles). Hence $\vec{E}(\vec{r}, t)$ is to be interpreted as the average value of the electric microfields in the volume element $d\vec{r}$ centered at position $\vec{r}$ at time t. The other field quantities are similarly defined (Ginzburg, 1970).

The current density, $\vec{J}'$, includes externally applied currents, $\vec{J}_{EXT}$, such as those associated with transmitting antennae which may be immersed in the plasma, and plasma currents, $\vec{J}$, arising from the net motion of charged plasma particles. Likewise, the charge density, ρ', consists of an externally applied part, ρ_{EXT}, and the plasma charge density, ρ. Hence one writes

$$\rho'(\vec{r}, t) = \rho_{EXT}(\vec{r}, t) + \rho(\vec{r}, t) \tag{2.5}$$

$$\vec{J}'(\vec{r}, t) = \vec{J}_{EXT}(\vec{r}, t) + \vec{J}(\vec{r}, t) \tag{2.6}$$

The external charge and current densities may generally be regarded as given quantities, independent of the field vectors $\vec{E}$, $\vec{H}$, $\vec{D}$ and $\vec{B}$. The charge and current densities are related by the charge continuity equation

$$\vec{\nabla} \cdot \vec{J}'(\vec{r}, t) = - \dot{\rho}'(\vec{r}, t) \tag{2.7}$$

Maxwell's equations combined with the charge continuity equation

amount to two vector relations (2.1-2) between the five vector unknowns $\vec{E}$, $\vec{H}$, $\vec{D}$, $\vec{B}$ and $\vec{J}$, along with three boundary conditions (2.3-4 and 2.7). To complete this system of equations, one requires a set of three vector equations relating the displacement, magnetic flux and current densities in the medium to the electric and magnetic field strengths. The required set of relations are called material or constitutive relations.

At an elementary level all matter may be considered to consist of charged particles; some free (ions, electrons) and others bound (neutral atoms or molecules). The formulation of the constitutive relations for a given material thus amounts to a description of the effects of the motion of these charged particles on the electromagnetic field vectors. The description of these effects may be approached from two different viewpoints; one macroscopic and the other microscopic.

At the macroscopic level the effects on the fields due to charge motion are taken into account by means of a set of constitutive parameters. The motion of free charges is described by means of the conductivity, σ, the translational motion of bound charges is described by means of the permittivity, ε, and the rotational motion of charges is described by means of the magnetic permeability, μ_M. The relationship between the field vectors in the medium are specified by the equations

$$\vec{D}(\vec{r}, t) = \varepsilon \vec{E}(\vec{r}, t) \tag{2.8}$$

$$\vec{B}(\vec{r}, t) = \mu_M \vec{H}(\vec{r}, t) \tag{2.9}$$

$$\vec{J}(\vec{r}, t) = \sigma \vec{E}(\vec{r}, t) \tag{2.10}$$

These simple relations are used extensively in the study of linear

electrodynamics (e.g. Jordan and Balmain, 1968) and apply to homogeneous, isotropic media. However, equations (2.8-10) are not, in general, applicable in ionospheric studies since the plasma can exhibit nonlinear, nonhomogeneous and anisotropic characteristics.

At the microscopic level, the electromagnetic properties of a medium are described in terms of the dynamical behavior of the elementary charges which comprise the medium. In this viewpoint one dispenses with the concept of a material medium per se, and instead considers the ensemble of plasma particles situated in free space. In any infinitesimal volume $d\vec{r}$, it is assumed that the number of positive and negative charges are equal so that there is no net charge in $d\vec{r}$ (i.e. $\rho(\vec{r}, t) = 0$). The physical reasoning behind this assumption is that if each $d\vec{r}$ had a net charge, there would be a potential difference between volume elements due to Coulomb forces and the plasma particles would quickly move between volume elements in such a way as to reduce the potential difference and restore neutrality (Yeh and Liu, 1972). In the presence of an electromagnetic field, the charges in the plasma (free or bound) are displaced by the Lorentz force due to the field

$$\vec{F}_s = q_s (\vec{E} + \vec{v}_s \times \vec{B}) \tag{2.11}$$

where q_s is the charge of the s-th type of plasma particle and $\vec{v}_s(\vec{r}, t)$ is the velocity of some s-type particle in $d\vec{r}$. This action gives rise to an average convection current

$$\vec{J} = \sum_s q_s n_s \langle \vec{v}_s \rangle \tag{2.12}$$

where $n_s(\vec{r}, t)$ is the number density of s-type particles in $d\vec{r}$ and $\vec{v}_s(\vec{r}, t)$ is the average velocity of the s-type particles in this volume. The plasma particles are situated in free space; hence, the permittivity and magnetic permeability are those of a vacuum: $\varepsilon = \varepsilon_o$, $\mu_M = \mu_o$. One therefore has

$$\vec{D} = \varepsilon_o \vec{E} \tag{2.13}$$

and

$$\vec{B} = \mu_o \vec{H}. \tag{2.14}$$

Equations (2.12-14) are the constitutive relations in the microscopic viewpoint.

Using the microscopic constitutive relations one can rewrite Maxwell's equations in the form

$$\vec{\nabla} \times \vec{H} = j\omega\varepsilon_o \vec{E} + \sum_s q_s n_s \langle \vec{v}_s \rangle \tag{2.15}$$

$$\vec{\nabla} \times \vec{E} = -j\omega\mu_o \vec{H} \tag{2.16}$$

$$\vec{\nabla} \cdot \vec{D} = 0 \tag{2.17}$$

$$\vec{\nabla} \cdot \vec{H} = 0 \tag{2.18}$$

where it has been assumed that the field vectors $\vec{E}$ and $\vec{H}$ vary sinusoidally as $e^{j\omega t}$ with angular frequency ω (i.e. monochromatic fields), and the medium is assumed to be free of externally applied sources (i.e. $\vec{J}_{EXT} = 0$, $\rho_{EXT} = 0$). In order to complete the system of equations (2.15-18) one must supplement them with a set of dynamical equations of motion for the plasma particles. The formulation of these dynamic equations is described in the following section.

2.2 The Kinetic Theory

The kinetic theory attempts to explain the physical properties of a plasma by considering the forces of interaction between the component particles of the plasma in the presence of externally applied force fields. In this theory the state of the plasma is described by distribution functions for each type of constituent. The distribution function $f_s(\vec{r}, \vec{v}_s, t)$ for the s-th particle type is defined such that the number of s-type particles in the differential volume $d\vec{r}$ located at position $\vec{r}$ at time t with velocity components in the range $\vec{v}_s$ to $\vec{v}_s + d\vec{v}_s$ is given by $f_s(\vec{r}, \vec{v}_s, t)\, d\vec{r}\, d\vec{v}_s$ where $d\vec{v}_s = dv_{sx} dv_{sy} dv_{sz}$ is a differential volume in velocity space centered at $\vec{v}_s$, and v_{sx}, v_{sy}, v_{sz} denote the cartesian components of $\vec{v}_s$. The number density of s-type particles at r and t is thus given by

$$n_s(\vec{r}, t) = \int_{-\infty}^{\infty} f_s(\vec{r}, \vec{v}_s, t)\, d\vec{v}_s \tag{2.19}$$

The fundamental equation governing the particle distribution functions is a plasma is the Boltzmann equation which is of the form (Holt and Haskell, 1965)

$$\frac{\partial}{\partial t} f_s = -\vec{v}_s \cdot \vec{\nabla} f_s - \vec{R}_s \cdot \vec{\nabla} f_s + \left(\frac{\partial}{\partial t} f_s \right)_{coll} \tag{2.20}$$

where $\vec{\nabla}_v$ is the differential velocity operator defined by the relation

$$\vec{\nabla}_v f_s = \frac{\partial}{\partial v_{sx}} f_s \hat{x} + \frac{\partial}{\partial v_{sy}} f_s \hat{y} + \frac{\partial}{\partial v_{sz}} f_s \hat{z} \,. \tag{2.21}$$

The term $\vec{R}_s$ is the force per unit mass on s-type particles due to

externally applied fields. For electromagnetic fields $\vec{R}_s$ is given by the Lorentz force per unit mass

$$\vec{R}_s = q_s (\vec{E}_T + \vec{v}_s \times \vec{B}_T)/m_s \tag{2.22}$$

where q_s and m_s are the charge and mass of s-type particles, and $\vec{E}_T$ and $\vec{B}_T$ are the total electric field and magnetic flux density acting on s-type particles. In this study $\vec{E}_T = \vec{E}$, the electric field of the heating wave and $\vec{B}_T = \mu_o \vec{H} + \vec{B}_E$ where $\vec{H}$ is the magnetic field of the heating wave and $\vec{B}_E$ is the magnetic flux density of the earth's magnetic field. Boltzmann's equation states the local variation in the distribution function, $\partial f_s/\partial t$, is equal to the variations in the distribution function due to streaming of particles in or out of a given volume, $\vec{v}_s \cdot \vec{\nabla} f_s$, externally applied forces, $\vec{R}_s \cdot \vec{\nabla}_v f_s$, and collisions of s-type particles with one another as well as with all other types of plasma particles, $(\partial f_s/\partial t)_{coll}$.

Particle collisions in a plasma are of two basic types: long range Coulomb interactions between charged particles (e.g. electron-electron, electron-ion or ion-ion collisions) and short range interactions involving at least one neutral particle (e.g. electron-neutral, ion-neutral or neutral-neutral encounters). The former type of collision is a multiple interaction in which a charged particle continuously interacts with the Coulomb fields of a large number of other charged particles. In contrast, the latter type of interaction is a localized encounter between two particles (i.e. a binary collision). Based on the relative importance of each of these types of collisions in determining the physical properties of the plasma, one can distinguish

between two different types of plasma: a strongly ionized plasma in which Coulomb collisions are dominant, and a weakly ionized plasma in which binary collisions overshadow Coulomb interactions. In the lower ionosphere the electron and ion densities are much smaller than the neutral density, and the properties of the plasma are governed primarily by electron-neutral and ion-neutral collisions; hence, only binary collisions are considered here.

The time rate of change of the distribution function, f_s, due to binary collisions between s-type particles and all other particles can be written as an integral of the form (e.g. McDaniel, 1964)

$$\left(\frac{\partial}{\partial t} f_s\right)_{coll} = \sum_k \int\int (\tilde{f}_s \tilde{f}_k - f_s f_k)\, g\, q_{sk}(g, \theta)\, d\Omega\, d\vec{v}_k \qquad (2.23)$$

where

$q_{sk}(g, \theta)\, d\Omega$ - differential scattering cross section for collisions between s and k type particles,

$g = |\vec{v}_s - \vec{v}_k|$ - relative speed between colliding particles,

$d\Omega = \sin\theta d\theta\, d\phi$ - differential solid angle, and

θ - angle between $\vec{v}_s - \vec{v}_k$ and $\tilde{\vec{v}}_s - \tilde{\vec{v}}_k$,

where the tilde above a given quantity indicates its value following the collision.

The collision integral includes all types of binary processes which occur in a plasma. Depending on the types of particles involved in the collision, these processes may include elastic scattering, inelastic encounters resulting in the excitation of rotational, vibrational or electronic energy levels of one or both of the colliding partners, collisional ionization, ion-electron recombination processes,

electron attachment to neutral particles, charge transfer and many other types of chemical reactions.

Given the distribution functions for a plasma, the mean value of any plasma property, $\Phi_s(\vec{r}, \vec{v}_s, t)$, associated with s-type particles (e.g. velocity, kinetic energy, etc.) is given by

$$\Phi_s(\vec{r}, t) = \frac{1}{n_s(\vec{r}, t)} \int_{-\infty}^{\infty} \Phi_s(\vec{r}, \vec{v}_s, t)\, f_s(\vec{r}, \vec{v}_s, t)\, d\vec{v}_s \qquad (2.24)$$

In particular the constitutive relation between the current density and the electromagnetic field in a plasma is given by

$$\vec{J}(\vec{r}, t) = \sum_s q_s \int_{-\infty}^{\infty} \vec{v}_s\, f_s(\vec{r}, \vec{v}_s, t, \vec{E}, \vec{H})\, d\vec{v}_s \qquad (2.25)$$

where the dependence of the individual distribution functions on the heating wave field vectors, $\vec{E}$ and $\vec{H}$, is specified by Boltzmann's equation.

2.3 Solutions of the Boltzmann Equation

For a homogeneous plasma on which no external fields are active, the steady state solution of the Boltzmann equation is the well-known Maxwellian distribution function

$$f_{s,0}^{M} = n_s \left(\frac{m_s}{2\pi K_B T_s} \right)^{3/2} e^{-m_s \vec{V}_s \cdot \vec{V}_s / 2 K_B T_s} \qquad (2.26)$$

where

T_s - characteristic temperature of the s-type particle distribution,

$K_B = 8.617 \times 10^{-5}$ eV/ K - Boltzmann's constant, and

$\vec{V}_s = \vec{v}_s - \langle \vec{v}_s \rangle$ - thermal speed of s-type particles.

if the mean thermal speed of s-type particles is much larger than their average velocity, one can write $\vec{v}_s \cdot \vec{v}_s \approx v_s^2$ so that the Maxwellian distribution is symmetrical (i.e. depends only on the magnitude of $\vec{v}_s$). This condition is usually satisfied for electrons and ions in the lower ionosphere (Gurevich, 1978).

If the distribution function of each particle type in the plasma is Maxwellian and all of the particle types are characterized by the same temperature, then the plasma is said to be in a state of thermal equilibrium. In this study, it will be assumed that, in the absence of heating wave fields, the plasma is in a state of thermal equilibrium characterized by the neutral gas temperature, T_n. This is a reasonable assumption in the lower ionosphere (i.e. < 100 km) where good thermal contact between the plasma particles is achieved due to the high density of the neutral particles and the corresponding high frequency of particle collisions (Banks and Kockarts, 1973). However, in the upper ionosphere, the neutral particle densities are smaller, particle collisions are less frequent, and the electron, ion and neutral temperatures can differ significantly (Schunk and Nagy, 1978).

For the general case of a plasma containing spatial gradients and acted upon by external fields, no exact solution of the Boltzmann equation is known. However, one can construct an approximate solution to this equation by expanding the distribution function as a series of spherical harmonics in velocity space and them making certain assumptions about the state of the plasma in order to make the problem mathematically more tractable.

The spherical harmonic expansion of the distribution function, f_s, in velocity space is of the form (Brandstatter, 1963)

$$f_s(\vec{r}, \vec{v}_s, t) = \sum_{n=0}^{\infty} \sum_{m=-n}^{n} f_{s,n}^{m}(\vec{r}, v_s, t)\, Y_n^m(\alpha, \beta) \tag{2.27}$$

where v_s, α, β are the spherical polar coordinates of $\vec{v}_s$ and the Y_n^m are normalized spherical harmonic functions defined by

$$Y_n^m(\alpha, \beta) = (-1)^m \left[\frac{(2n+1)\ (n-m)!}{4\pi\ \ (n+m)!}\right]^{\frac{1}{2}} \sin^m\alpha\ \frac{d^m}{d(\cos\alpha)^m}\ P_n(\cos\alpha)\ e^{jm\beta} \tag{2.28}$$

where $P_n(\cos\alpha)$ is a Legendre polynomial of order n; and

$$(Y_n^m)^* = (-1)^m\, Y_n^{-m} \tag{2.29}$$

where $(Y_n^m)^*$ is the complex conjugate of Y_n^m. The spherical harmonic functions satisfy the orthogonality condition (Arfken, 1970)

$$\int_0^{2\pi} \int_0^{\pi} Y_{n_1}^{m_1 *}(\alpha, \beta)\ Y_{n_2}^{m_2}(\alpha, \beta)\ \sin\alpha\, d\alpha\, d\beta = \delta_{n_1, n_2}\, \delta_{m_1, m_2} \tag{2.30}$$

where δ_{n_1, n_2} is the Kronecker delta function,

$$\delta_{n_1, n_2} = \begin{cases} 1, & n_1 = n_2 \\ 0, & n_1 \neq n_2 \end{cases} \tag{2.31}$$

The general procedure for solving Boltzmann's equation using the spherical harmonic expansion is to substitute (2.27) into the Boltzmann equation, multiply the resultant equation by $Y_{n'}^{m'*}$ and integrate over $\sin\alpha d\alpha d\beta$. Using the orthogonality relation for the spherical harmonics to eliminate the double summation over n and m, one generates

a series of equations involving the functions, $f^{m}_{s,n}$. If one can solve these equations for the $f^{m}_{s,n}$ up to some order n = N, then (2.27) can be used to write an N-th order approximation to the distribution function (e.g. Gurevich, 1978). A modified form of this procedure will be used in the following section to study the electron distribution function.

2.4 The Electron Distribution Function

This section outlines a first order solution of the Boltzmann equation for the electron component of a weakly ionized plasma in the presence of a heating wave field and a constant geomagnetic field of flux density, $\vec{B}_E$. The objective of this analysis is to develop an expression for the electron current density, $\vec{J}_e$, induced by the electromagnetic field of the heating wave. Since one is concerned only with the field induced current, the effects of gravity and spatial gradients will be neglected. It is also assumed that the plasma is nonrelativistic so that the force exerted on the plasma by the magnetic field of the heating wave is much smaller than that due to the corresponding electric field, and can thus be neglected. Finally, the electric field of the heating, $\vec{E}$, is assumed to vary harmonically as $e^{j\omega t}$. Under these conditions the Boltzmann equation becomes

$$\frac{\partial}{\partial t} f_e - \frac{e}{m_e} (\vec{E} + \vec{v}_e \times \vec{B}_E) \cdot \vec{\nabla}_v f_e = \left(\frac{\partial}{\partial t} f_e \right)_{coll} \qquad (2.32)$$

where $-e = q_e$.

From equations (2.27-28), one has to the first order in n

$$f_e = \left(\frac{1}{4\pi}\right)^{\frac{1}{2}} f_{e,0}^{0} - \left(\frac{3}{8\pi}\right)^{\frac{1}{2}} \sin\alpha\, e^{j\beta} f_{e,1}^{1} + \left(\frac{3}{4\pi}\right)^{\frac{1}{2}} \cos\alpha\, f_{e,1}^{0} + \left(\frac{3}{8\pi}\right)^{\frac{1}{2}} \sin\alpha\, e^{-j\beta} f_{e,1}^{-1} \tag{2.33}$$

or more compactly

$$f_e = f_{e,0} + \hat{a}_e \cdot \vec{f}_{e,1} \tag{2.34}$$

where

$$f_{e,0} = \left(\frac{1}{4\pi}\right)^{\frac{1}{2}} f_{e,0}^{0}$$

$$\vec{f}_{e,1} = \left(\frac{3}{4\pi}\right)^{\frac{1}{2}} (f_{e,1}^{1}\,\hat{e}_1 + f_{e,1}^{0}\,\hat{e}_2 + f_{e,1}^{-1}\,\hat{e}_3)$$

and

$$\hat{a}_e = \vec{v}_e / v_e = \frac{-\sin\alpha\, e^{j\beta}}{\sqrt{2}}\hat{e}_1 + \cos\alpha\,\hat{e}_2 + \frac{\sin\alpha\, e^{-j\beta}}{\sqrt{2}}\hat{e}_3$$

with $\hat{e}_1$, $\hat{e}_2$, $\hat{e}_3$ being a set of complex orthonormal vectors.

Substituting (2.34) into (2.32) and integrating over $\sin\alpha\, d\alpha\, d\beta$, one obtains

$$\frac{\partial}{\partial t} f_{e,0} - \frac{e}{m_e} \vec{E} \cdot \frac{1}{3v_e^2} \frac{\partial}{\partial v_e} (v_e^2 \vec{f}_{e,1}) = \left(\frac{\partial}{\partial t} f_{e,0}\right)_{coll} \tag{2.35}$$

where

$$\left(\frac{\partial}{\partial t} f_{e,0}\right)_{coll} = \frac{1}{4\pi} \int_0^{2\pi}\int_0^{\pi} \left(\frac{\partial}{\partial t} f_e\right)_{coll} \sin\alpha\, d\alpha\, d\beta \tag{2.36}$$

Similarly, by inserting (2.34) into (2.32) and integrating over $\vec{v}_e \sin\alpha \, d\alpha \, d\beta$, one obtains

$$\frac{\partial}{\partial t} \vec{f}_{e,1} - \frac{e}{m_e} \vec{E} \frac{\partial}{\partial v_e} f_{e,0} - \frac{e}{m_e} \vec{B}_E \times \vec{f}_{e,1} = \left(\frac{\partial}{\partial t} \vec{f}_{e,1} \right)_{coll} \tag{2.37}$$

where

$$\left(\frac{\partial}{\partial t} \vec{f}_{e,1} \right)_{coll} = \frac{3}{4\pi} \int_0^{2\pi} \int_0^{\pi} \hat{a}_e \left(\frac{\partial}{\partial t} f_e \right)_{coll} \sin\alpha \, d\alpha \, d\beta \tag{2.38}$$

Considering the expansion (2.34), one notes that the terms $f_{e,0}$ and $\vec{f}_{e,1}$ depend only on the magnitude of $\vec{v}_e$; hence from (2.24) and the identities

$$\int_0^{2\pi} \int_0^{\pi} \vec{v}_e \sin\alpha \, d\alpha \, d\beta = 0 \tag{2.39}$$

$$\int_0^{2\pi} \int_0^{\pi} \vec{v}_e \vec{v}_e \sin\alpha \, d\alpha \, d\beta = \frac{4\pi}{3} v_e^2 \underline{I} \tag{2.40}$$

where $\underline{I}$ is a unit diagonal matrix, one finds that

$$\left\langle \vec{v}_e \right\rangle = \frac{4\pi}{3n_e} \int_0^{\infty} v_e^3 \vec{f}_{e,1} \, dv_e \tag{2.41}$$

and

$$\left\langle v_e^2 \right\rangle = \frac{4\pi}{n_e} \int_0^{\infty} v_e^4 f_{e,0} \, dv_e \tag{2.42}$$

Thus, the average electron momentum, $m_e \left\langle \vec{v}_e \right\rangle$ and the electron current density

$$\vec{J}_e = - e \, n_e \left\langle \vec{v}_e \right\rangle \tag{2.43}$$

are related to $\vec{f}_{e,1}$, while the average electron energy, $m_e \left\langle v_e^2 \right\rangle / 2$,

is related to $f_{e,0}$. The corresponding collision terms $(\partial \vec{f}_{e,1}/\partial t)_{coll}$ and $(\partial f_{e,0}/\partial t)_{coll}$ describe the transfer of momentum and energy, respectively, from electrons to the neutral gas.

In order to evaluate the collision terms (2.36, 2.38), one must first evaluate the collision integral $(\partial f_e/\partial t)_{coll}$ which is given by (2.23). In the weakly ionized plasma of the lower ionosphere, electrons collide primarily with neutral particles, principally N_2 and O_2. Since these particles are much more massive than an electron, one could assume as a lowest order approximation that the neutral particles are infinitely massive (i.e. they are initially at rest and do not recoil as a result of collisions with electrons). This assumption implies that $\tilde{v}_e = v_e = g$, $\tilde{f}_k = f_k$, and since $f_{e,0}$ and $\vec{f}_{e,1}$ depend only on the magnitude of $\vec{v}_e$, one has $\tilde{f}_{e,0} = f_{e,0}$, $\tilde{\vec{f}}_{e,1} = \vec{f}_{e,1}$. From these conditions and the collision geometry given in Figure 2.1, one finds that

$$\tilde{f}_e \tilde{f}_k - f_e f_k = (\tilde{\hat{a}}_e - \hat{a}_e) \cdot \vec{f}_{e,1} f_k \qquad (2.43)$$

$$= [\sin\theta \cos\phi \sin\psi + (1-\cos\theta)] \cos\psi \; f_{e,1} f_k$$

Substituting (2.43) into (2.23) and integrating over $d\phi$ and $d\vec{v}_k$, one finds that the collision integral can be written as

$$\left(\frac{\partial}{\partial t} f_e \right)_{coll} = - \sum_k \nu_{ek} \hat{a}_e \cdot \vec{f}_{e,1} \qquad (2.44)$$

where

$$\nu_{ek}(v_e) = 2\pi n_k v_e \int_0^{\pi} (1-\cos\theta) \, q_{ek}(v_e,\theta) \sin\theta \, d\theta \qquad (2.45)$$

is the electron-neutral collision frequency for momentum transfer

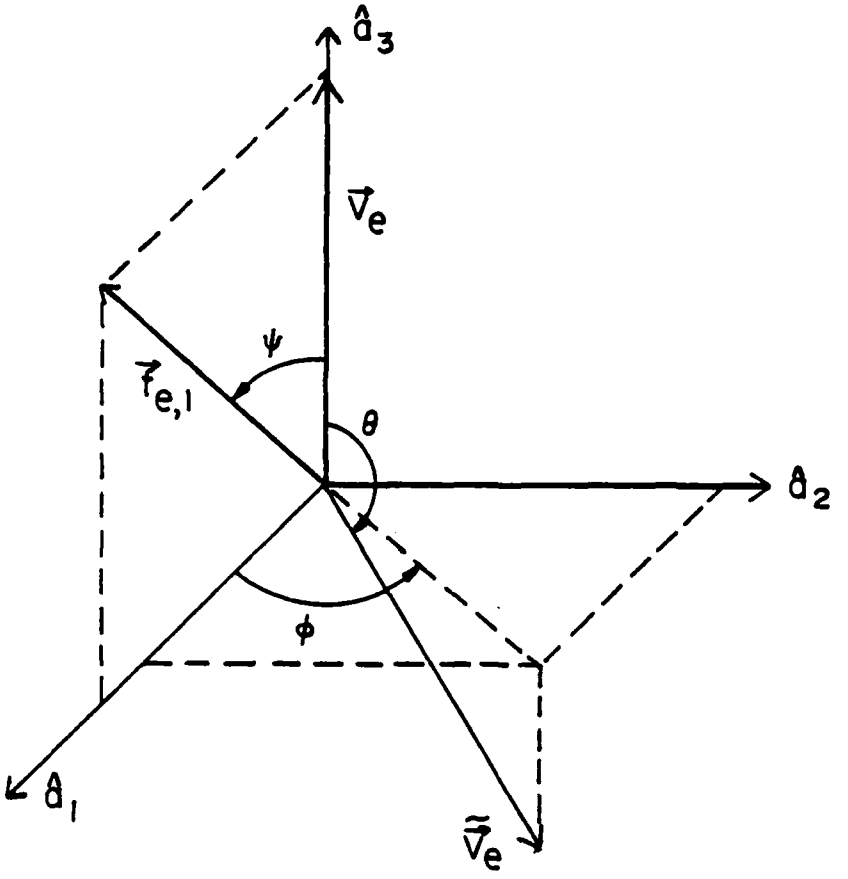

Figure 2.1 Geometry of momentum transfer collisions.

with the k-th type of neutral constituent. Inserting (2.44) into (2.38) and applying (2.40), one finds that

$$\left(\frac{\partial}{\partial t} \vec{f}_{e,1} \right)_{coll} = - \sum_k \nu_{ek} \vec{f}_{e,1} , \tag{2.46}$$

and substituting (2.44) into (2.36) and applying (2.39), one obtains

$$\left(\frac{\partial}{\partial t} f_{e,0} \right)_{coll} = 0 \tag{2.47}$$

Equation (2.47) states that for infinitely massive neutral particles, there is no energy transfer from the electrons to the neutral particles during collisions. In order to allow for energy transfer, one must recompute the collision integral for the case where $\tilde{v}_e \neq v_e$ (i.e. $m_e \tilde{v}_e^2/2 \neq m_e v_e^2/2$). This shall be done presently.

Focusing on $\vec{f}_{e,1}$, one has from (2.37) and (2.46)

$$\frac{\partial}{\partial t} \vec{f}_{e,1} - \frac{e}{m_e} \vec{E} \frac{\partial}{\partial v_e} f_{e,0} - \frac{e}{m_e} \vec{B}_E \times \vec{f}_{e,1} = \sum_k \nu_{ek} \vec{f}_{e,1} \tag{2.48}$$

Since one is only interested in that part of the current density which is induced by the electric field and $\vec{E}$ is assumed to vary harmonically as $e^{j\omega t}$, one may assume that $\vec{f}_{e,1}$ also varies as $e^{j\omega t}$. Equation (2.48) can therefore be written as

$$j\omega \vec{f}_{e,1} - \frac{e}{m_e} \vec{B}_E \times \vec{f}_{e,1} + \nu_{en} f_{e,1} = \frac{e}{m_e} \vec{E} \frac{\partial}{\partial v_e} f_{e,0} \tag{2.49}$$

where

$$\nu_{en} = \sum_k \nu_{ek} \tag{2.50}$$

This equation may be put in a more compact from by defining the following quantities:

$$\vec{Y} = - e \vec{B}_E / m_e \omega \tag{2.51}$$

$$Z = \nu_{en} / \omega \tag{2.52}$$

and

$$U = 1 - j Z \tag{2.53}$$

Rewriting (2.49) in terms of these quantities, one has

$$U \vec{f}_{e,1} - j \vec{Y} \times \vec{f}_{e,1} = - j \frac{e}{m_e \omega} \vec{E} \frac{\partial}{\partial v_e} f_{e,0} \tag{2.54}$$

Let $\hat{x}_1$, $\hat{x}_2$ and $\hat{x}_3$ be a set of orthonormal unit vectors chosen such that $\vec{Y}$ is parallel to $\hat{x}_3$: $\vec{Y} = Y \hat{x}_3$. Writing the left hand side of (2.54) in matrix one has

$$\underline{A} \vec{f}_{e,1} = - j \frac{e}{m_e \omega} \vec{E} \frac{\partial}{\partial v_e} f_{e,0} \tag{2.55}$$

where

$$\underline{A} = \begin{bmatrix} U & jY & 0 \\ -jY & U & 0 \\ 0 & 0 & U \end{bmatrix} \tag{2.56}$$

in the above coordinate system.

Solving (2.55) by matrix inversion, one has

$$\vec{f}_{e,1} = - j \frac{e}{m_e \omega} \underline{A}^{-1} \vec{E} \frac{\partial}{\partial v_e} f_{e,0} \tag{2.57}$$

where

$$\underline{A}^{-1} = \frac{1}{U(U^2 - Y^2)} \begin{bmatrix} U^2 & -jUY & 0 \\ jUY & U^2 & 0 \\ 0 & 0 & U^2 - Y^2 \end{bmatrix} \tag{2.58}$$

One can now write the electron current density (2.43) as

$$\vec{J}_e = \frac{4\pi}{3} j \frac{e^2}{m_e \omega} \int_0^\infty \underline{A}^{-1} v_e^3 \frac{\partial}{\partial v_e} f_{e,0} \, dv_e \, \vec{E} \tag{2.59}$$

From the above equation, it is apparent that one can write $\vec{J}_e$ as a conduction current

$$\vec{J}_e = \underline{\sigma}_e \vec{E} \tag{2.60}$$

where $\underline{\sigma}_e$ is the electron conductivity matrix defined by

$$\underline{\sigma}_e = \begin{bmatrix} \sigma_T & -\sigma_H & 0 \\ \sigma_H & \sigma_T & 0 \\ 0 & 0 & \sigma_L \end{bmatrix} \tag{2.61}$$

and

$$\sigma_T = \frac{4\pi}{3} j \frac{e^2}{m_e \omega} \int_0^\infty \frac{U}{U^2 - Y^2} v_e^3 \frac{\partial}{\partial v_e} f_{e,0} \, dv_e \tag{2.62}$$

$$\sigma_H = \frac{-4\pi}{3} \frac{e^2}{m_e \omega} \int_0^\infty \frac{Y}{U^2 - Y^2} v_e^3 \frac{\partial}{\partial v_e} f_{e,0} \, dv_e \tag{2.63}$$

$$\sigma_L = \frac{4\pi}{3} j \frac{e^2}{m_e \omega} \int_0^\infty \frac{1}{U} v_e^3 \frac{\partial}{\partial v_e} f_{e,0} \, dv_e \tag{2.64}$$

where σ_T, σ_H, and σ_L are the transverse, Hall and longitudinal conductivities, respectively.

2.5 Energy Transfer

In order to specify the electron conductivity completely, one must solve equation (2.35) for $f_{e,0}$. As noted earlier, the collision term in (2.35), $(\partial f_{e,0}/\partial t)_{coll}$, is zero for the case of electron

collisions with infinitely massive neutral particles; hence, there is no energy transfer from the electrons to the neutral particles. In order to allow for energy transfer, the assumptions used in deriving the collision integral (2.44) shall be relaxed by letting $\tilde{f}_{e,0}(\tilde{v}_e) = f_{e,0}(v_e + \Delta v_e)$. Since the electron energy is governed by $f_{e,0}$, it is again assumed that $\tilde{f}_{e,1} = f_{e,1}$. The assumptions that the neutral particles are initially stationary, $g = v_e$, and that the neutral particle distribution functions, f_k, are not significantly altered by electron neutral collisions, $\tilde{f}_k = f_k$, are also retained. Applying this set of assumptions to equation (2.23) and integrating over $d\vec{v}_k$, one has

$$\left(\frac{\partial f_e}{\partial t}\right)_{coll} = \sum_k n_k \int [f_{e,0}(v_e+\Delta v_e) - f_{e,0}(v_e)]\, v_e\, q_{ek}\, d\Omega - \sum_k \nu_{ek}\, \hat{a}_k \cdot \vec{f}_{e,1} \qquad (2.65)$$

Substituting this result into (2.36) and integrating over $\sin\alpha\, d\alpha\, d\beta$ one finds that

$$\left(\frac{\partial}{\partial t} f_{e,0}\right)_{coll} = \sum_k n_k \int \left[f_{e,0}(v_e+\Delta v_e) - f_{e,0}(v_e)\right] v_e\, q_{ek}\, d\Omega \qquad (2.66)$$

For elastic electron-neutral collisions, the collision integral (2.66) can be written as (e.g. Holt and Haskell, 1965)

$$\left(\frac{\partial}{\partial t} f_{e0}\right)_{el} = \frac{1}{2v_e^2} \frac{\partial}{\partial v_e}\left\{ v_e^2 \left(\sum_k G_{ek}^{el} \nu_{ek}\right)\left[v_e f_{e0} + (K_B T_n/m_e) \frac{\partial}{\partial v_e} f_{e0}\right]\right\} \qquad (2.67)$$

where the neutral particles are assumed to be in a state of thermal equilibrium characterized by the temperature T_n, and $G_{ek}^{el} = 2\, m_e/m_k$ is the mean fractional energy loss for elastic collisions between electrons and the k-th type of neutral particle.

The inelastic collision integral for the symmetrical part of the distribution function, f_{e0}, has been analyzed by Holstein (1946) and is of the form

$$\left(\frac{\partial f_{e0}}{\partial t}\right)_{in} = \frac{-2}{m_e v_e} \sum_k \left\{ \sum_{i,j} n_{ki} \left[(u+u_{ij}^k)\, f_{e0}\,(u+u_{ij}^k)\, \sigma_{ek}^{ij}\,(u+u_{ij}^k) \right.\right.$$
$$- u\, f_{e0}(u)\, \sigma_{ek}^{ij}\,(u) + (u-u_{i,-j}^k)\, f_{e0}\,(u-u_{i,-j}^k)\sigma_{ek}^{ij}(u-u_{i,-j}^k)$$
$$\left.\left. - u\, f_{e0}(u)\, \sigma_{ek}^{i,-j}\,(u)\right]\right\} \qquad (2.68)$$

where

$u = m_e v_e^2/2$,

u_{ij}^k - transition energy for the k-th neutral particle type from state i to state i + j,

$\sigma_{ek}^{ij} = q_{ek}^{ij}\, d\Omega$ - total cross section for the excitation of the i → i + j transition in k-type particles, and

n_{ki} - number density of k-type particles in state i.

The first two terms in (2.68) describe the excitation of k-type particles due to the transfer of energy u_{ij}^k from the electrons to the k-type particles, while the last two terms describe de-excitation of the k-type particles due to the transfer of energy $u_{i,-j}^k$ to the electrons.

In the lower ionosphere electrons lose energy by inelastic collisions resulting in the excitation of rotational and vibrational energy levels in N_2 and O_2. For diatomic molecules such as N_2 and O_2, Gerjouy and Stein (1955) have shown that the total cross sections for the excitation of rotational energy levels are given by

$$\sigma_{ek}^{ij} = \sigma_J^k \, \delta_{iJ} \, \delta_{j,\, J+2} \tag{2.69}$$

$$\sigma_{ek}^{i,-j} = \sigma_{-J}^{k} \, \delta_{iJ} \, \delta_{-j,\, J-2} \tag{2.70}$$

where

$$\sigma_J^k = \sigma_0^k \frac{(J+2)\ (J+1)}{(2J+3)\,(2J+1)} \left[1 - \frac{(4J+6)}{u} \ B_0^k \right]^{\frac{1}{2}},$$

$$\sigma_{-J}^{k} = \sigma_0^k \frac{J\ (J-1)}{(2J-1)\,(2J+1)} \left[1 + \frac{(4J-2)}{u} \ B_0^k \right]^{\frac{1}{2}},$$

$$\sigma_0^k = 8\pi \, Q_k \, a_0^2/15,$$

$$a_0 = 5.29 \times 10^{-9} \text{ cm - Bohr radius,}$$

Q_k - quadrapole moment for the k-th type diatomic molecule and

B_0^k - the corresponding rotational constant.

The energy of the rotational quanta are given by

$$u_{ij}^{k} = (4J+6) \ B_0^k \, \delta_{iJ} \, \delta_{j,\, J+2}$$

$$u_{i,-j}^{k} = (4J-2) \ B_0^k \, \delta_{iJ} \, \delta_{-j,\, J-2}$$

Using the cross sections (2.69-70), Gurevich (1978) has shown that (2.67) reduces to

$$\left(\frac{\partial}{\partial t} f_{e0}\right)_{rot} = \frac{1}{2v_e^2} \frac{\partial}{\partial v_e} \left\{ v_e^2 \left(\sum_k R_{rot}^k \right) \left[f_{e0} + (K_B T_n / m_e) \frac{\partial f}{\partial v_e} e0 \right] \right\} \quad (2.71)$$

provided that $u >> B_0^k$ and $K_B T_n >> B_o^k$

where $$R_{rot}^k (v_e) = \frac{8 B_0^k \sigma_0^k n_k}{m_e v_e}$$

and $$n_k = \sum_k n_{ki}.$$

In the lower ionosphere, $u \sim K_B T_n \simeq 2 \times 10^{-2}$ eV while $B_o^{N_2} = 2.48 \times 10^{-4}$ eV (Herzburg, 1950); hence, the conditions on (2.71) are satisfied.

If one writes $(\partial f_{e0}/\partial t)_{coll}$ as the sum of (2.67) and (2.71) and substitutes this sum into (2.35), it is found that f_{e0} is governed by an equation of the form

$$\frac{\partial}{\partial t} f_{e0} = \frac{1}{2v_e^2} \frac{\partial}{\partial v_e} \left\{ v_e^2 \left[\frac{2}{3} \frac{e}{m_e} \vec{E} \cdot \vec{f}_{el} + \sum_k G_{ek} \nu_{ek} \left(v_e f_{e0} + \frac{K_B T_n}{m_e} \frac{\partial}{\partial v_e} f_{e0} \right) \right] \right\} \quad (2.72)$$

where $$G_{ek}(v_e) = G_{ek}^{el} + R_{rot}^k (v_e) / \nu_{ek}(v_e)$$

For steady state conditions in which the harmonic perturbations to f_{e0} have been time averaged over the period $2\pi/\omega$, equation (2.72) can be reduced to (Holt and Haskell, 1965)

$$\frac{\partial}{\partial v_e}\left\{v_e^2\left[\frac{2}{3}\,\frac{e}{m_e}\,\overrightarrow{\overrightarrow{E}\cdot\overrightarrow{f}_{e1}} + \sum_k G_{ek}\,\nu_{ek}\left(v_e\,f_{e0} + \frac{K_B T_n}{m_e}\,\frac{\partial f}{\partial v_e}\right)\right]\right\} = 0 \tag{2.73}$$

where $$\overrightarrow{\overrightarrow{E}\cdot\overrightarrow{f}_{e1}} = \frac{\omega}{2\pi}\int_0^{2\pi/\omega}\left[\mathrm{Re}\,\{\vec{E}\}\cdot\mathrm{Re}\,\{f_{e1}\}\right]dt$$

and $\mathrm{Re}\,\{\vec{E}\}$ denotes the real part of $\vec{E}$. From (2.57) one has

$$\vec{f}_{e1} = \vec{\Gamma}\,\frac{\partial}{\partial v_e}\,f_{e0} \tag{2.74}$$

where $$\vec{\Gamma} = -j\,\frac{e}{m_e\omega}\,\underline{A}^{-1}\,\vec{E},$$

therefore

$$\overrightarrow{\overrightarrow{E}\cdot\overrightarrow{f}_{e1}} = \overrightarrow{\overrightarrow{E}\cdot\vec{\Gamma}}\;\;\frac{\partial}{\partial v_e}\,f_{e0}. \tag{2.75}$$

Substituting (2.75) into (2.73) and integrating over dv_e, one has

$$\frac{1}{f_{e0}}\;\frac{\partial}{\partial v_e}\,f_{e0} = \frac{m_e\,v_e}{\left[K_B\,T_n + 2c\,\overrightarrow{\overrightarrow{E}\cdot\vec{\Gamma}}/3\;(\sum_k G_{ek}\,\nu_{ek})\right]} \tag{2.76}$$

Integrating once more over dv_e, one obtains

$$f_{e0} = C\,\exp\left\{-\int_0^{v_e}\frac{m_e\,v_e\,dv_e}{\left[K_B\,T_n + 2e\,\overrightarrow{\overrightarrow{E}\cdot\vec{\Gamma}}/3(\sum_k G_{ek}\,\nu_{ek})\right]}\right\} \tag{2.77}$$

where the constant of integration, C, is determined from the normalization condition (2.19):

$$n_e = \int_{-\infty}^{\infty} f_e\,d\vec{v}_e = 4\pi\int_0^{\infty} v_e^2\,f_{e0}\,dv_e \tag{2.78}$$

From (2.77), it is apparent that the symmetrical part of the distribution function is Maxwellian only when $2e\,\overline{\vec{E}\cdot\vec{\Gamma}}/3(\sum_k G_{ek}\,\nu_{ek}) \ll K_B\,T_n$. In general, f_{e0} is non-Maxwellian due to the v_e dependence of $\vec{\Gamma}$ and $\sum_k G_{ek}\,\nu_{ek}$. The above analysis has included only elastic and rotational energy transfer processes; however, if one includes vibrational cooling, a similar result is obtained (Gurevich, 1978).

As a lowest order approximation, it is assumed that the denominator of the integrand in (2.77) can be written as $K_B\,T_e$ where T_e is an effective electron temperature. The symmetric part of the distribution function is therefore approximated as a Maxwellian distribution

$$f_{e0} = n_e \left(\frac{m_e}{2\pi\,K_B\,T_e}\right)^{3/2} \exp\left\{-\frac{m_e\,v_e^2}{2\,K_B\,T_e}\right\} \tag{2.79}$$

and the effect of the heating wave field on the distribution function is accounted for by describing the variation in T_e due to the heating wave field. The equation governing the variation of T_e can be derived from (2.35) by multiplying this equation by $m_e\,v_e^2/2$ and integrating over $4\pi\,v_e^2\,dv_e$ The resultant equation is

$$\frac{\partial}{\partial t}\left(\frac{3}{2}\,n_e\,K_B\,T_e\right) = \overline{\vec{E}\cdot\vec{J}_e} - L_e^{\,coll} \tag{2.80}$$

where

$$L_e^{\,coll} = \int_{-\infty}^{\infty} \frac{1}{2}\,m_e\,v_e^2 \left(\frac{\partial f_e}{\partial t}\right)_{coll} d\vec{v}_e \tag{2.81}$$

is the rate of electron energy loss due to collisions. As in (2.76), the harmonic variations in T_e have been time averaged over $2\pi/\omega$,

hence, one has $\overline{\vec{E} \cdot \vec{J}_e}$ rather than $\vec{E} \cdot \vec{J}_e$. The time derivative in (2.80) is thus to be applied to the long term variations of T_e: variations on a time scale $t >> 2\pi/\omega$.

Since f_{e0}, as specified by (2.77), is a function of the electric field strength, E, the normalization condition (2.78) suggests that n_e also varies with E. The equation describing the long term variations in n_e due to electric field of a heating wave can be derived from (2.35) by integrating this equation over $4\pi\, v_e^2\, dv_e$. Following this procedure, one finds that

$$\frac{\partial n_e}{\partial t} = S_e^{\text{coll}} \tag{2.82}$$

where

$$S_e^{\text{coll}} = \int_{-\infty}^{\infty} \left(\frac{\partial f_e}{\partial t} \right)_{\text{coll}} d\vec{v}_e \tag{2.83}$$

is the rate at which electrons are gained or lost due to collisions and photoionization of the neutral gas. If one characterizes the field induced variation in the distribution function by the effective electron temperature, T_e, then S_e^{coll} varies with T_e and causes a corresponding variation in n_e as defined by (2.82).

With f_{e0} defined by (2.79), one has $\partial f_{e0}/\partial v_e = -m_e\, v_e\, f_{e0}/K_B\, T_e$ so that the electron conductivity (2.61) becomes

$$\underline{\sigma}_e\,(T_e) = \frac{-4\pi}{3}\, j\, \frac{e^2}{K_B\, T_e\, \omega} \int_0^{\infty} \underline{A}^{-1}\, v_e^4\, f_{e0}\,(v_e, T_e)\, dv_e \tag{2.84}$$

Since f_{eo} depends on the electric field strength, it is apparent from (2.59) that the relation between $\vec{J}_e$ and $\vec{E}$ is nonlinear. In

equation (2.84), this nonlinearity is described in terms of T_e which, of course, depends directly on the field strength via (2.80).

2.6 The Dispersion Equation

In terms of the kinetic theory, the total current density induced by the electric field of a heating wave can be written as

$$\vec{J}\,(\vec{E}) = \sum_s \vec{J}_s\,(\vec{E}) = \sum_s q_s \int_{-\infty}^{\infty} \vec{v}_s\, f_s\,(\vec{v}_s, \vec{E})\, d\vec{v}_s \qquad (2.85)$$

where it is assumed that f_s is symmetrical when $\vec{E} = 0$. In the previous two sections an expression for $\vec{J}_e\,(\vec{E})$ has been developed. In order to completely specify $\vec{J}\,(\vec{E})$, one must also include any field induced ion currents. In order to specify these currents, one could proceed as in Section 2.3 to expand each of the ion distribution functions as a series of spherical harmonics:

$$f_i = f_{i0} + \hat{a}_i \cdot f_{i,1} + \ldots \qquad (2.86)$$

The first order solution of the Boltzmann equation for the ionic components of a weakly ionized plasma follows that given in Section 2.4 for the electrons, the primary difference being that, unlike the electron, the mass of a typical ion is of the same order as that of the neutral particles. From elementary considerations, Gurevich (1978) has shown that the ion currents are small in comparison with the electron current provided

$$\left(\frac{f}{f_G}\right)^2 >> \frac{m_e}{m_i}\,\frac{\langle \nu_{en} \rangle}{\langle \nu_{in} \rangle} \qquad (2.87)$$

where $f = \omega/2\pi$

$f_G = \frac{eB_E}{2\pi m_e}$ - electron gyrofrequency

m_i - mass of i-th ion type, and

ν_{in} - ion-neutral momentum transfer collision frequency

In the lower ionosphere one has $m_e/m_i \lesssim 10^{-6}$, $f_G = 0.85 - 1.7$ MHz (Yeh and Lui, 1972) and $\nu_{in} \sim \nu_{en}$ (Banks and Kockarts, 1973), hence, (2.87) is satisfied for HF fields. One can therefore write $\vec{J}(\vec{E}) = \vec{J}_e(\vec{E})$.

Using this result one can write the first of Maxwell's equation (2.15) as

$$\vec{\nabla} \times \vec{H} = \dot{\vec{D}} + \vec{J} = j\omega\varepsilon_0 \vec{E} + \underline{\sigma}_e \vec{E} \tag{2.88}$$

where $\dot{\vec{D}} = j\omega\varepsilon_0 \vec{E}$ - free space displacement current, and

$\vec{J} = \underline{\sigma}_e \vec{E}$ - electron conduction current.

In ionospheric studies, one often equates the right hand side of (2.88) to an effective displacement current

$$\dot{\vec{D}}' = j\omega\varepsilon_0 (1 - j\,\underline{\sigma}_e/\varepsilon_0\omega)\,\vec{E} \tag{2.89}$$

so that the plasma is characterized as a dielectric with relative permittivity tensor

$$\underline{\varepsilon}_R' = (\underline{I} - j\,\underline{\sigma}_e/\varepsilon_0\omega) \tag{2.90}$$

In this viewpoint the currents induced in the plasma by the electric wave field are polarization currents

$$\dot{\vec{P}}' = j\omega\,\vec{P}' = \underline{\sigma}_e \vec{E} \tag{2.91}$$

where $\vec{P}'$ is the effective plasma polarization vector defined by the relation

$$\vec{D}' = \varepsilon_0 \vec{E} + \vec{P}' \tag{2.92}$$

The above viewpoint shall be adopted in the following discussion of the wave and dispersion equations.

By susbtituting (2.84) into (2.90), the relative permittivity tensor may be written out explicity as

$$\underline{\varepsilon}_R'(\omega, T_e) = \underline{I} - \frac{4\pi}{3} \frac{e^2}{\varepsilon_0 K_B T_e \omega^2} \int_0^\infty \underline{A}^{-1}(v_e, \omega) \, f_{e0}(v_e, T_e) \, v_e^4 \, dv_e \tag{2.93}$$

The dependence of ε_R' on T_e leads to a nonlinear relationship between $\vec{D}'$ and $\vec{E}$ via (2.80), while the dependence of ε_R' on ω corresponds to frequency dispersion. Frequency dispersion arises from the fact that the effective polarization, $\vec{P}'$, of the plasma in the presence of a harmonic electromagnetic field cannot respond instantaneously to changes in the field due to the inertia of the plasma charges and the collisional forces to which they are subject (Ginzburg, 1970).

Following the usual procedure, the wave equation for the electric field vector, $\vec{E}$, can be derived by taking the curl of (2.16) and then applying (2.88) to eliminate $\vec{H}$. One obtains

$$\vec{\nabla}\vec{\nabla} \cdot \vec{E} - \nabla^2 \vec{E} = K_0^2 \underline{\varepsilon}_R' \vec{E} \tag{2.94}$$

where $K_0 = \frac{\omega}{c}$ - free space propagation constant, and

$c = \frac{1}{\sqrt{\varepsilon_0 \mu_0}}$ - speed of light in vacuo.

If one assumes that $\vec{E}$ has the form of a monochromatic plane wave with wave vector $\vec{K}$,

$$\vec{E} = \vec{E}_0 \, e^{j(\omega t - \vec{K} \cdot \vec{r})} \tag{2.95}$$

then (2.93) can be written as

$$(\vec{K} \cdot \vec{K})\,\vec{E} - (\vec{K} \cdot \vec{E})\,\vec{K} + K_0^2\,\underline{\varepsilon}'_R\,\vec{E} = 0 \qquad (2.96)$$

or

$$\underline{L}\,\vec{E} = 0 \qquad (2.97)$$

where the matrix $\underline{L}$ has elements

$$L_{ij} = K^2\,\delta_{ij} - K_i\,K_j - K_0^2\,\varepsilon'_{Rij}\,(\omega) \qquad (2.98)$$

Equation (2.96) has a nontrivial solution if and only if the determinant of $\underline{L}$ vanishes:

$$\det\,(\underline{L}) = 0 \qquad (2.99)$$

Equation (2.99) is the dispersion equation for a homogeneous, anisotropic plasma. The dispersion equation describes the relationship between the wave vector $\vec{K}$ and the wave frequency in the presence of the plasma. Since $\underline{\varepsilon}'_R\,(\omega)$ is known, equation (2.99) specified those values of $\vec{K}$ for which waves of the form (2.95) can propagate in the plasma.

In order to solve the dispersion equation, one must first evaluate the integral in (2.93). From equations (2.52-53) and (2.58), one notes that the velocity dependence of $\underline{A}^{-1}$ arises from the term U which is proportional to the electron-neutral collision frequency, ν_{en}. Thus, in order to evaluate (2.93) one must specify the velocity dependence of ν_{en}. In the lower ionosphere the neutral gas is about 78% N_2 and 21% O_2; hence, one can write from (2.50)

$$\nu_{en}(u) \approx n_{air}\left(\frac{2}{m_e}\right)^{1/2} u^{1/2}\,[0.78\,\sigma_{eN_2}(u) + 0.21\,\sigma_{eO_2}(u)] \qquad (2.100)$$

where $u = m_e v_e^2/2$,

$$\sigma_{ek}(u) = 2\pi \int_0^{\pi} (1 - \cos\theta)\, q_{ek}(v_e,\theta)\, \sin\theta d\theta$$

q_{ek} - momentum transfer cross section for electron collisions with the k-th netural particle type, and

n_{air} - number density of air.

The momentum transfer cross sections for N_2 and O_2 are given by (Banks and Kockarts, 1973)

$$\sigma_{eN_2}(u) = (18.3 - 7.3\, u)\, u^{\frac{1}{2}} \times 10^{-16}\ cm^2 \qquad (2.101)$$

and

$$\sigma_{eO_2}(u) = (2.2 + 5.1\, u^{\frac{1}{2}}) \times 10^{-16}\ cm^2 \qquad (2.102)$$

where u is in electron volts. Figure 2.2 shows a plot of ν_{en} as a function of u based on the above cross sections. For $u < 1$ eV, one has to a good approximation that ν_{en} is proportional to u. Budden (1965) has evaluated (2.93) for this case and has shown that

$$\underline{\varepsilon}_R' = \begin{bmatrix} (\varepsilon_1 + \varepsilon_2)/2 & j(\varepsilon_1 - \varepsilon_2)/2 & 0 \\ -j(\varepsilon_1 - \varepsilon_2)/2 & (\varepsilon_1 + \varepsilon_2)/2 & 0 \\ 0 & 0 & \varepsilon_3 \end{bmatrix} \qquad (2.103)$$

where

$$\varepsilon_1 = 1 - \frac{X}{Z_m}\left[\alpha_0\, C_{3/2}(\alpha_0) + j\,\frac{5}{2}\, C_{5/2}(\alpha_0)\right]$$

$$\varepsilon_2 = 1 - \frac{X}{Z_m}\left[\alpha_x\, C_{3/2}(\alpha_x) + j\,\frac{5}{2}\, C_{5/2}(\alpha_x)\right]$$

$$\varepsilon_3 = 1 - \frac{X}{Z_m}\left[Z_m^{-1} C_{3/2}(Z_m^{-1}) + j\,\frac{5}{2}\, C_{5/2}(Z_m^{-1})\right]$$

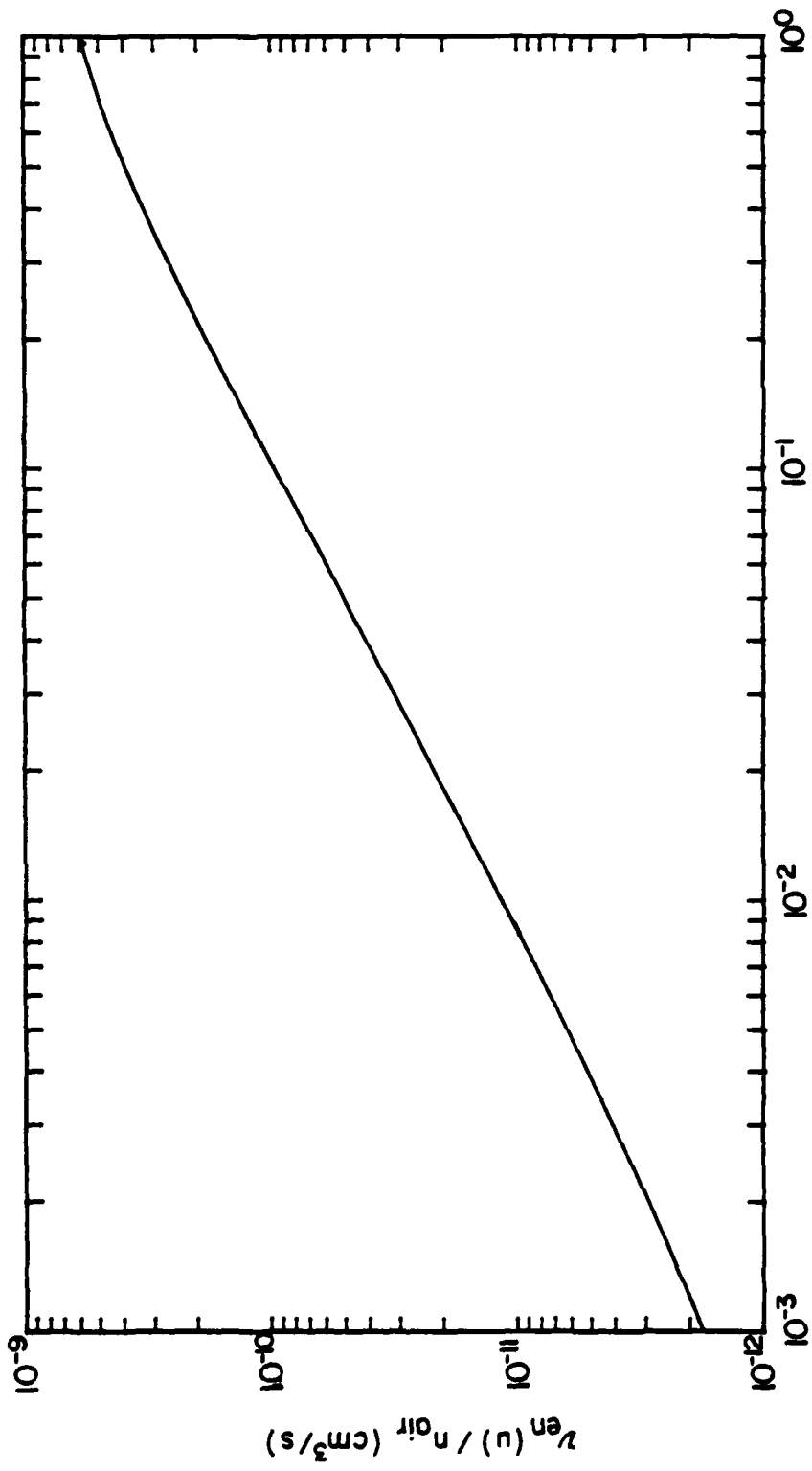

Figure 2.2 Electron-neutral collision frequency as a function of electron energy.

$$\alpha_0 = (1 + Y)/Z_m$$

$$\alpha_x = (1 - Y)/Z_m$$

$$X = \omega_e^2/\omega^2$$

$$\omega_e = \left(\frac{n_e e^2}{m_e \varepsilon_0}\right)^{1/2} \text{ - angular electron plasma frequency}$$

$$Z_m = \nu_m/\omega$$

$$\nu_m = \nu_{en}(K_B T_e) \text{ - electron-neutral momentum transfer collision frequency evaluated at the most probably electron energy}$$

and (Dingle et al., 1957; Hara, 1963)

$$C_p(X) = \frac{1}{p!}\int_0^\infty \frac{\xi^p}{(\xi^2 + X^2)}\, e^{-\xi}\, d\xi.$$

Equation (2.103) applies to the coordinate system illustrated in Figure 2.3, which was used in defining $\underline{A}$ (see 2.56). If one chooses the wave vector to be in the $\hat{x}_1$, $\hat{x}_3$ plane, then one can easily show that

$$\vec{K}\cdot\vec{K}\vec{E} - \vec{K}\cdot\vec{E}\vec{K} = \begin{bmatrix} K^2\cos^2\theta & 0 & -K^2\cos\theta\sin\theta \\ 0 & K^2 & 0 \\ -K^2\cos\theta\sin\theta & 0 & K^2\sin^2\theta \end{bmatrix} \begin{bmatrix} E_1 \\ E_2 \\ E_3 \end{bmatrix} \qquad (2.104)$$

where $\vec{E} = E_1\,\hat{x}_1 + E_2\,\hat{x}_2 + E_3\,\hat{x}_3$ and θ is the angle between $\vec{Y}$ and $\vec{K}$.

By substituting (2.103-104) into (2.99) and solving for K (e.g. Yeh and Liu, 1972), one finds that

$$K = K_0\,\eta$$

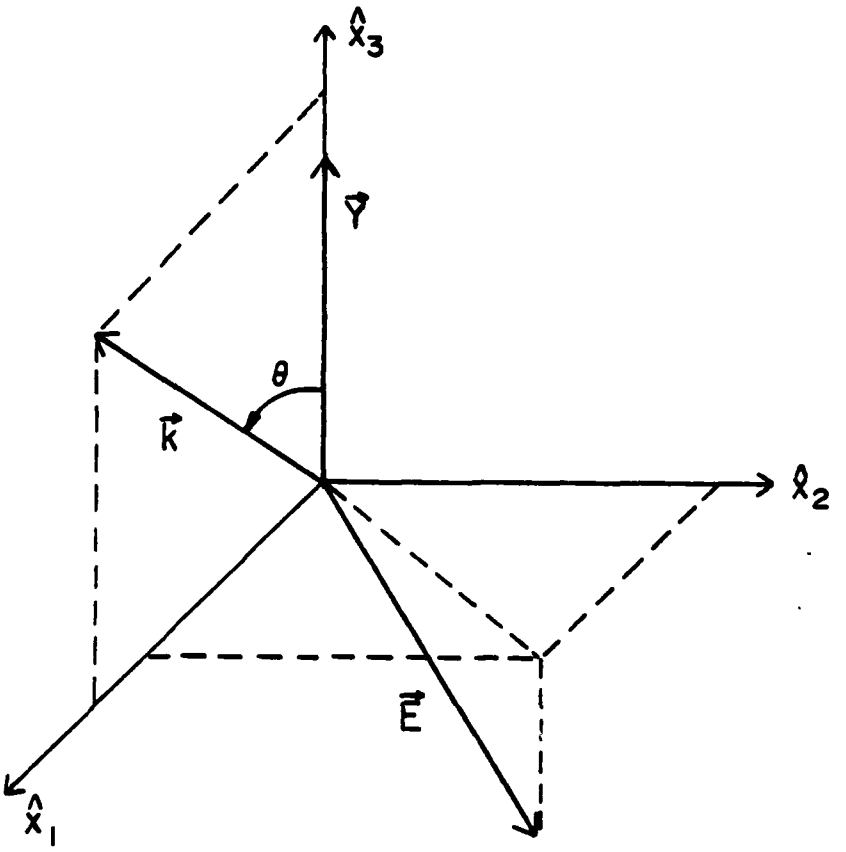

Figure 2.3 Geometry for the dispersion equation.

where η is the complex index of refraction defined by (Budden, 1965)

$$\eta^2 = \frac{\varepsilon_1 \varepsilon_2 \sin^2\theta + \frac{1}{2}\varepsilon_3(\varepsilon_1+\varepsilon_2)(1+\cos^2\theta)}{(\varepsilon_1+\varepsilon_2)\sin^2\theta + 2\varepsilon_3\cos^2\theta} \pm \frac{\{\sin^4\theta\,\varepsilon_1\varepsilon_2 - \frac{1}{2}\varepsilon_3(\varepsilon_1+\varepsilon_2)^2 + \cos^2\theta\,\varepsilon_3^2(\varepsilon_1-\varepsilon_2)\}^{\frac{1}{2}}}{(\varepsilon_1+\varepsilon_2)\sin^2\theta + 2\varepsilon_3\cos^2\theta} \quad (2.106)$$

Equation (2.106) is the generalized magnetoionic formula for a homogeneous, anisotropic plasma which was first developed by Sen and Wyller (1960). It is apparent that η^2 has two values: one corresponding to the plus sign in (2.106) and the other to the minus sign. The ionospheric is thus a birefringent medium which supports the propagation of waves of two different types. These two wave types correspond to two different polarizations (e.g. Budden, 1966) and are denoted the ordinary or O-mode, η_O (plus sign), and the extraordinary or X-mode, η_X (minus sign).

CHAPTER III

IONOSPHERIC HEATING

3.1 The Energy Balance Equation

The objectives of this chapter are to determine the magnitude and time scale of electron temperature modifications in the lower ionosphere induced by a strong electromagnetic wave and the corresponding variation in the heating wave fields due to self-absorption.

Electron temperature modifications due to radiowave heating are governed by the energy balance equation (2.80). In order to simplify the analysis of this equation, it shall be assumed throughout this chapter that the time scale for electron density modifications is much larger than that for the electron temperature so that one may write $\partial n_e/\partial t = 0$. The validity of this assumption will be examined in Chapter IV. Applying this assumption to (2.80), the energy balance equation becomes

$$\frac{3}{2} n_e K_B \frac{\partial}{\partial t} T_e = \overline{\vec{E} \cdot \vec{J}} - \sum_s \frac{\partial}{\partial t} U_{es} \tag{3.1}$$

where $\overline{\vec{E} \cdot \vec{J}}$ is the rate of electron heating due to the wave field, and $\sum_s \partial U_{es}/\partial t = L_e^{coll}$ is the rate of electron energy loss due to collisions with neutral particles.

From equations (2.16) and (2.88), one has

$$\vec{E} \cdot \vec{J}_e = \vec{E} \cdot (\vec{\nabla} \times \vec{H} - j\omega\varepsilon_o \vec{E}) \tag{3.2}$$

$$= -\vec{\nabla} \cdot (\vec{E} \times \vec{H}) - j\omega(\varepsilon_o E^2 + \mu_o H^2)$$

By computing the time average of $\vec{E} \cdot \vec{J}_e$ over $\omega/2\pi$, one finds that (e.g. Brandstatter, 1965)

$$\overline{\vec{E} \cdot \vec{J}_e} = -\nabla \cdot \vec{S} \tag{3.3}$$

where $$\vec{S} = \frac{1}{2} R_e \{\vec{E} \times \vec{H}^*\} \tag{3.4}$$

is the average power density of the heating wave. The final form of the production term (3.3) to be used in the solution of (3.1) will be developed in the following section.

The electron energy loss term $\sum_s \partial U_{es}/\partial t$ includes a number of collisional processes including elastic electron-neutral collisions and electron impact excitation of the rotational, vibrational and electronic energy levels of neutral particles. The rate of electron cooling due to elastic electron-neutral collisions has been calculated by Banks (1966) and is given by

$$\frac{\partial}{\partial t} U_{es}(T_e)\Big|_{elastic} = 3 \frac{m_e}{m_s} n_e \left\langle \nu_{es}(T_e) \right\rangle (T_e - T_n). \tag{3.5}$$

Elastic collisions are not very effective in cooling electrons due to the unfavorable mass ratio, m_e/m_s, and these processes are generally overshadowed by inelastic collisions. At present, a precise analytic theory of inelastic cooling does not exist; however, numerical formulae for most of the important ionospheric electron cooling processes based on laboratory data are available, and have been summarized in works by Stubbe and Varnum (1972), Banks and Kockarts (1973) and Shunk and Nagy (1978). The primary electron cooling processes in the ionosphere for $T_e \leq 10\ T_n$ are rotational and vibrational excitation of N_2 and O_2, and the excitation of fine structure levels on atomic oxygen.

Figures 3.1 - 2 illustrate the electron temperature variation of

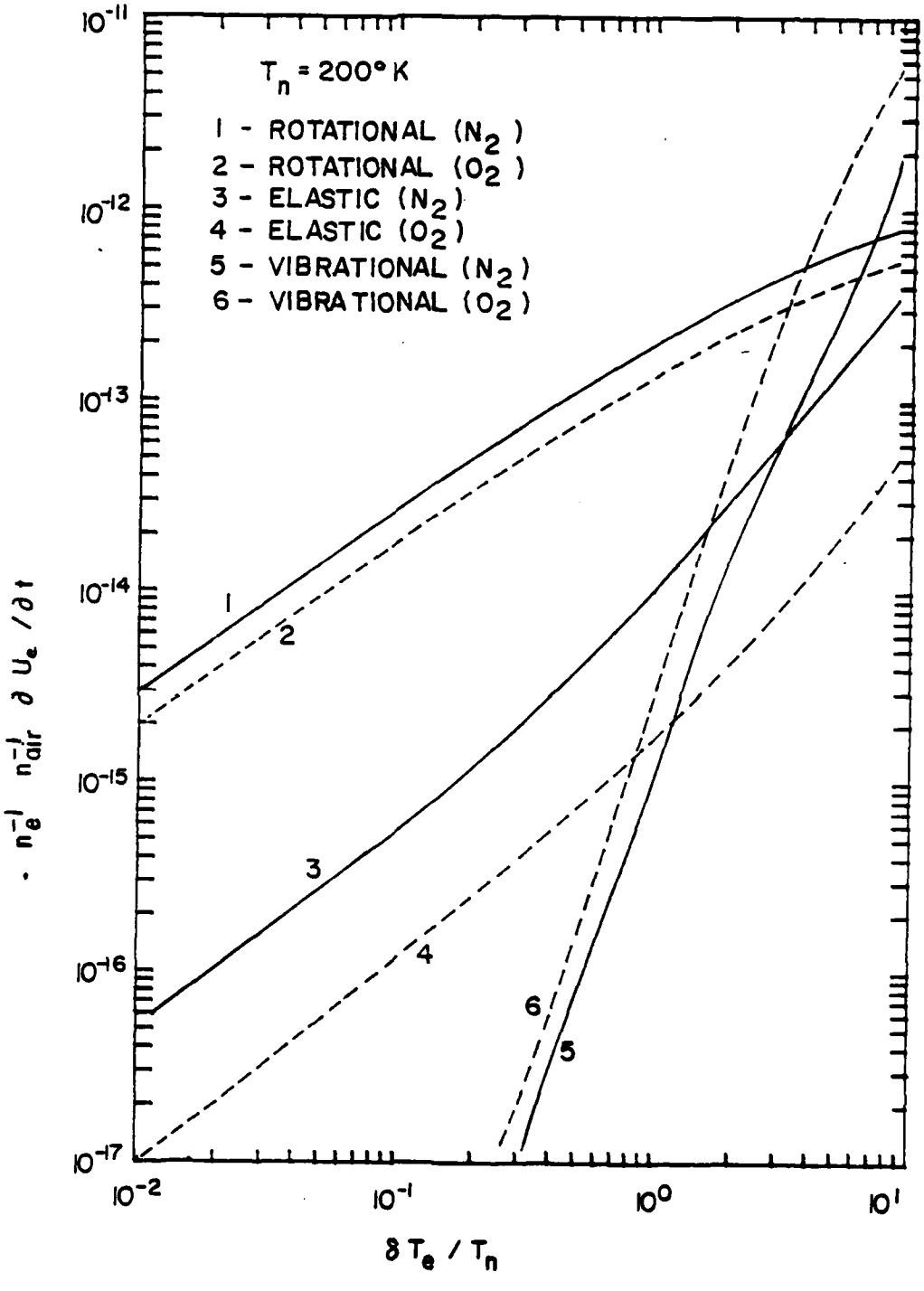

Figure 3.1 Normalized electron cooling rates for various processes in air as a function of the fractional change in electron temperature.

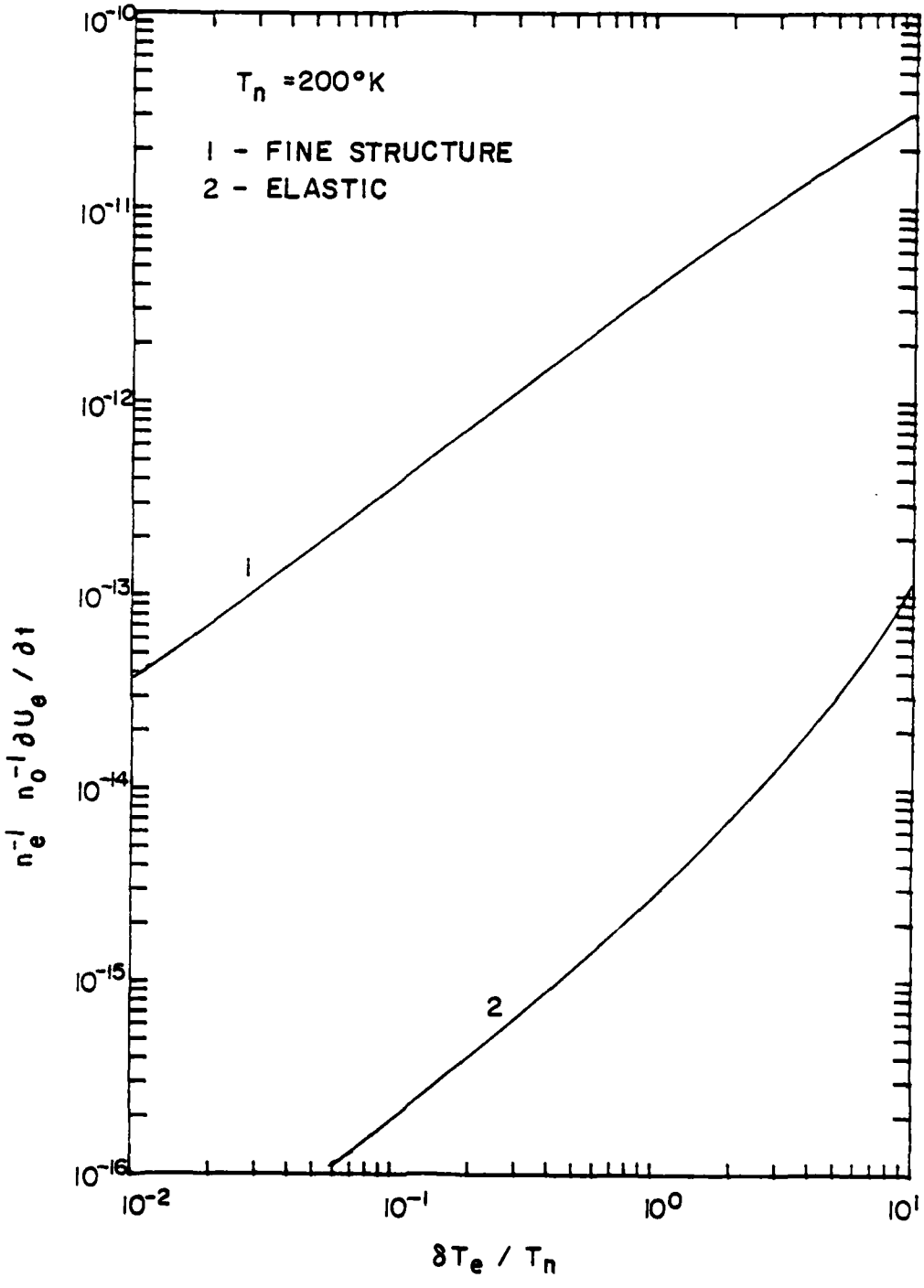

Figure 3.2 Normalized electron cooling rates for collisions with atomic oxygen as a function of the fractional change in electron temperature.

the electron energy transfer rates for various types of collisional processes based on the summary of formulae given by Stubbe and Varnum (1972). In Figure 3.1, the mixing ratio for the major neutral gases has been assumed to be constant with N_2 being 78% of the total neutral (air) content and O_2 being 21%. The cooling rates have been made independent of the electron and neutral particle densities by dividing $\partial U_e/\partial t$ for each process by n_e and n_{air}. These normalized rates are plotted as a function of the normalized change in electron temperature above ambient: $\delta T_e/T_n = (T_e - T_n)/T_n$. For $\delta T_e/T_n \lesssim 1$, rotational cooling is dominant; however, for higher electron temperatures, vibrational cooling becomes important.

In the D-region, one has $n_O << n_{O_2}$ and n_{N_2}, hence, electron cooling due to collisions with atomic oxygen is relatively unimportant, but in the E-region, $n_O \sim n_{O_2}$ and these processes must be considered. Figure 3.2 shows a plot of the normalized cooling rates for electron collisions with atomic oxygen as a function of $\delta T_e/T_n$. Electron cooling due to electron impact induced fine structure transitions in O is clearly dominant over the corresponding elastic cooling process over the range of electron temperatures of interest in this study.

3.2 The Heating Wave Fields

The source of the heating wave is assumed to be a powerful ground-based HF transmitter which is excited by a sinusoidally varying current of angular frequency ω. At a point r from the HF transmitter (i.e. $r >> 1/K_o$) but below the base of the ionosphere (~ 50 km) the heating wave fields are given by (Jordan and Balmain, 1968)

$$\vec{E}(\vec{r}, t) = -j K_o Z_o \frac{e^{j(\omega t - K_o r)}}{r} \int \vec{J}_{EXT}(\vec{r}') \, e^{-jK_o \vec{r}' \cdot \hat{r}} \, d\vec{r}' \quad (3.6)$$

and $$\vec{H}(\vec{r}, t) = \frac{1}{Z_o} \hat{r} \times \vec{E}(\vec{r}, t) \quad (3.7)$$

where $Z_o = \sqrt{\mu_o/\varepsilon_o}$ - characteristic impedance of free space,

and

$\hat{r}$ - a unit vector in the direction of $\vec{r}$.

The fields incident upon the ionosphere therefore have the form of spherical waves.

In deriving the magnetoionic formula (2.106), it is assumed that the wave fields have the form of plane waves. If one were instead to assume that the wave fields are spherical, then the application of the del operator, $\vec{\nabla}$, to the electric field in (2.94) gives rise to terms of order 1/r as well as those of order K. Clearly if one has $1/r \ll K$, then the dispersion equation (2.96) and its solution (2.106) are also valid for spherical waves. At the base of the ionosphere this condition reduces to $\omega \gg 6 \times 10^3$/s which is easily satisfied at frequencies in the HF band. Thus, while the wave fronts of the radiation field from the transmitter are spherical, by the time they reach the base of the ionosphere the radius of curvature of the fronts are so large that the wave is very nearly a plane wave. The wave fields in a plasma far from the wave source are therefore of the forms

$$\vec{E}(\vec{r}, t) = \vec{E}_o \left(\frac{r_o}{r}\right) e^{j[\omega t - \vec{K} \cdot (\vec{r} - \vec{r}_o)]} \quad (3.8)$$

and

$$\vec{H}(\vec{r}, t) = \vec{H}_o \left(\frac{r_o}{r}\right) e^{j[\omega t - \vec{K} \cdot (\vec{r} - \vec{r}_o)]} \quad (3.9)$$

where $\vec{E}_o$ is the value of $\vec{E}$ at some reference point $\vec{r}_o$ and by (2.16)

$$\vec{H}_o = \frac{1}{\omega\mu_o} \vec{K} \times \vec{E}_o \tag{3.10}$$

The above formulae apply to a homogeneous plasma. However, as noted in Chapter I, the ionosphere is a nonhomogeneous medium. For a nonhomogeneous medium the spherical wave solutions for the field vectors given above are not valid and one must generally resort to a full wave analysis of Maxwell's equations to determine the field vectors (e.g. Budden, 1965). At wave frequencies above 1 MHz, the properties of the ionosphere are slowly varying over distances of the order of a wavelength. One may therefore consider the plasma to be locally homogeneous and approximate solutions for the wave fields can be obtained by the WKB method. Since the largest variation in the properties of the ionosphere is in the vertical direction, these properties are assumed to be a function of height, h, only. The WKB solutions for the portion of the spherical wave front that is vertically incident on a horizontally homogeneous ionosphere are given approximately by (Budden, 1966)

$$\vec{E}\ (h,\ t) = \vec{E}_o \left(\frac{h_o}{h}\right) \eta^{-\frac{1}{2}}(h)\ \exp\left\{ j\omega t - j\ K_o \int_{h_o}^{h} \eta(h')\ dh' \right\} \tag{3.11}$$

and

$$\vec{H}\ (h,\ t) = \vec{H}_o \left(\frac{h_o}{h}\right) \eta^{\frac{1}{2}}(h)\ \exp\left\{ j\omega t - j\ K_o \int_{h_o}^{h} (h')\ dh' \right\} \tag{3.12}$$

where

$$\vec{H}_o = \hat{z} \times \vec{E}_o / Z_o \tag{3.13}$$

Substituting (3.11-13) into (3.4), one finds that the average power density is given approximately by

$$\vec{S}(h) = \vec{S}_o \left(\frac{h_o}{h}\right)^2 \exp\left\{-2K_o \int_{h_o}^{h} \chi(h') \, dh'\right\} \qquad (3.14)$$

where $\chi(h)$ is the imaginary part of the index of refraction

$$\eta(h) = \mu(h) - j\,\chi(h) \qquad (3.15)$$

and $\mu(h)$ is the real part. The quantity $\vec{S}_o$ is the average power density which is vertically incident on the base of the ionosphere, h_o, and is given by

$$\vec{S}_o = \frac{1}{2} \frac{E_o^2}{Z_o} \hat{z} = \frac{P_T G}{4\pi h_o^2} \hat{z} \qquad (3.16)$$

where P_T - total transmitter power, and

G - zenith gain of the transmitting antenna array.

Taking the divergence of equation (3.14), one finds that

$$\vec{\nabla} \cdot \vec{S}(h) = \frac{-2}{h} S(h) - 2\,K_o\,\chi(h)\,S(h) \qquad (3.17)$$

The first term on the righthand side of (3.17) accounts for the decrease in the power density of the HF wave as its front spreads with increasing height, while the second term represents the power dissipation per unit volume as a result of absorption by electrons. The rate of electron heating due to the wave field is therefore given by

$$\overline{\vec{E} \cdot \vec{J}_e} = 2\,K_o\,\chi(h)\,S(h) \qquad (3.18)$$

Substituting this result into the electron energy balance equation, one obtains

$$\frac{3}{2} n_e(h)\,K_B \frac{\partial}{\partial t} T_e(h) = 2\,K_o\,\chi(h, T_e)\,S(h, T_e) - \sum_s \frac{\partial}{\partial t} U_{e,s}(h, T_e) \qquad (3.19)$$

where the electron temperature dependence of χ and S arises from the collision frequency, $\nu_{en}(K_B T_e)$, which is a parameter in the formula for the index of refraction.

As a heating wave propagates through the ionosphere, energy is absorbed from it by the plasma electrons, causing an increase in the electron temperature as dictated by (3.19). The increase in electron temperature changes the plasma absorption index from its ambient value, $\chi(h, T_n)$ to a heated value, $\chi(h, T_e)$, along the wave path which in turn causes additional absorption on the wave. From (3.14), one finds that the self-absorption experienced by a heating wave as it propagates from h_o to h is given by

$$L_s = 8.686\, K_o \int_{h_o}^{h} [\chi(h', T_e) - \chi(h', T_n)]\, dh' \qquad (3.20)$$

where L_s is in decibels above the ambient absorption level.

3.3 Electron Heating in a Weak Field: Analytic Theory

In the following analysis, the heating wave field is assumed to be weak so that the electron temperature is only slightly perturbed from its ambient value: $\delta T_e << T_n$. In this temperature regime, the dominant electron energy loss process is rotational cooling with N_2 and O_2 (see Figure 3.1), and the total cooling rate can be written as (Mentzoni and Row, 1963; Shunk and Nagy, 1978)

$$\sum_s \frac{\partial}{\partial t} U_{e,s}(T_e) \approx a\, n_e\, T_e^{-\frac{1}{2}}\, \delta T_e \qquad (3.21)$$

where

$$a = 1.17 \times 10^{-10} (.78\, n_{N_2} Q_{N_2}^2 B_o^{N_2} + .21\, n_{O_2} Q_{O_2}^2 B_o^{O_2})$$

Since $T_e \approx T_n$, one can neglect self-absorption effects and the electron energy balance equation can be written as

$$\frac{\partial}{\partial t} T_e = P_e (T_n) - \frac{\delta T_e}{\tau_H(T_n)} \tag{3.22}$$

where

$$P_e (T_n) = \frac{4 K_o \chi(T_n) S(T_n)}{3 n_e K_B} \tag{3.23}$$

and

$$\tau_H (T_n) = \frac{3 K_B T_n^{\frac{1}{2}}}{2 a} \tag{3.24}$$

For an HF wave of duration Δt_H initiated at time $t = 0$, one finds from equation (3.22) that for $0 \leq t \leq \Delta t_H$

$$T_e(t) = T_n + P_e(T_n) \tau_H(T_n) [1 - e^{-t/\tau_H(T_n)}] \tag{3.25}$$

where

$$\delta T_e(\Delta t_H) = P_e(T_n) \tau_H(T_n) [1 - e^{-\Delta t_H/\tau_H(T_n)}] \tag{3.26}$$

3.4 Electron Heating in a Strong Field: Computational Method

This section describes a numerical procedure for solving the energy balance equation for a strong wave field in a nonhomogeneous plasma which takes into account the self-absorption of the heating wave.

Let h_o denote the base of the ionosphere and let the plasma above this height be subdivided into a large number of horizontal layers of thickness $\Delta h_i = h_{i+1} - h_i$ where h_{i+1} and h_i are the height of the upper and lower boundaries of the i-th layer. Each Δh_i is chosen such that the plasma is essentially homogeneous over the layer. In particular, it is required that $\Delta h_i \ll 1/(2 K_o \Delta\chi_i)$ where $\Delta\chi_i = \chi(h_{i+1}) - \chi(h_i)$

so that the incremental absorption over each h_i is small compared to the integral absorption from h_o to h_i.

Consider an HF pulse of duration Δt_H incident upon h_o at $t_o = h_o/c$ and propagating upwards with velocity c. If one chooses $t_i \ll \tau_H(h_i, T_n)$ where Δt_i is the size of the time increments within the i-th layer, the electron temperature within the i-th layer can be approximated as

$$T_e(h_i, t_j) = T_e(h_i, t_{j-1}) + \Delta t_i \frac{\partial T_e}{\partial t}(h_i, t_{j-1}, S(h_i, t_j)) \quad (3.27)$$

where $t_j = t_{j-1} + \Delta t_i$, and $\partial T_e/\partial t$ is given by equation (3.19) with χ and $\sum_s \partial U_{es}/\partial t$ evaluated at $T_e(h_i, t_{j-1})$. T_e is computed for each t_j starting at h_o and moving upwards in steps of Δh_i. The power density is recomputed after each altitude increment for fixed t_j using equation (3.14) and is employed in evaluating T_e for the layer. The boundary conditions on the solutions for T_e and S are

$$S(h_o, t) = \begin{cases} S_o, & t_o \leq t \leq t_o + \Delta t_H \\ 0, & \text{otherwise} \end{cases} \quad (3.28)$$

and

$$T_e(h_i, t) = T_n(h_i), \quad t < h_i/c \quad (3.29)$$

3.5 Electron Heating in a Strong Field: Results

The above procedure has been used to compute the transient and steady state response of T_e and S for a strong wave field. The absorption index was calculated from the Sen-Wyller formula (2.106). The gyro frequency was taken as $f_G = 1.135$ MHz and the angle between $\vec{K}$ and $\vec{Y}$, $\theta = 40.65^\circ$, corresponding to geomagnetic conditions at Arecibo

for a vertically incident wave. The collision frequency was calculated from the energy dependent cross sections given by Banks and Kockarts (1973) and was evaluated at the most probably electron energy, $K_B T_e$. The neutral particle densities and the neutral temperature were taken from CIRA (1972). The plasma frequency model, $\omega_e(h)$, corresponds to the daytime electron density distribution at a solar zenith angle, $\chi_s = 30^o$ and a moderate level of solar activity.

Figure 3.3 shows the electron temperature variation at 70 km due to a 250μs, 5 MHz X-mode heating pulse for several values of the effective radiated power, $P_T G$. One notes that the electron temperature reaches a steady state in less than 250μs for all heating powers and that the plasma cools somewhat faster than it heats. The power density at 70 km (not shown) is proportional to the heating power and is constant with time. This is not the case in the upper D-region (90 km) as illustrated in Figure 3.4. Here, the power density drops abruptly from its initial value, corresponding to the leading edge of the heating pulse, to a steady state value on a time scale of about 500μs. This effect is due to self-absorption and it parallels the time scale for electron temperature changes in the 70 to 80 km region, which is the region of maximum heating as illustrated in Figure 3.5. The electron temperature at 90 km, on the other hand, responds much more slowly than the power density, requiring about 3.5 ms to reach a steady state level.

Self-absorption severely limits the available heating power in the upper D-region leading to a steep temperature gradient between 80 and 90 km as shown in Figure 3.5. Moreover, the limitations imposed by

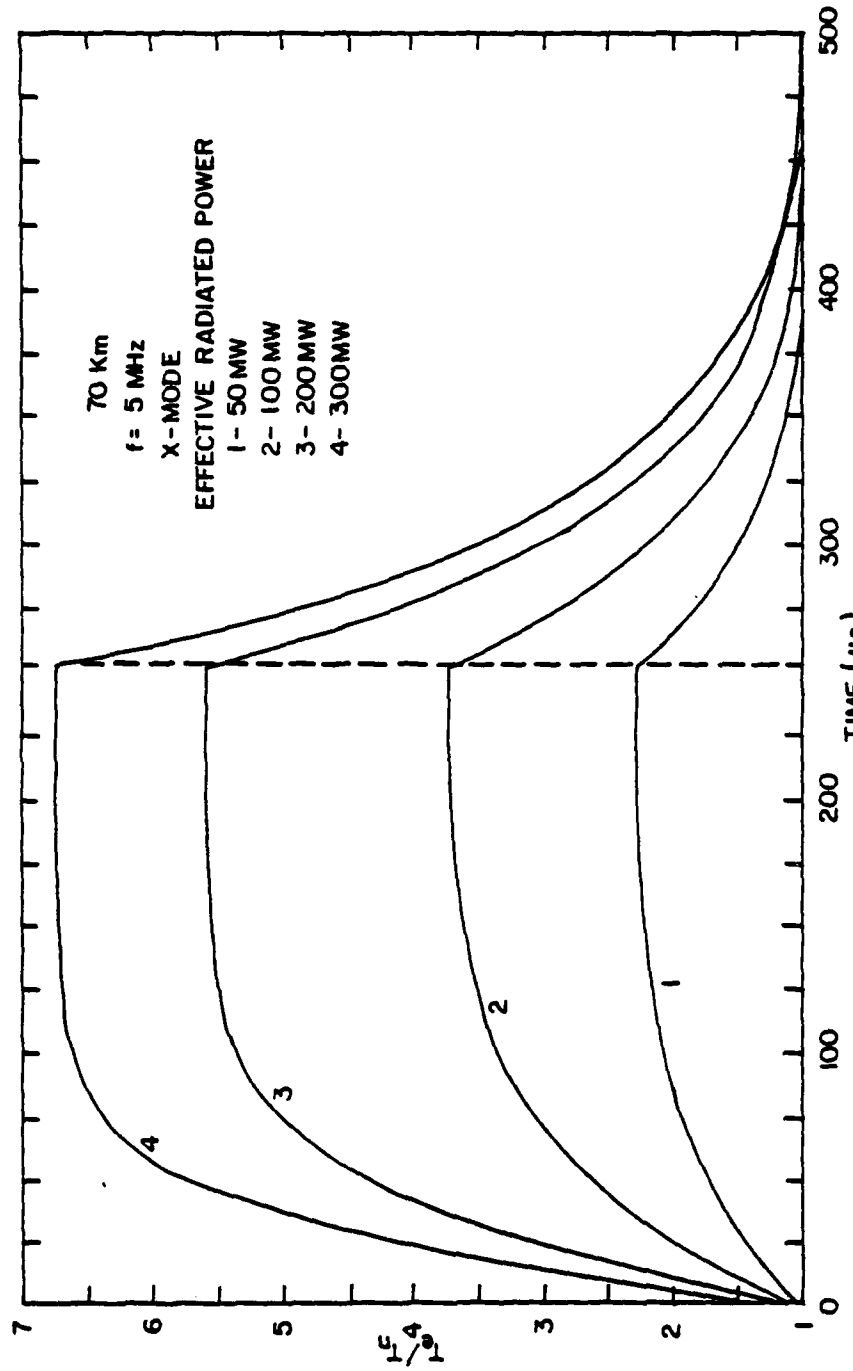

Figure 3.3 Electron temperature variation at 70 km due to a 250 μs heating pulse.

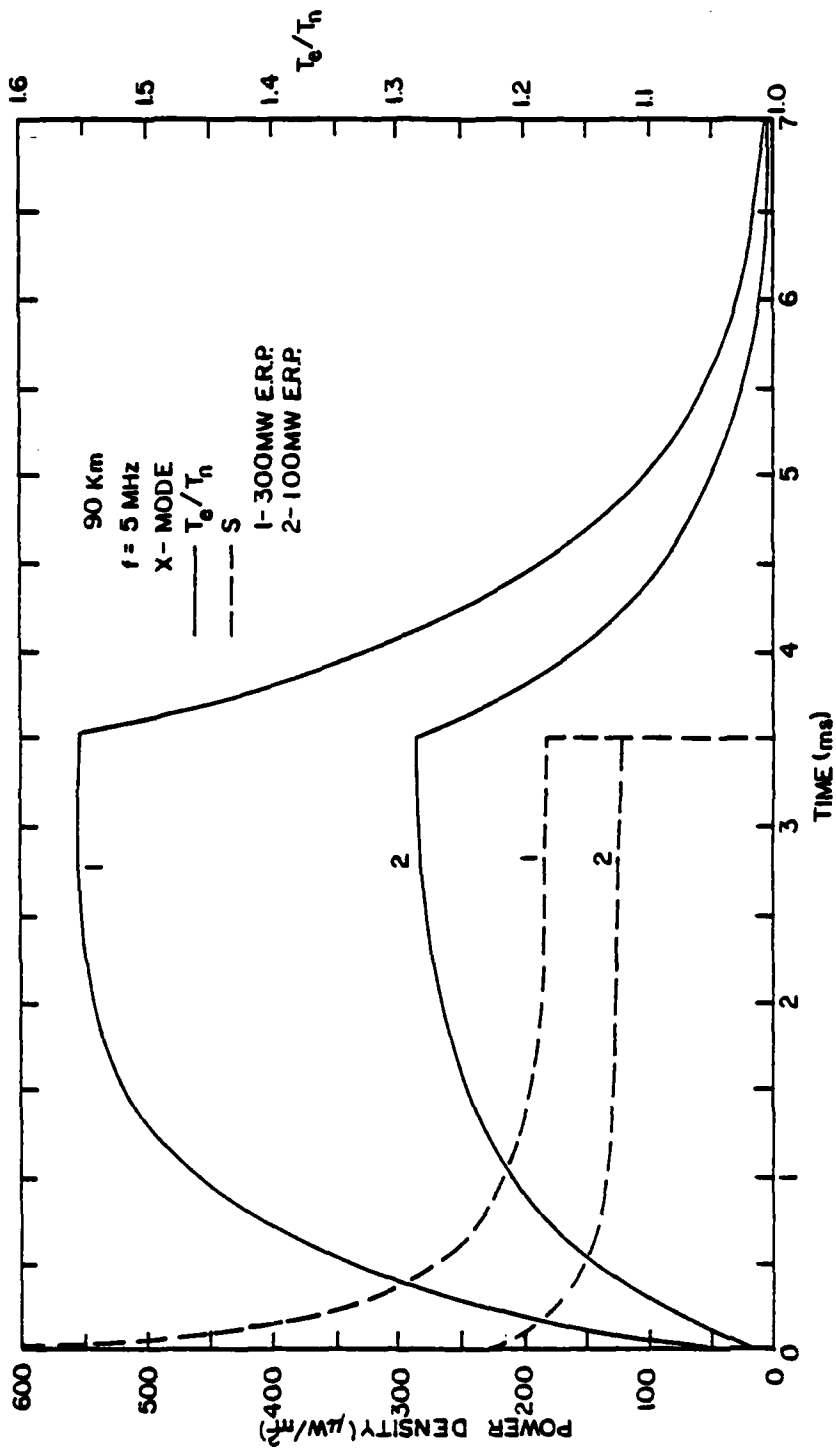

Figure 3.4 Power density and electron temperature variation at 90 km due to a 3.5 ms heating pulse.

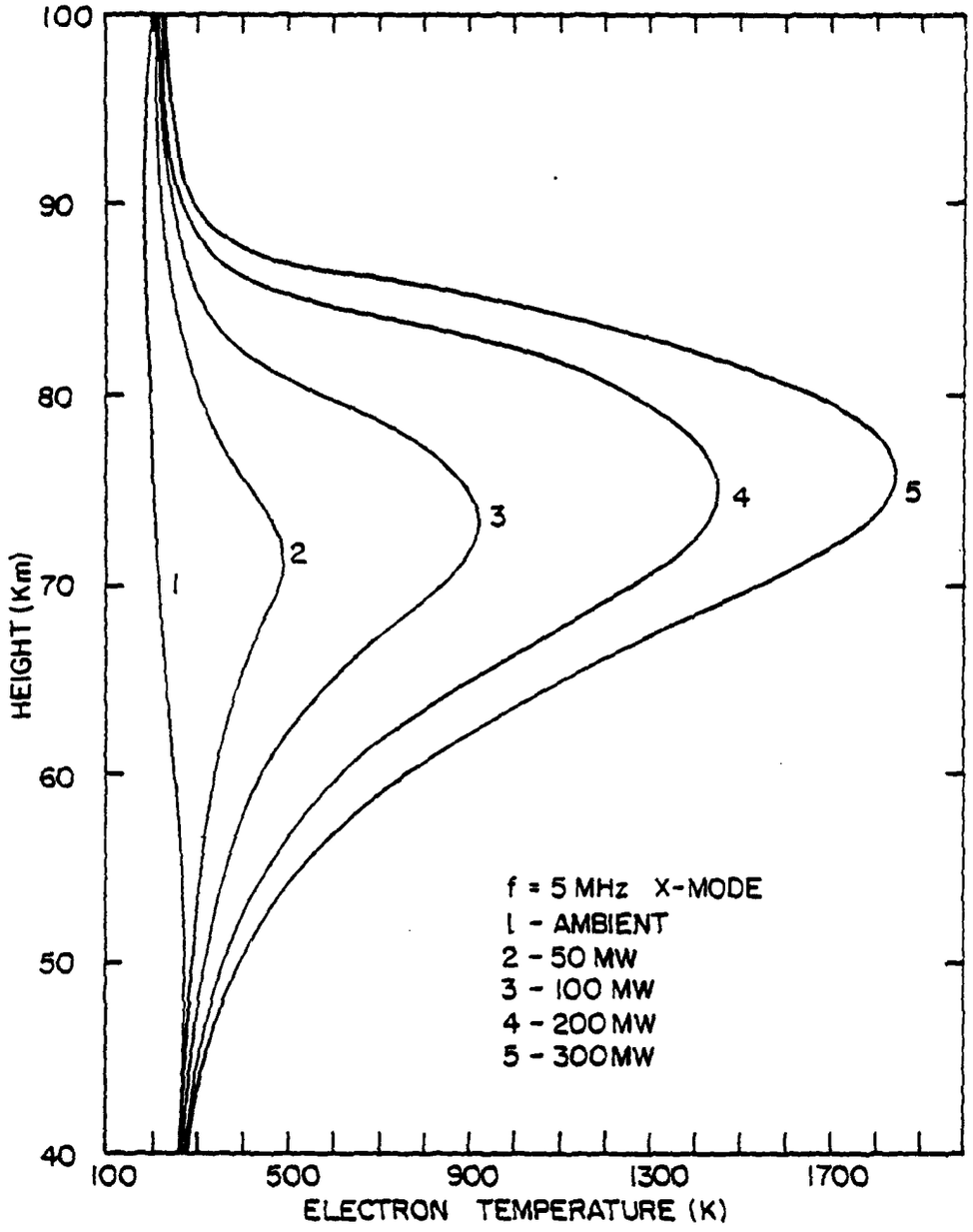

Figure 3.5 Steady state electron temperature profiles for various heating powers.

self-absorption on upper ionospheric heating cannot be readily overcome simply by increasing the heating power. In Figure 3.6, the initial (leading edge) and steady state power densities are plotted as a function of heating power at 5 MHz X-mode. The initial power density increases in proportion to the heating power; however, the self-absorption also increases with heating power, with the effect that the net gain in steady state power density is very small. For example, at 100 km the self-absorption is about 3dB for 100 MW of heating. If one doubles the heating power to 200 MW, the self-absorption rises to more than 5dB resulting in a net gain in power density of less than 30%.

Figure 3.7 shows the initial and steady state power density as a function of heating frequency. The power density available for heating in the upper ionosphere decreases sharply at the lower end of the heating frequency range due to rapid absorption in the middle D-region. As a consequence, the electron temperature in the middle D-region is greatly enhanced (Figure 3.8). As one moves to higher heating frequencies, the D-region absorption significantly decreases and consequently so does the D-region electron temperature. The self-absorption component of the D-region absorption also decreases with increasing heating frequency as shown by the convergence of the initial and steady state power density curves in Figure 3.7. At the higher frequencies, the power density available for upper ionospheric heating becomes nearly independent of frequency and is controlled by the heating power. While the available power density is much larger at the higher frequencies, the heating above 90 km is not significantly increased, as

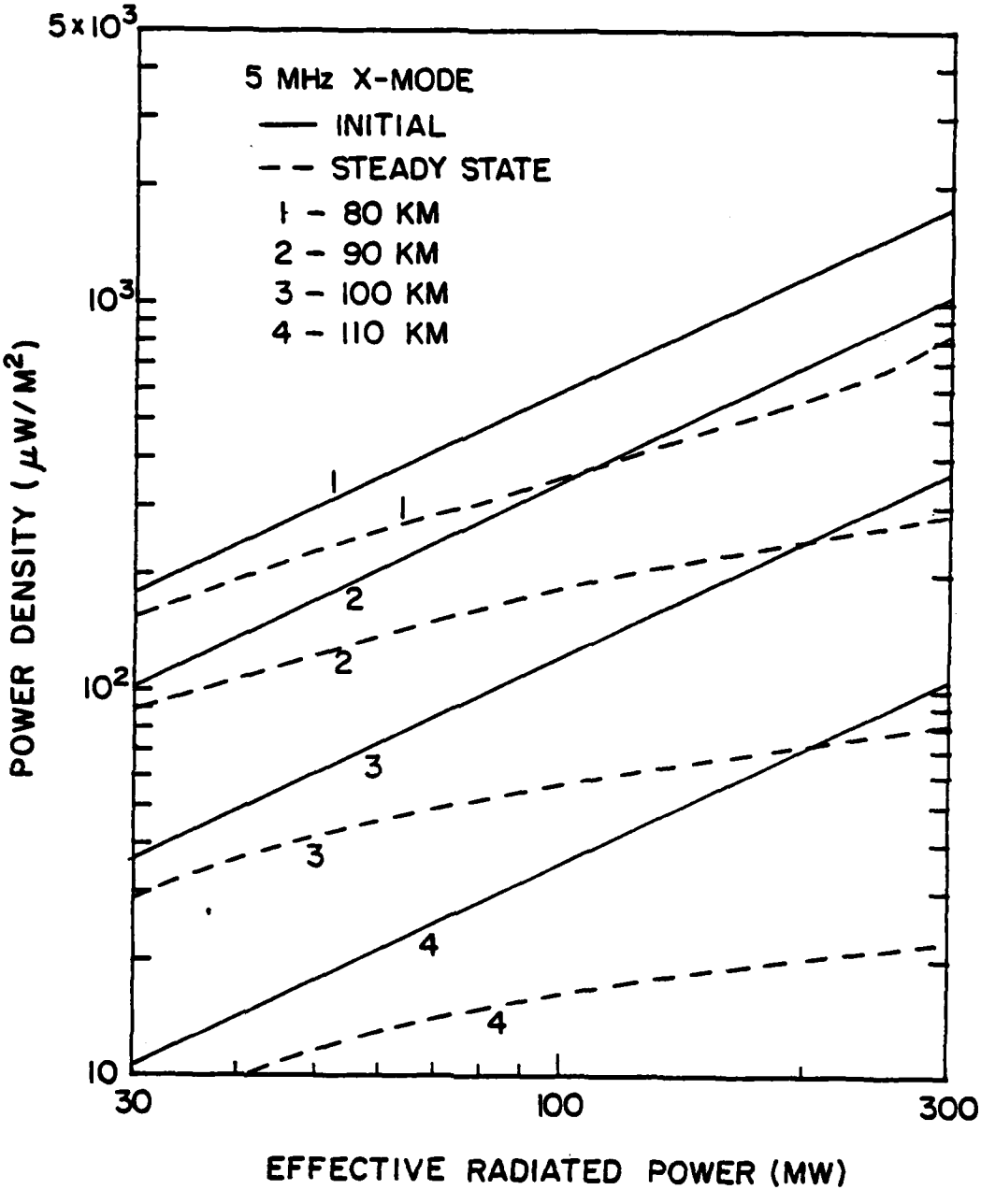

Figure 3.6 Power density as a function of effective radiated power for 5 MHz X-mode heating.

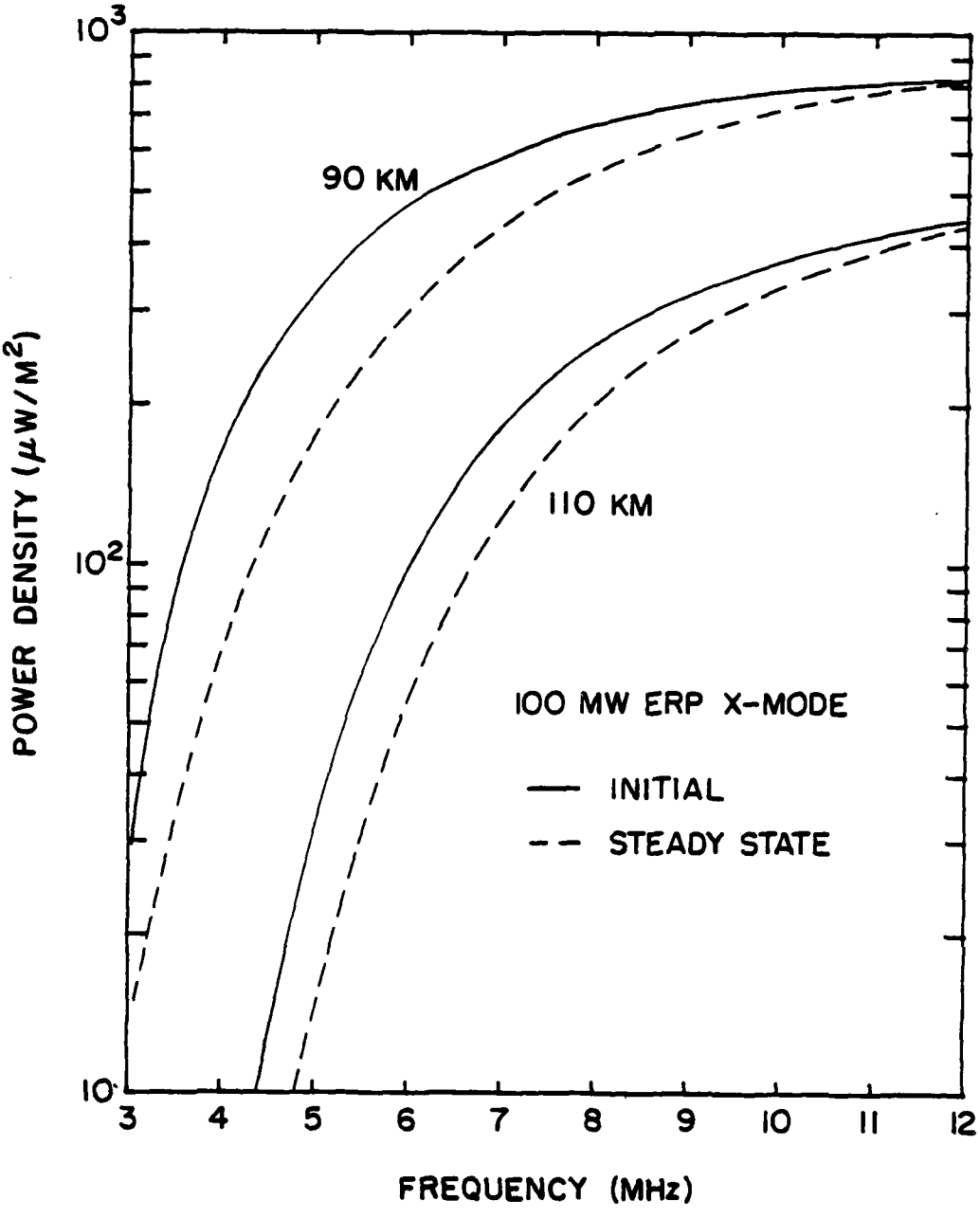

Figure 3.7 Power density as a function of heating frequency.

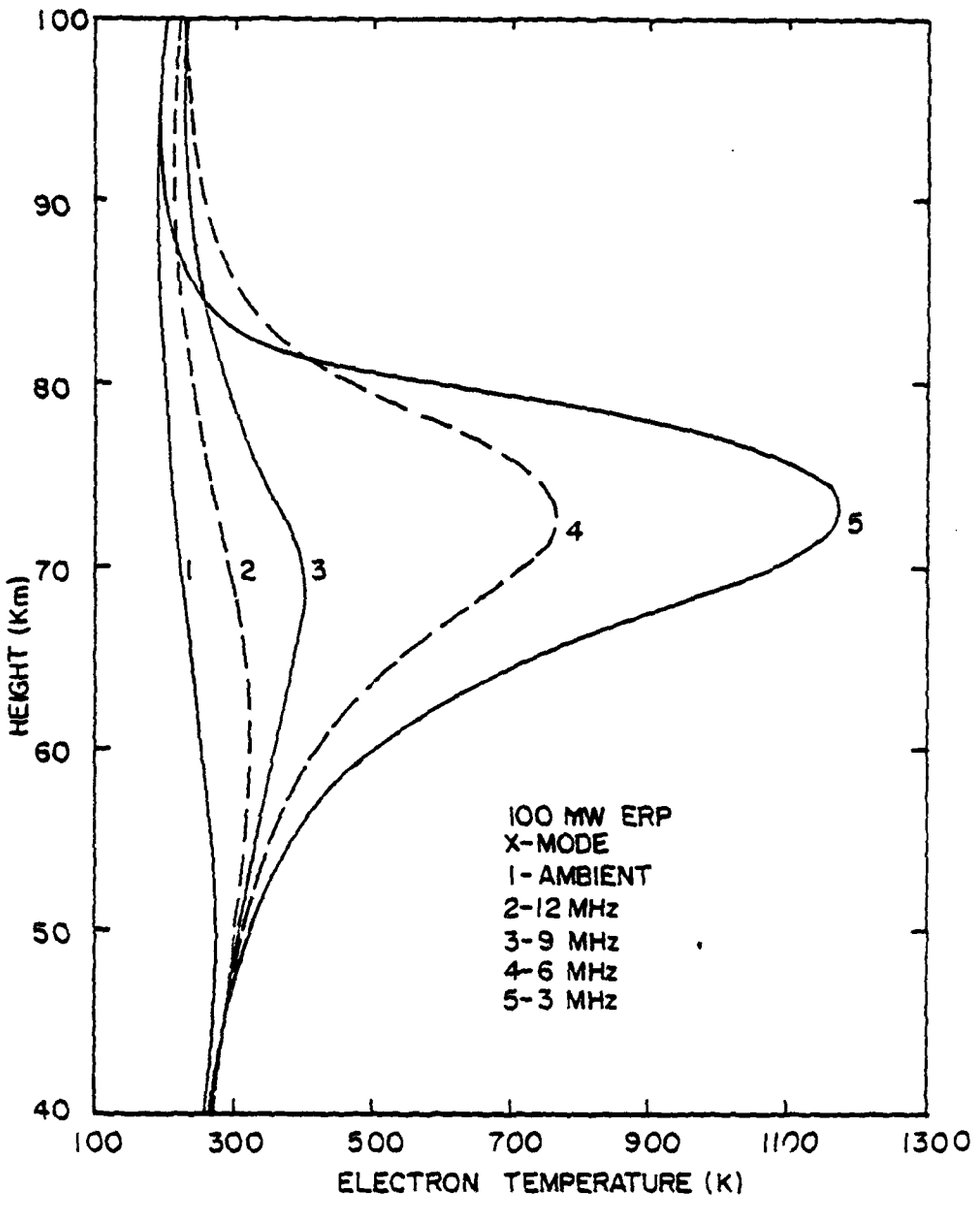

Figure 3.8 Electron temperature profiles for various heating frequencies.

shown in Figure 3.8, because the critical power density, S_c, required to produce large temperature enhancements increases with heating frequency, varying approximately as f^2 (Meltz et al., 1974).

The results presented above can be influenced by a number of factors. The effect of two of these factors, variations in electron density and uncertainties in the total electron energy loss rate, are considered in Figure 3.9. The ambient ($T_e = T_n$) temperature model and that for 100 MW ERP, 5 MHz X-mode are illustrated as curves (1) and (2), respectively. Curves (3) and (4) show the effect of a factor of two changes in the electron density at all heights on the electron temperature during heating. Increasing the total electron concentration (3) results in only a moderate decrease in T_e, primarily near the temperature maximum (73 km). On the other hand, decreasing n_e (4) causes a considerable enhancement in electron temperature in the upper D-region, which suggests that the upper ionosphere is heated more effectively as the solar zenith angle increases. Curves (5) and (6) illustrate the effect of a factor of 2 increase and decrease in the total electron energy loss rate, $\sum_s \frac{\partial}{\partial t} U_{e,s}$, on the electron temperature distribution. The electron temperature maximum varies roughly as the inverse of the total loss rate. This result could be anticipated from the analysis given in Section 3.3. From (3.25) one expects the steady state electron temperature, T_{eo}, for the strong field case to be given approximately by

$$T_{eo} = P_e(T_{eo})\ \tau_H(T_{eo}) \qquad (3.30)$$

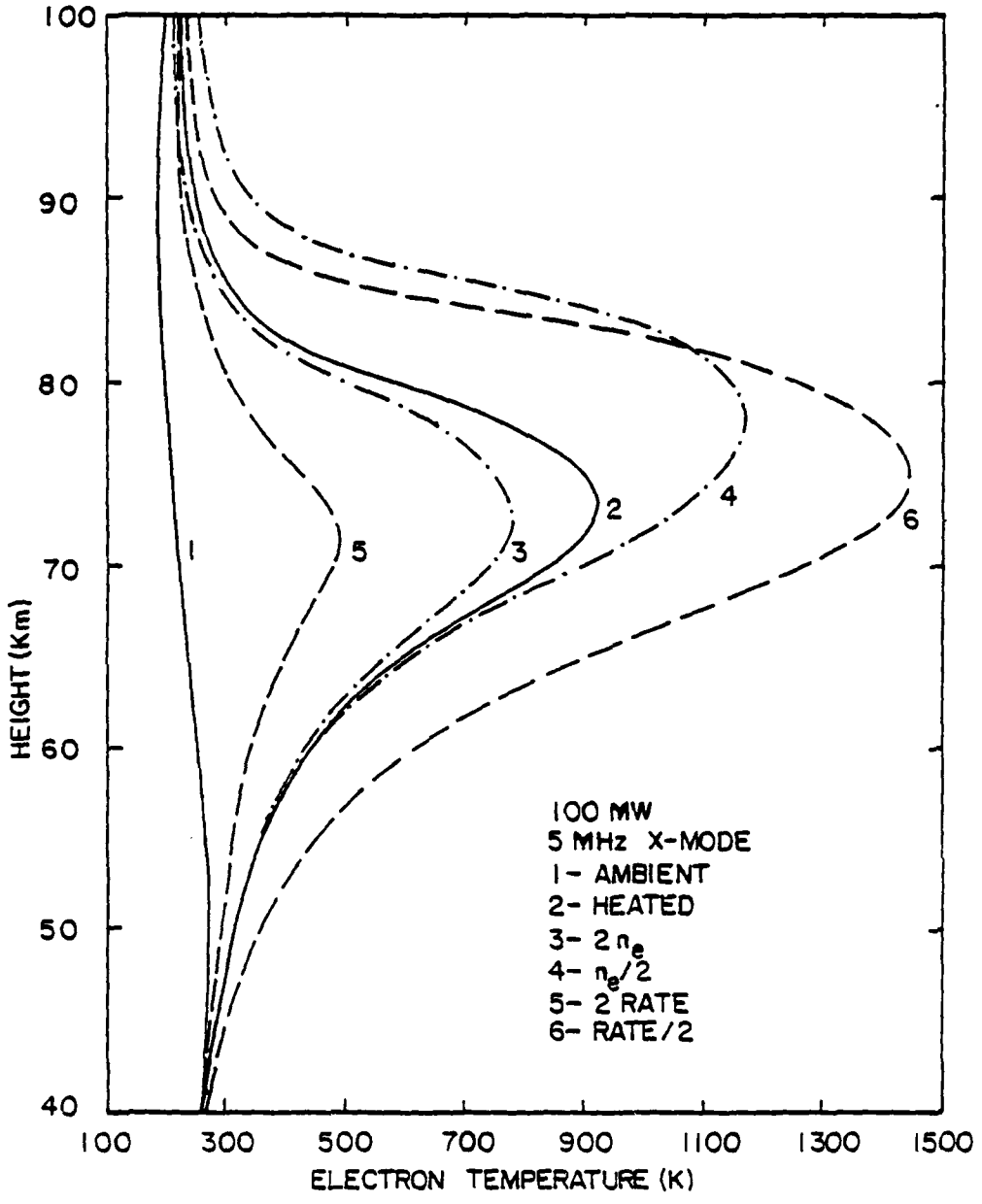

Figure 3.9 Effect of electron density and total loss rate on the electron temperature distribution.

where the analogous form of (3.24) is

$$\tau_H(T_{eo}) = \frac{3}{2} n_e K_B \delta T_{eo} / \sum_s \partial U_{es}/\partial t \qquad (3.31)$$

Thus, T_{eo} is inversely proportional to the total electron energy loss rate.

CHAPTER IV

ION CHEMISTRY MODIFICATIONS

4.1 Continuity Equations

In the previous chapter, it was shown that a substantial increase in electron energy can occur when the ionosphere is irradiated by high power electromagnetic waves. Since the chemical processes which determine the composition of the ionospheric plasma, and in particular, the electron density, are collisional in nature, they depend directly upon the energies of the colliding particles. An increase in electron energy due to heating by electromagnetic waves can therefore alter the reaction rates for chemical processes in which electrons participate and thus modify the composition of the plasma.

In Chapter III it was assumed that the time scale for HF heating induced electron density variations is much larger than that for the electron temperature so that one could write $\partial n_e/\partial t = 0$ in the electron energy balance equation. The objectives of this chapter are to ascertain the validity of this assumption and to explore the types of chemistry modifications that can result from HF heating.

The electron content of the ionospheric plasma is governed by the continuity equation (2.82) which can be written out explicitly in terms of the various electron production and loss processes as

$$\frac{\partial}{\partial t} n_e = Q_e + \sum_{i-} \gamma_{i-}\, n_{i-} - \beta_e\,(T_e)\, n_e - \sum_{j+} \alpha_{j+}\,(T_e)\, n_{j+}\, n_e \tag{4.1}$$

where Q_e - electron production rate per unit volume due to

ionization of neutral atmospheric constituents,

γ_i - rate of electron detachment from the i-th negative ion type,

$\beta_e(T_e)$ - rate of electron attachment to neutral constituents, and

$\alpha_{j+}(T_e)$ - rate coefficient for electron recombination with the j-th positive ion type.

The electron attachment rate and the electron-ion recombination coefficients depend directly on the electron temperature as emphasized in (4.1). Strictly speaking, the electron production rate may also depend on T_e due to electron impact ionization of neutral particles (Gurevich et al., 1977b), or Q_e may depend directly on the electric field strength of the heating wave, $\vec{E}$. The latter dependence results from the breakdown of the neutral gas in the presence of very strong electric fields (Lombardini, 1965). The effects of electron production enhancements due to the heating wave field shall be commented on later in this chapter. In the present discussion, it is assumed that Q_e is independent of T_e and $\vec{E}$ and is given by the sum of the production rates due to ionization of the neutral gas by solar photons and cosmic rays.

In the upper D and lower E regions, the predominant positive ions are NO^+ and O_2^+, there are very few negative ions, and electron attachment and detachment processes are relatively unimportant. From the plasma charge neutrality condition, $\rho = 0$, one has

$$n_e \simeq n_{NO^+} + n_{O_2^+} \tag{4.2}$$

In this region the electron continuity equation can be written in the simple form

$$\frac{\partial}{\partial t} n_e = Q_e - \alpha_{eff}(T_e)\, n_e^2 \qquad (4.3)$$

where $\alpha_{eff}(T_e)$ is the effective electron-ion recombination coefficient defined by

$$\alpha_{eff}(T_e) = \sum_{j+} \alpha_{j+}(T_e)\, n_{j+} / \sum_{i+} n_{i+} \qquad (4.4)$$

Holway and Meltz (1973) have employed an analytic model of this form to calculate the electron density variation due to various levels of heating. They have found that the electron density increases from its unheated value on a time scale of minutes to a level which is inversely proportional to the square root of the recombination coefficient.

While simple models of plasma density modification based strictly upon heating induced changed in the recombination rate may be adequate in the upper D and lower E regions, the complex nature of the ion chemistry governing the plasma composition in the lower D-region requires a more detailed analysis. Below 85 km the identity of the predominant positive ions switches from NO^+ and O_2^+ to water cluster ions of the forms $H^+ \cdot (H_2O)_n$ and $NO^+ \cdot (H_2O)_m$ which are formed through a complicated sequence of reactions (e.g. Rowe et al., 1974). Electron recombination with these heavier ions will also be influenced by HF heating. Moreover, below 75 km negative ions become a significant portion of the total ion density due to the attachment of electrons to neutral constituents, primarily through the three body reaction $e + O_2 + M \rightarrow O_2^- + M$. The

rate for this reaction, β, should increase with electron temperature up to about 700°K for ambient neutral temperatures of 200-300°K then slowly decrease (Chanin et al., 1962). Thus, HF heating of the lower D-region could decrease the electron density due to increased three body attachment. However, this process must compete with any electron increase due to decreased recombination.

Equation (4.1) is inadequate for describing the chemically rich lower ionosphere since some of the electron production and loss terms depend on the ion densities which are unknown. One must therefore develop a set of continuity equations for the ionic components of the plasma. The ion continuity equations can be derived directly from Boltzmann's equation (2.20) by integrating over $d\vec{v}_s$ (e.g. Holt and Haskell, 1965). Neglecting transport effects, one finds that the i-th type of positive ion is described by a continuity equation of the form

$$\frac{\partial}{\partial t} n_{i+} = Q_{i+} + \sum_{j+} (R_{i+,j+} n_{j+} - R_{j+,i+} n_{i+}) \qquad (4.5)$$

$$- (\alpha_{i+}(T_e) n_e + \sum_{j-} \alpha_{i+,j-} n_{j-}) n_{i+}$$

while the i-th type of negative ion is governed by a continuity equation of the form

$$\frac{\partial}{\partial t} n_{i-} = \beta_{i-}(T_e) n_e + \sum_{j-} (R_{i-,j-} n_{j-} - R_{j-,i-} n_{i-}) \qquad (4.6)$$

$$- (\gamma_{i-} + \sum_{j+} \alpha_{j+,i-} n_{j+}) n_{i-}$$

where

Q_{i+} - production rate per unit volume of the i-th positive ion type resulting from the ionization of neutral atmospheric constituents by solar radiation and cosmic rays,

$R_{i\pm,j\pm}$ - rate at which the i-th positive/negative ion type is created from the j-th positive/negative ion type through charge transfer and atom-ion interchange with neutral constituents,

$\alpha_{i+,j-}$ - ion-ion recombination rate coefficient for the i-th positive ion type and j-th negative ion type, and

β_{i-} - rate at which the i-th negative ion type is formed by the attachment of electrons to neutral constituents.

The system of equations (4.1), (4.5-6) are not independent, but are related by the plasma neutrality condition

$$n_e = \sum_{j+} n_{j+} - \sum_{i-} n_{i-} \tag{4.7}$$

Equations (4.5-7) specify the composition of the plasma provided one knows the electron temperature distribution. As shown in Chapters II and III, the electron temperature distribution depends on the heating wave field strength, which in turn depends on the electron temperature and electron density through the index of refraction of the plasma. Therefore, a complete description of heating wave induced plasma modification requires a simultaneous solution of the system of equations (4.5-7), the

electron energy balance equation, and the heating wave power density equation (see Chapter III). A simultaneous solution of this set of equations is complicated by the fact that the lower ionosphere contains a large number of different types of ions and many of the reaction rates leading to the formation and destruction of these ions are not known. Accordingly, the following section describes a simplified ion chemistry scheme which avoids some of the complexity and uncertainty inherent in detailed models of the lower ionosphere.

4.2 The Mitra-Rowe Ion Chemistry Model

The ion chemistry model adopted in this work is the simple six ion scheme proposed by Mitra and Rowe (1972). This model has been shown to satisfactorily reproduce the major features of the lower ionosphere during quiet and disturbed conditions while eliminating many of the complex and often hypothetical steps in the complete ion chemistry reaction sequence (Mitra, 1975a, b; Rowe et al., 1974). The reaction chain for the six ion model is outlined in Figure 4.1 and specific reactions included in the model are listed in Table 4.1.

The primary ions formed by the ionization of neutral atmospheric constituents are N_2^+, O_2^+ and NO^+. The ions N_2^+ and O_2^+ are formed by two different mechanisms: photoionization of the neutral gas by solar X-rays and extreme ultraviolet radiation, and collisional ionization of N_2 and O_2 by high energy cosmic particles (i.e. cosmic rays). Nitric oxide is a minor neutral constituent (i.e. $n_{NO} << n_{O_2}$ or n_{N_2}) but is very effectively ionized by the solar Lyman α line at 1215.7 A, forming NO^+.

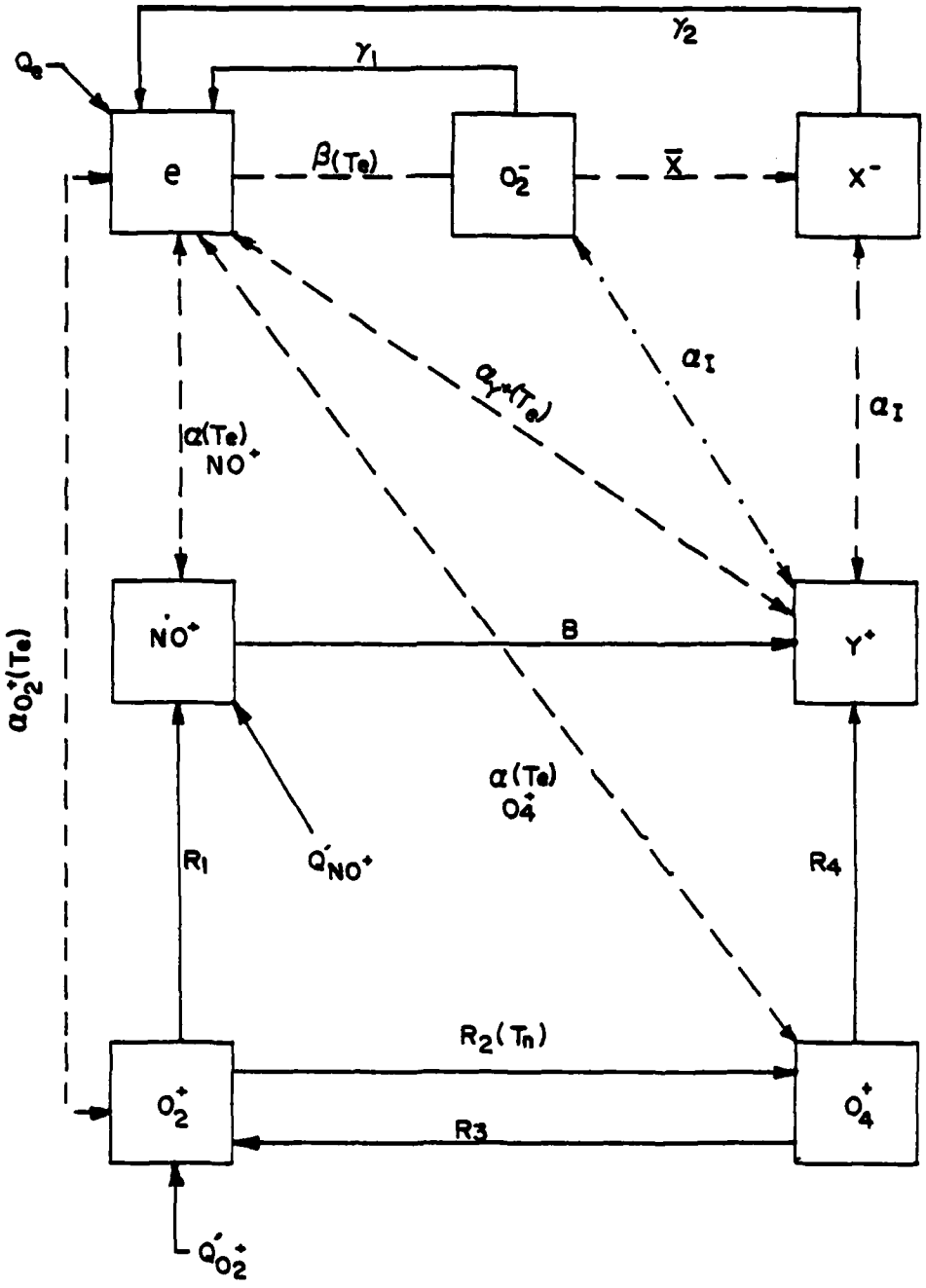

Figure 4.1 The Mitra-Rowe six ion model (all ion-ion lines not shown).

Table 4.1 Reactions included in the six ion scheme

1. $N_2^+ + O_2 \rightarrow O_2^+ + N_2$; $K_1 = 5.0 \times 10^{-11}$ cm^3/s
2. $N_2^+ + O \rightarrow NO^+ + N$; $K_2 = 1.4 \times 10^{-10}$ cm^3/s
3. $O_2^+ + NO \rightarrow NO^+ + O_2$; $K_3 = 4.4 \times 10^{-10}$ cm^3/s
4. $O_2^+ + N_2 \rightarrow NO^+ + NO$; $K_4 = 10^{-16}$ cm^3/s
5. $O_2^+ + O_2 + O_2 \rightarrow O_4^+ + O_2$; $K_5 = 2.8 \times 10^{-30}(300^oK/T_n)cm^3/s$
6. $O_4^+ + O \rightarrow O_2^+ + O_3$; $K_6 = 3 \times 10^{-10}$ cm^3/s
7. $O_4^+ + H_2O \rightarrow O_2 + O_2^+ \cdot H_2O$; $K_7 = 1.5 \times 10^{-9}$ cm^3/s
8. $O_2^- + O \rightarrow O_3 + e$; $K_8 = 3 \times 10^{-10}$ cm^3/s
9. $O_2^- + O_2\ (^1\Delta g) \rightarrow 2\ O_2 + e$; $K_9 = 2 \times 10^{-10}$ cm^3/s
10. $h\nu + O_2^- \rightarrow O_2 + e$; $\gamma_p = 0.3\ s^{-1}$

The rate of production of the i-th ion type per unit volume at height h due to the photoionization of the i-th type of neutral constituent by all solar radiations is given by (e.g. Rishbeth and Carriott, 1969; Banks and Kockarts, 1973)

$$Q_{i+}^{PH}(h) = \int_{\lambda'} \sigma_i^I(\lambda')\, n_i(h)\, \Phi(h, \lambda')\, d\lambda' \qquad (4.8)$$

where

$\sigma_i^I(\lambda')$ - the ionization cross section at wavelength λ' for the i-th neutral constituent, and

$\Phi(h, \lambda')$ - the solar radiation flux of wavelength λ' a height h.

For ionizing collisions of the i-th neutral particle type with high energy particles (i.e. > 100 KeV) the corresponding production rate is given by (Velinov, 1968)

$$Q_{i+}^{CR}(h) = \frac{2\pi}{u_1} \int_{u_j}^{\infty} \left(\frac{du}{dh}\right)_{ij} f_j(u)\, du \qquad (4.9)$$

where

u_1 - the energy required for the formation of one electron/ion pair ($\approx$ 35 eV)

u_j - the geomagnetic cutoff energy for energetic particles of type j,

$\left(\frac{du}{dh}\right)_{ij}$ - the energy loss per unit height by the j-th type of energetic particle due to collisions with neutral particles of type i, and

$f_j(u)$ - the energy spectrum of the j-th type of energetic particle at the top of the earth's atmosphere.

The production rates for N_2^+, O_2^+ and NO^+ used in this work have been calculated from the above formulae using a computer code developed by Rowe (1972). Typical daytime values of $Q_{N_2^+}$, $Q_{O_2^+}$ and Q_{NO^+} are given in Figure 4.2.

Since N_2^+ is rapidly converted to O_2^+ or NO^+ by reactions (1) and (2) of Table 4.1, only O_2^+ and NO^+ are explicitly included in the chemistry model. The effective production rates for these ions are denoted $Q'_{O_2^+}$ and Q'_{NO^+}, respectively, and are defined by

$$Q'_{O_2^+} = Q_{O_2^+} + \frac{1}{1 + A} Q_{N_2^+} \tag{4.10}$$

and

$$Q'_{NO^+} = Q_{NO^+} + \frac{A}{1 + A} Q_{N_2^+} \tag{4.11}$$

where

$$A = K_2[O]/K_1[O_2]$$

The brackets denote the number density of the indicated constituent (e.g. $[O_2] = n_{O_2}$).

In addition to the primary ions O_2^+ and NO^+, the positive ion scheme includes the intermediate ion O_4^+ and a hydrated ion group Y^+, which includes $H^+(H_2O)_n$ and $NO^+(H_2O)_m$. The primary negative ion formed by electron attachment is O_2^-. All other negative ions are assumed to be formed by reactions with O_2^- and are lumped into the group X^-.

The rates for conversion of one positive ion type into another as indicated in Figure 4.1 are

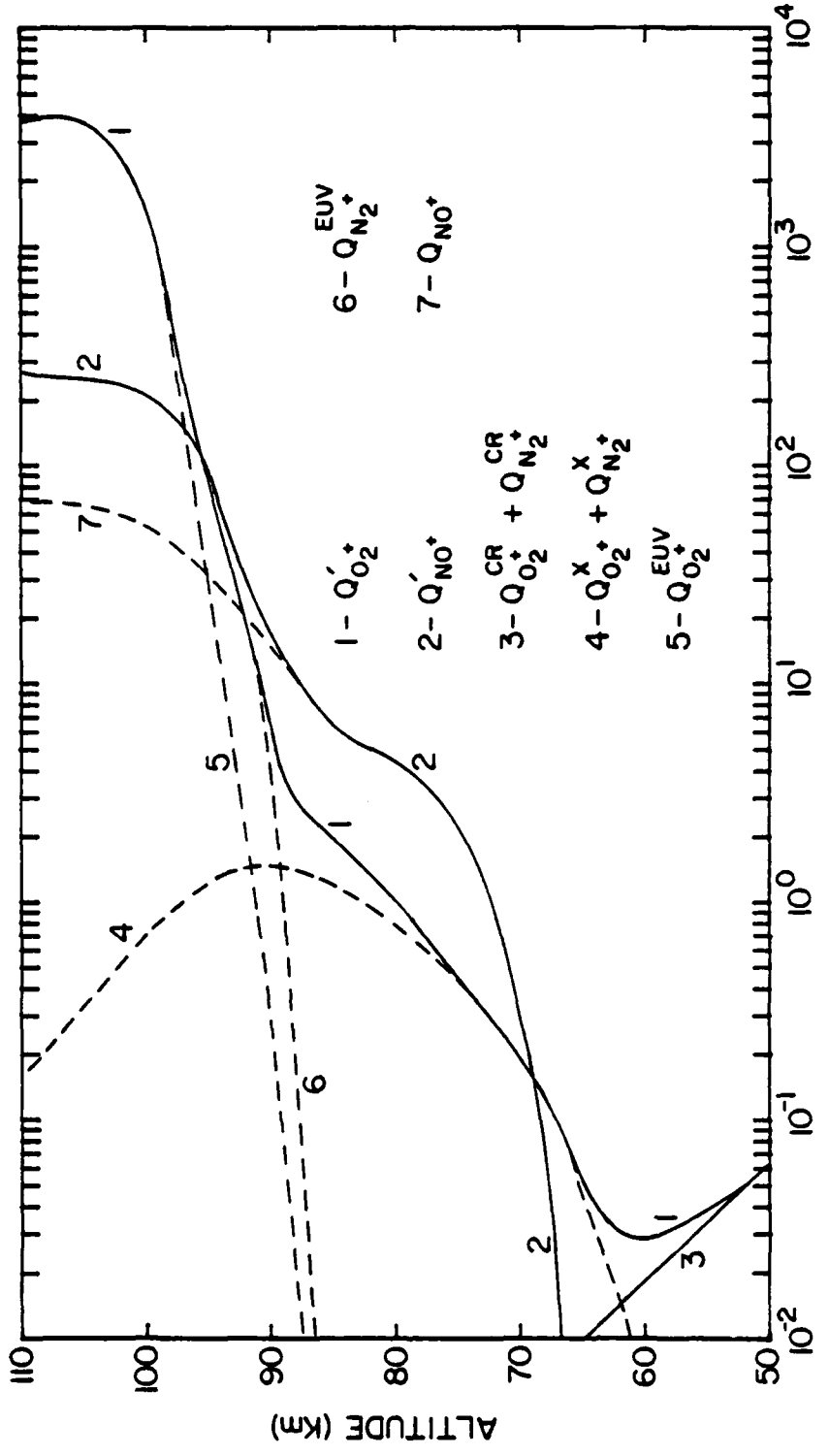

Figure 4.2 Ion production rates as a function of height.

$$R_1 = K_3 [O] + K_4 [N_2] \tag{4.12}$$

$$R_2 = K_5 [O_2]^2 \tag{4.13}$$

$$R_3 = K_6 [O] \tag{4.14}$$

and

$$R_4 = K_7 [H_2O]. \tag{4.15}$$

The bulk rate for conversion of NO^+ into $H^+(H_2O)_n$, B, has been estimated from positive ion composition measurements and is given approximately by

$$B = 10^{-31} [air]^2 \text{ in } s^{-1} \tag{4.16}$$

(Rowe et al., 1974). Other parameters included in the model are the electron detachment rate from O_2^-,

$$\gamma_1 = \gamma_p + K_8 [O] + K_9 [O_2(^1\Delta g)], \tag{4.17}$$

the bulk rate for conversion of O_2^- into X^-,

$$\overline{X} = 10^{-30} [O_2] [air] + 3 \times 10^{-10} [O_3] \text{ in } s^{-1} \tag{4.18}$$

(Mitra, 1975b). The ion-ion recombination coefficients are assumed to be the same for all ions $\alpha_I = 10^{-7}$ cm^3/s.

One addition parameter employed in the model is the bulk detachment rate from X^-, γ_2. Rowe et al. (1974) have shown that γ_2 plays a key role in determining the size of the electron density and negative ion to electron ratio, λ, below 70 km. Estimates of γ_2 at 60 km based upon electron and total positive ion density measurements range from $0.1s^{-1}$ to $4s^{-1}$. The effect of γ_2 on n_e and λ is illustrated in

AD-A103 538 PENNSYLVANIA STATE UNIV UNIVERSITY PARK IONOSPHERE R--ETC F/G 20/14
NONLINEAR PHENOMENA ARISING FROM RADIO WAVE HEATING OF THE LOWE--ETC(U)
AUG 81 A A TOMKO N00014-81-K-0276
UNCLASSIFIED PSY-TRL-SCI-470 NL

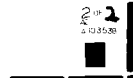

END
DATE FILMED
10-81
DTIC

Figure 4.3. The solid curves represent the ambient profiles which will be adopted in subsequent calculations. The corresponding values of γ_2 are given in Table 4.2. The dashed curves in Figure 4.3 are for fixed γ_2 as indicated.

Electron attachment in the lower ionosphere is believed to take place primarily through the three body reaction $e + O_2 + O_2 \rightarrow O_2^- + O_2$. A large number of experimental studies of this reaction have been performed, and it is perhaps the best documented of all negative ion reactions (Caledonia, 1975). For unheated conditions, $T_e \simeq T_n$, the attachment coefficient for this reaction is given by (Truby, 1972)

$$K_a\ (T_n) = 4 \times 10^{-30}\ e^{-196/T_n}\ cm^6/s;\ 100 < T_n < 600^oK \qquad (4.19)$$

Measurements of the electron energy dependence of the three body process for fixed values of T_n (Chanin et al., 1962; Pack and Phelps, 1965) have shown that K_a increases rapidly for $\langle u \rangle > 3K_B\ T_n/2$, reaching a peak at an average electron energy of $\langle u \rangle = 0.09$ eV and then decreasing slowly at higher energies. The 0.09 eV peak corresponds to the fourth vibrational level of O_2^-. High resolution electron beam measurements by Spence and Schulz (1972) have shown that K_a has secondary maxima at energies corresponding to the higher vibrational levels of O_2^-.

The above mentioned experimental data has been used to construct a numerical formula for the simultaneous T_e and T_n dependence of K_a (see Appendix A). The electron temperature variation of K_a computed from this formula is compared with the experimental data in Figure 4.4, and is in good agreement. The electron attachment rate employed in the

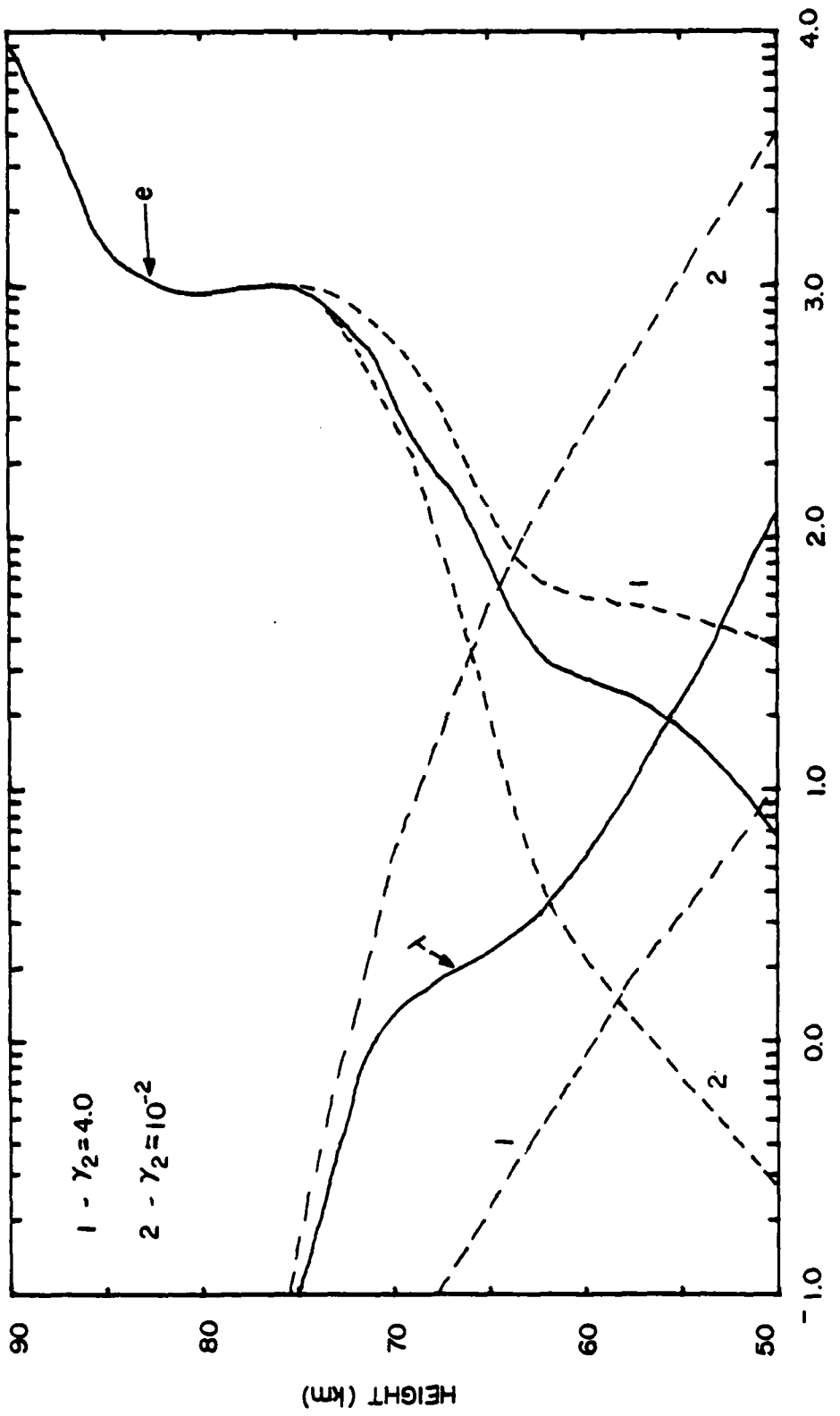

Figure 4.3 Effect of γ_2 on the electron density and the negative ion to electron ratio, λ.

Table 4.2 Typical values of key chemistry parameters

h(km)	X	γ_1	γ_2	β	a	ξ	b
50	130	4	0.3	40	134	30	0.3
60	14	5	0.5	3	19	1.9	0.5
70	1	5	0.02	0.2	6	0.03	0.02
80	0.1	13	0.02	0.01	13	8×10^{-5}	0.02

(Note: All values are in units of s^{-1}.)

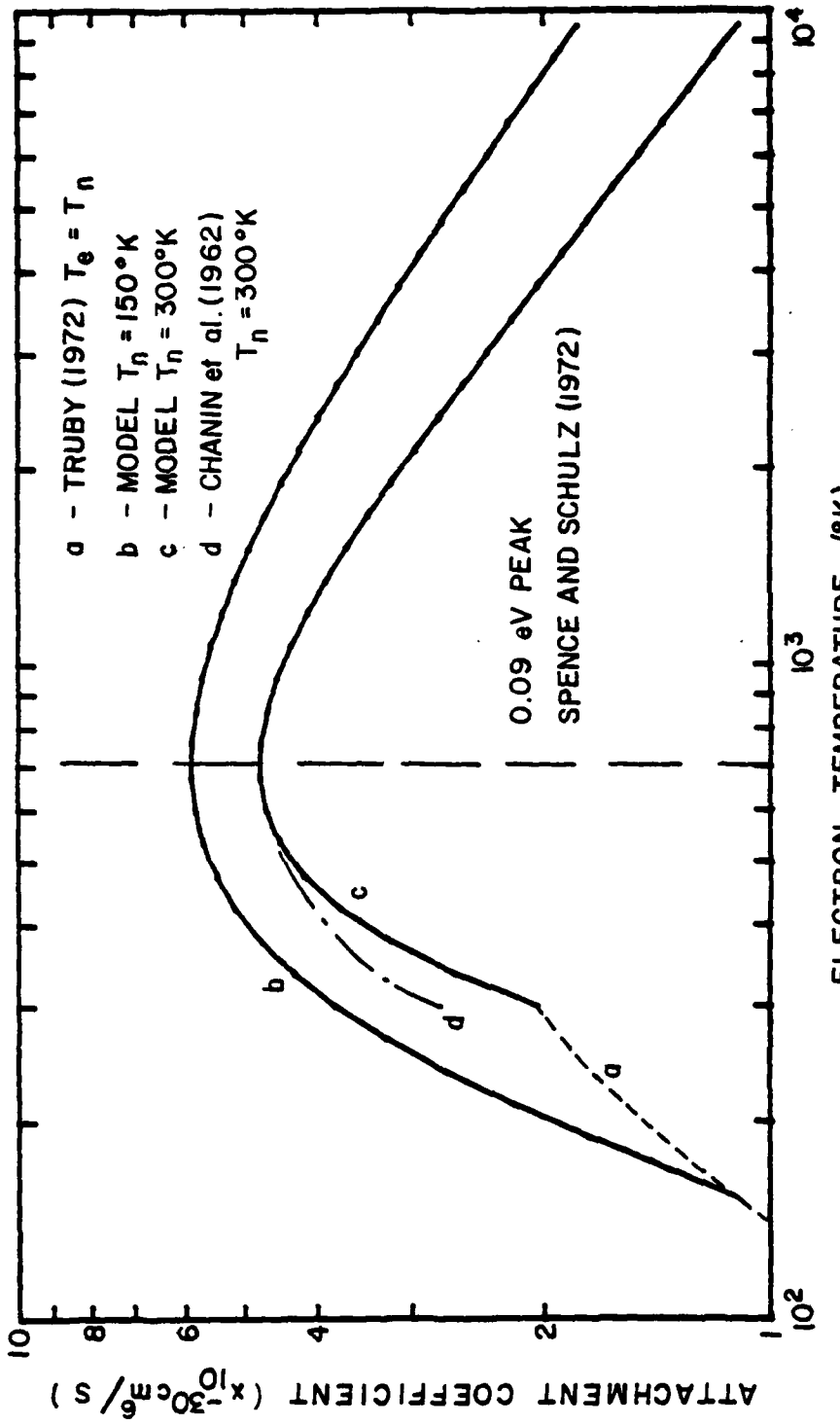

Figure 4.4 Electron attachment coefficient as a function of electron temperature.

Mitra-Rowe chemistry scheme is given by

$$\beta(T_e, T_n) = K_a(T_e, T_n) [O_2]^2 \qquad (4.20)$$

Reviews of the available experimental data on atmospheric electron-ion recombination processes have been given by Biondi (1969, 1975). In the lower ionosphere electron-ion pairs are removed by the highly efficient dissociative recombination process. Estimates of the dissociative recombination coefficients for O_2^+ and NO^+ are

$$\alpha_{O_2^+}(T_e) = {}_{O_2^+}(T_n) \, (T_e/T_n)^{-0.6} \qquad (4.21)$$

where

$$\alpha_{O_2^+}(T_n) = 2.1 \times 10^{-7} \, (T_n/300^oK)^{-0.7} \; cm^3 s^{-1} \qquad (4.22)$$

and

$$\alpha_{NO^+}(T_e) = \alpha_{NO^+}(T_n) \, (T_e/T_n)^{-0.5} \qquad (4.23)$$

where

$$\alpha_{NO^+}(T_n) = 4.1 \times 10^{-7} \, (T_n/300^oK)^{-1.0} \; cm^3 s^{-1}; \; 200 \leq T_n \leq 300^oK \qquad (4.24)$$

More recent measurements of dissociative recombination cross sections for O_2^+ and NO^+ by Mul and McGowan (1979) suggest that both $\alpha_{O_2^+}$ and α_{NO^+} vary as $T_e^{-0.5}$.

The dissociative recombination coefficient for O_4^+ is approximately $\alpha_{O_4^+} = 2.3 \times 10^{-6} \; cm^3 s^{-1}$ at $T_e = T_n = 205^oK$ and is assumed to vary as $T_e^{-1.0}$.

The effective recombination coefficient for the water cluster ion group, Y^+, is given approximately by

$$\alpha_{Y^+}(T_e) = \sum_n \alpha_n(T_n) \frac{[H^+ \cdot (H_2O)_n]}{[Y^+]} \frac{T_e}{T_n}^{-b} \qquad (4.25)$$

where $\alpha_n(T_n)$ denotes the recombination coefficient for the hydrate $H^+ \cdot (H_2O)_n$ as given by Leu et al. (1973), with a neutral temperature dependence of $T_n^{-0.2}$. The electron temperature dependence of the effective recombination coefficient is uncertain, but typical estimates are $0 < b < 1$. Recent measurements by Huang et al. (1978) favor a small value of $b = 0.08$. The relative concentration of the individual hydrated ions $[H^+ \cdot (H_2O)_n]/[Y^+]$ may be calculated from the equilibrium rate constants for the reactions $H_2O + H^+ \cdot (H_2O)_{n-1} \rightleftarrows H^+ \cdot (H_2O)_n$ as given by Kebarle et al. (1967).

The reaction rates used in the Mitra-Rowe chemistry scheme vary as a function of altitude due to their dependence on the neutral particle densities. The neutral atmospheric model adopted in this work is illustrated in Figure 4.5. The densities of the major neutral constituents N_2 and O_2 are taken from CIRA (1972), while the concentrations of the minor constituents O, H_2O, $O_2(^1\Delta g)$, O_3 and NO are based upon the recent review of experimental data by Thomas (1980) and a summary figure given by Mitra (1979). The altitude variation of the reaction rates used in the Mitra-Rowe scheme based on this neutral model are presented in Figure 4.6.

4.3 Steady State Results

The system of continuity equations (4.5-7) corresponding to the chemical model of Figure 4.1 have been solved under steady state

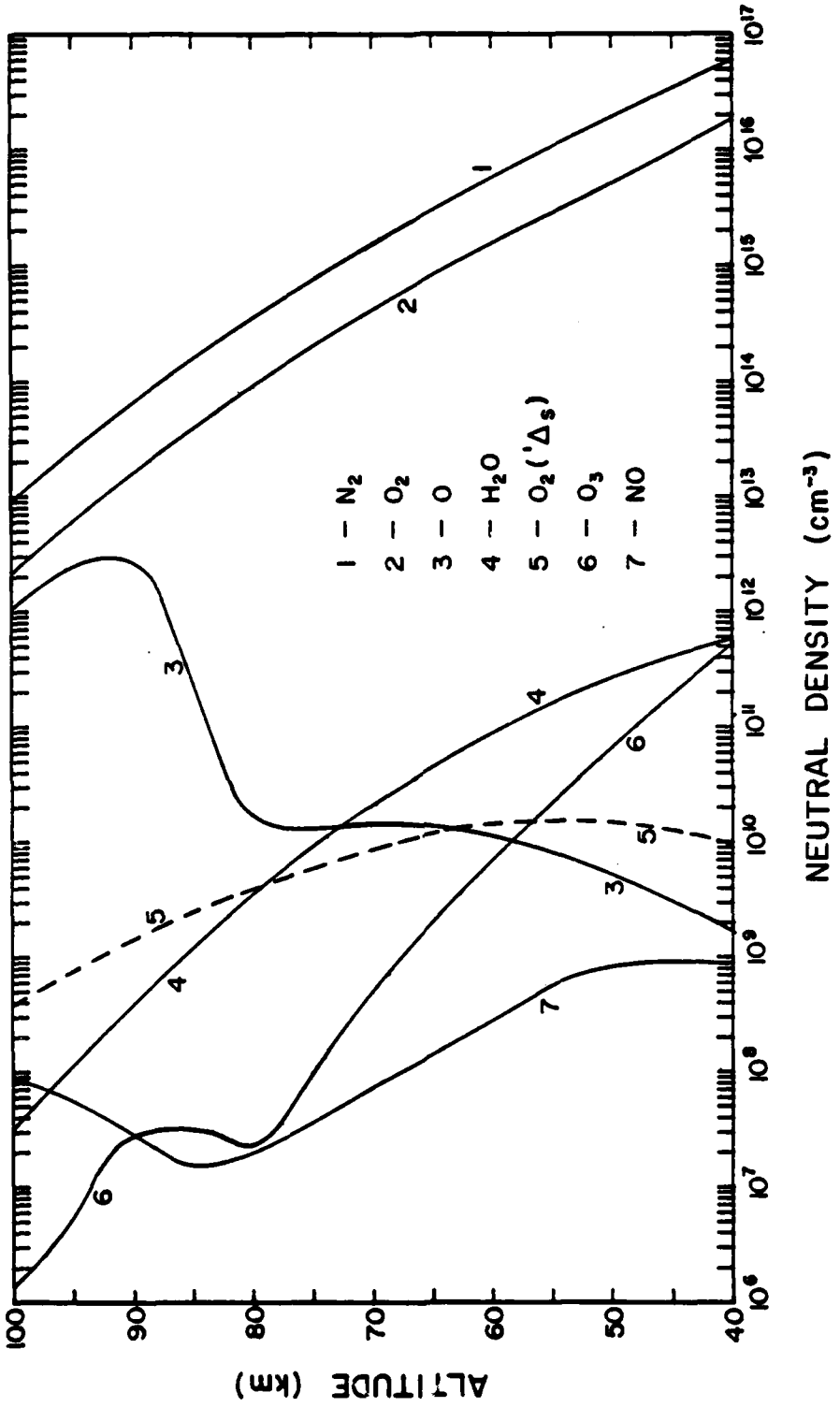

Figure 4.5 Neutral atmospheric model.

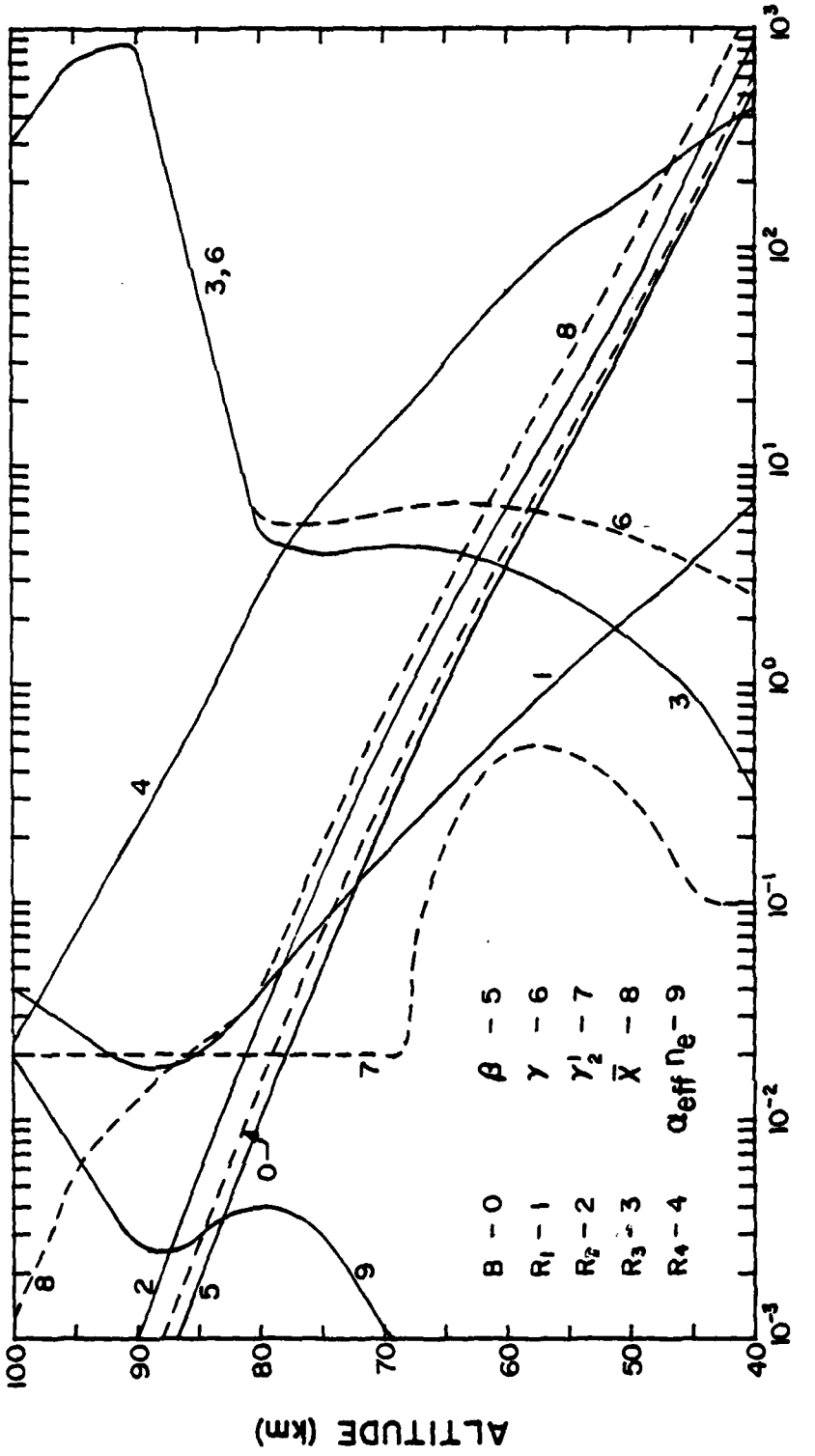

Figure 4.6 Altitude variation of the reaction rates employed in the Mitra-Rowe model.

conditions (i.e. $\partial n_{\pm}/\partial t = 0$) for fixed values of T_e using the method of false positions as in the work of Rowe (1972). Figure 4.7 shows the steady state ion and electron density distributions predicted by the Mitra-Rowe scheme for the daytime ionosphere under unheated conditions (i.e. $T_e = T_n$). Above 85 km the density of water cluster ions is small and equation (4.2) is satisfied while below 85 km, Y^+ becomes the dominant positive ion. In the lower D-region, negative ions become important and one has $[e] << [Y^+] \simeq [X^-]$.

Figure 4.8 shows the variation of the steady state electron density with electron temperature for the daytime ionosphere. Both n_e and T_e have been normalized to their respective unheated values. Two different models of the electron temperature dependence of α_{Y+} have been used: b = 0.2 (solid curves) and b = 0.5 (dashed curves). All other T_e dependent rates are as given previously.

At 50 km the change in n_e with T_e is controlled by β with n_e reaching a minimum at $T_e/T_n = 2.5$ which corresponds to the maximum value of β. In the 60 to 70 km region, if one assumes a slow variation of α_{Y+} with T_e (b = 0.2) then n_e is again largely controlled by β. However, if α_{Y+} varies more rapidly with T_e (b = 0.5), then the decrease in n_e due to increasing β is offset by the increase in n_e with decreasing α_{Y+}, so that n_e begins to increase before the maximum value of β is reached. At 80 km α_{Y+} governs the variation of n_e with T_e, and n_e increases more rapidly with T_e as b is increased. Above 80 km, the identity of the dominant positive ion type switches from Y^+ to NO^+, hence the n_e variation with T_e is controlled by α_{NO^+} which is assumed

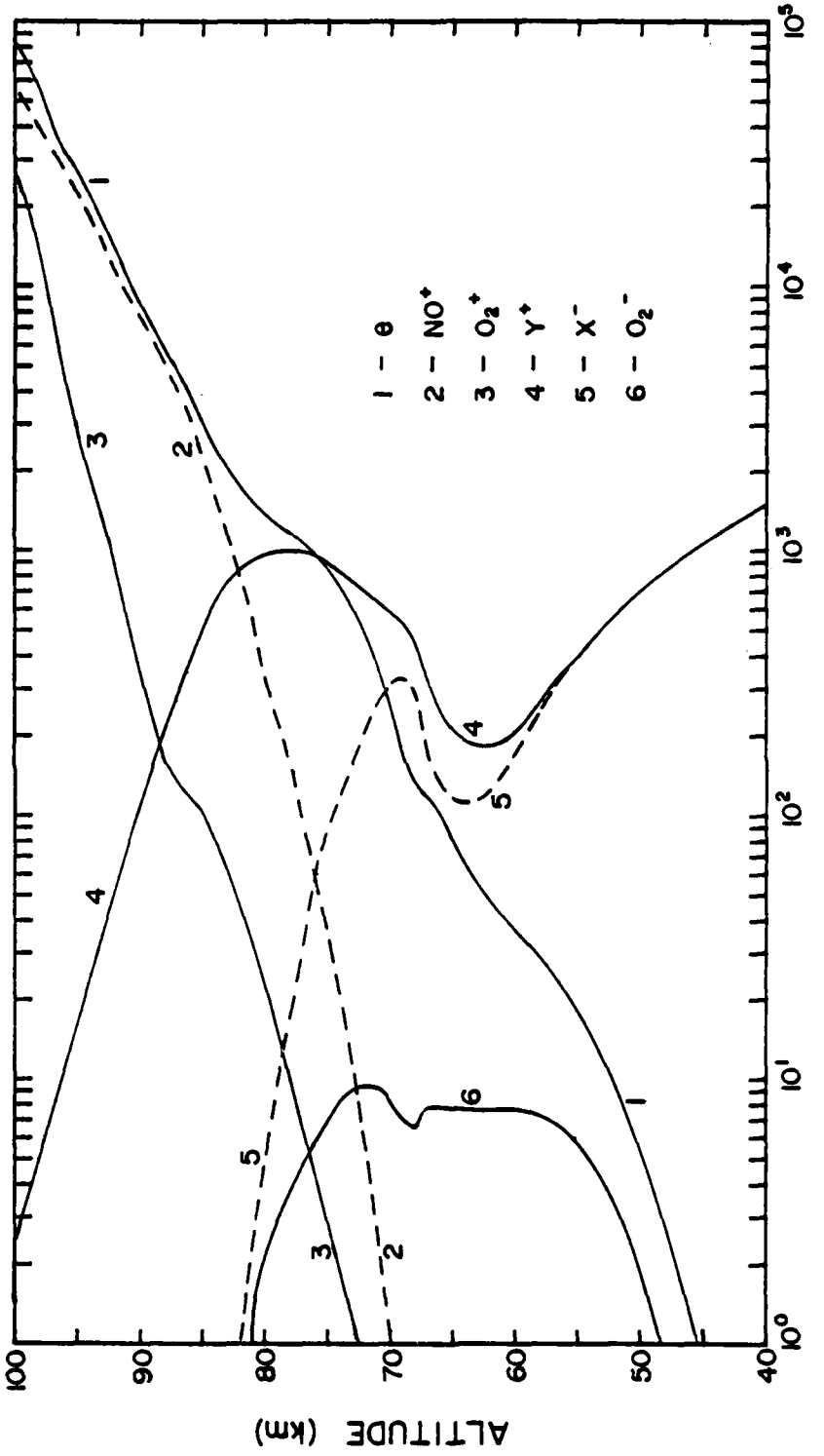

Figure 4.7 Steady state ion and electron density distributions for unheated conditions.

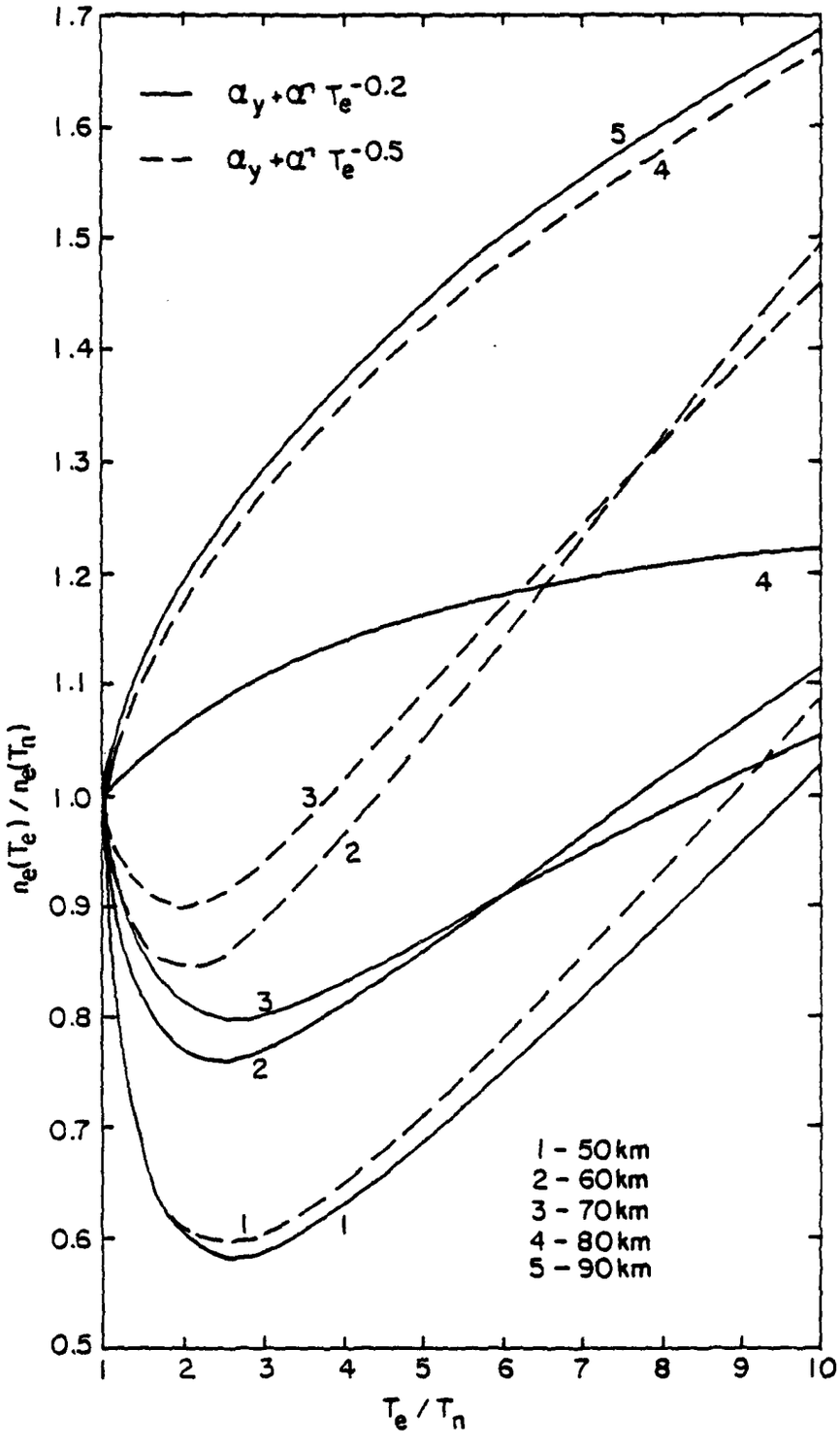

Figure 4.8 Steady state electron density as a function of electron temperature (normalized to ambient).

to vary as $T_e^{-0.5}$. Variations in $\alpha_{O_2^+}$ effect n_e primarily in the E-region during normal daytime conditions, but can have a significant effect on n_e at D-region heights during disturbed conditions (Mitra, 1975b). Heating induced changed in $\alpha_{O_4^+}$ have no significant effect on n_e since the density of O_4^+ is relatively small.

4.4 Time Dependent Solutions

The continuity equations for the six ion model have been solved silutaneously along with the equations for electron energy and power flow using basic numerical integration techniques (e. g. Ralston and Wift, 1960). Figures 4.9 through 4.13 illustrate the resultant time variation of key ionospheric parameters due to a period of 10^3 seconds of CW heating and during the subsequent return of the plasma to unheated conditions following termination of heating. The results presented here are for heating at 5 MHz, X-mode with an effective radiated power of 100 MW. The electron cooling rates, $\frac{\partial}{\partial t} U_{e,j}$, and electron neutral collision frequency used in these calculations were taken from Banks and Kockarts (1973). The calculations include rotational, vibrational and fine structure cooling as well as elastic processes. The ambient ionosphere used in these calculations is that given in Figure 4.7. The value b = 0.5 has been assumed for the electron temperature dependence of α_Y^+. The parameters presented in Figures 4.9 through 4.12 have been normalized to their respective ambient (unheated) values which are denoted by a zero subscript.

Prior to the initiation of CW heating, the ionosphere is assumed to be in a steady state with $T_e = T_n$. Once the heating transmitter is

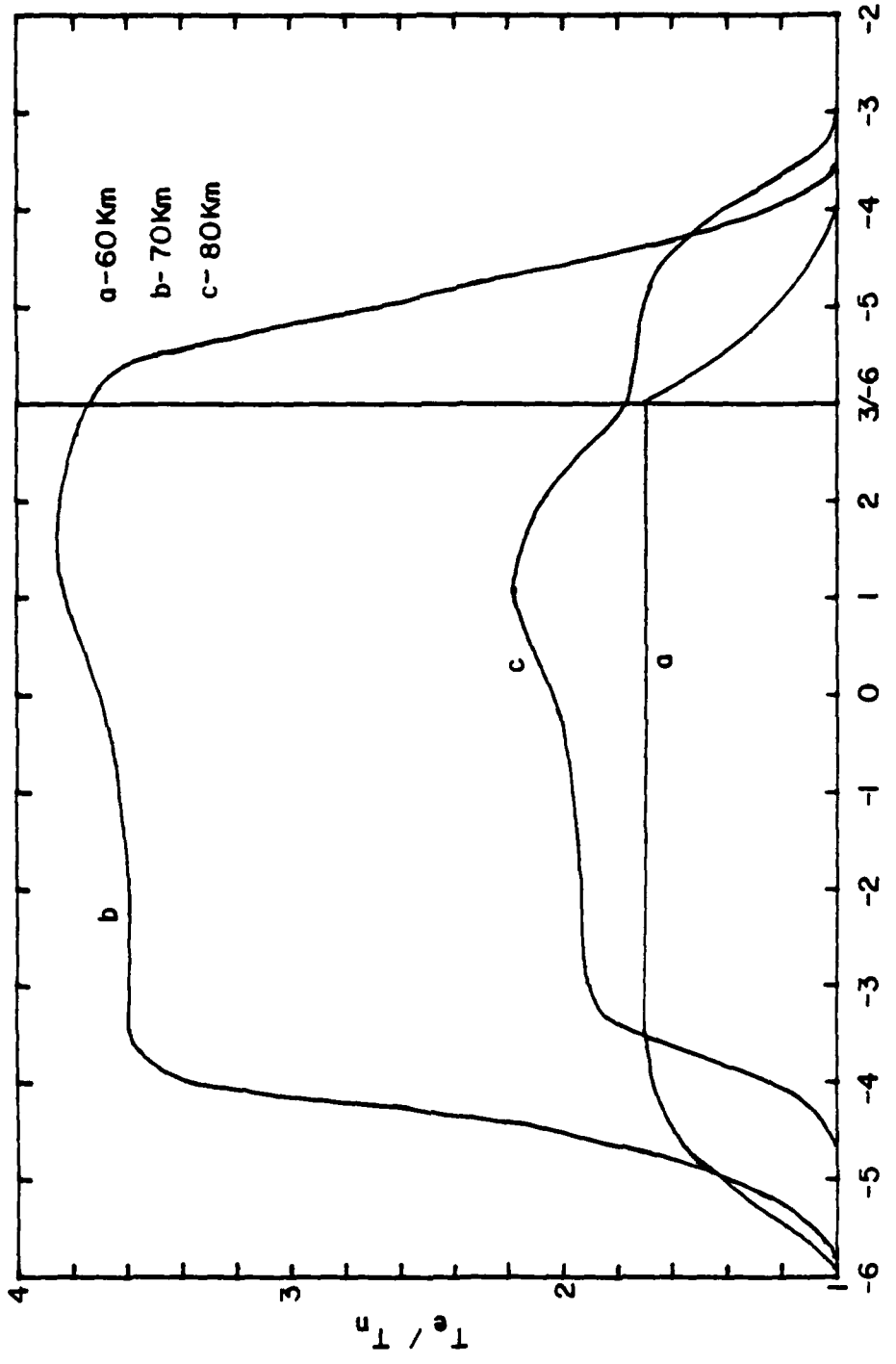

Figure 4.9 Electron temperature variation during and following a period of CW heating.

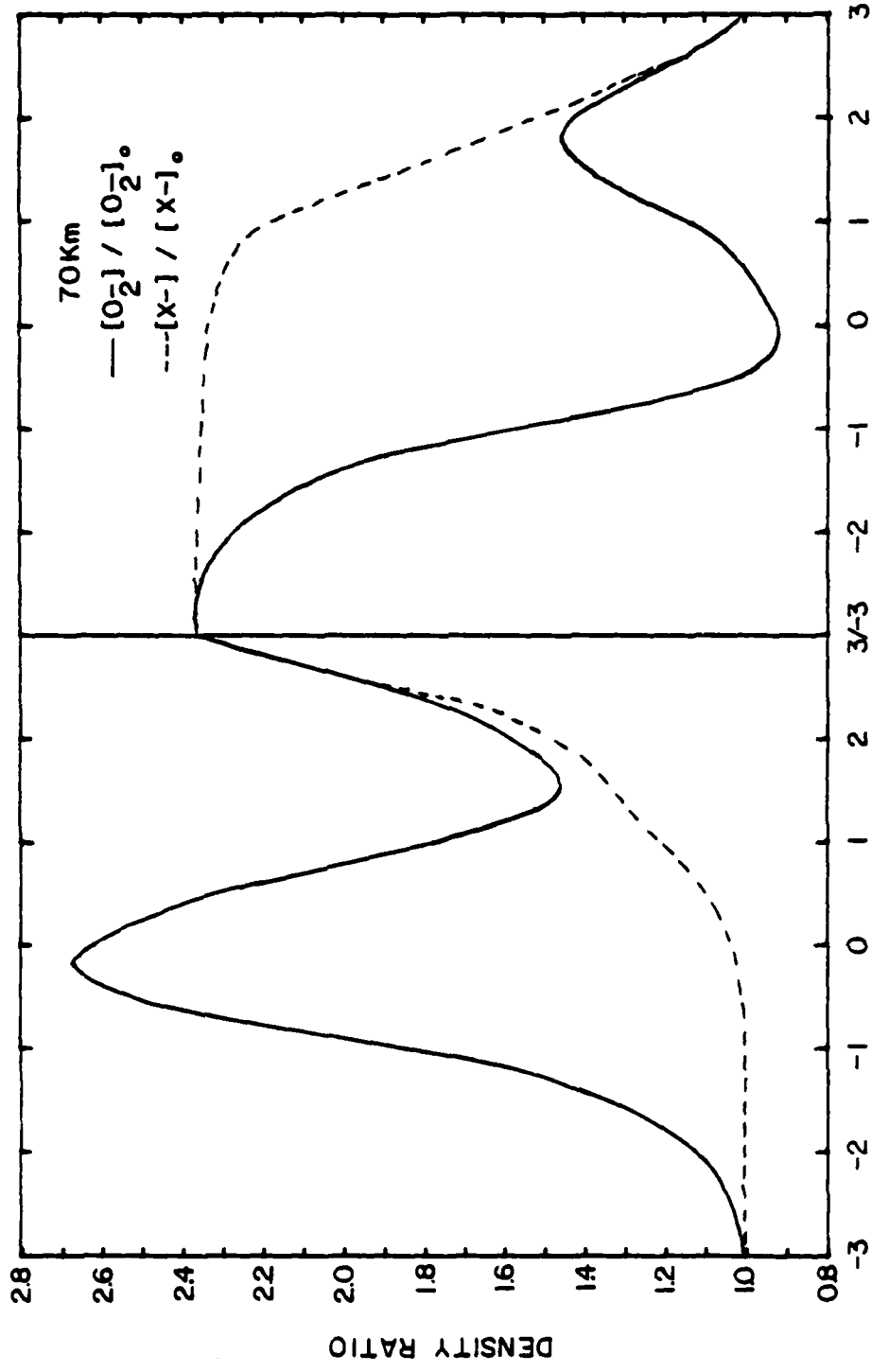

Figure 4.10 Negative ion density variation during and following a period of CW heating.

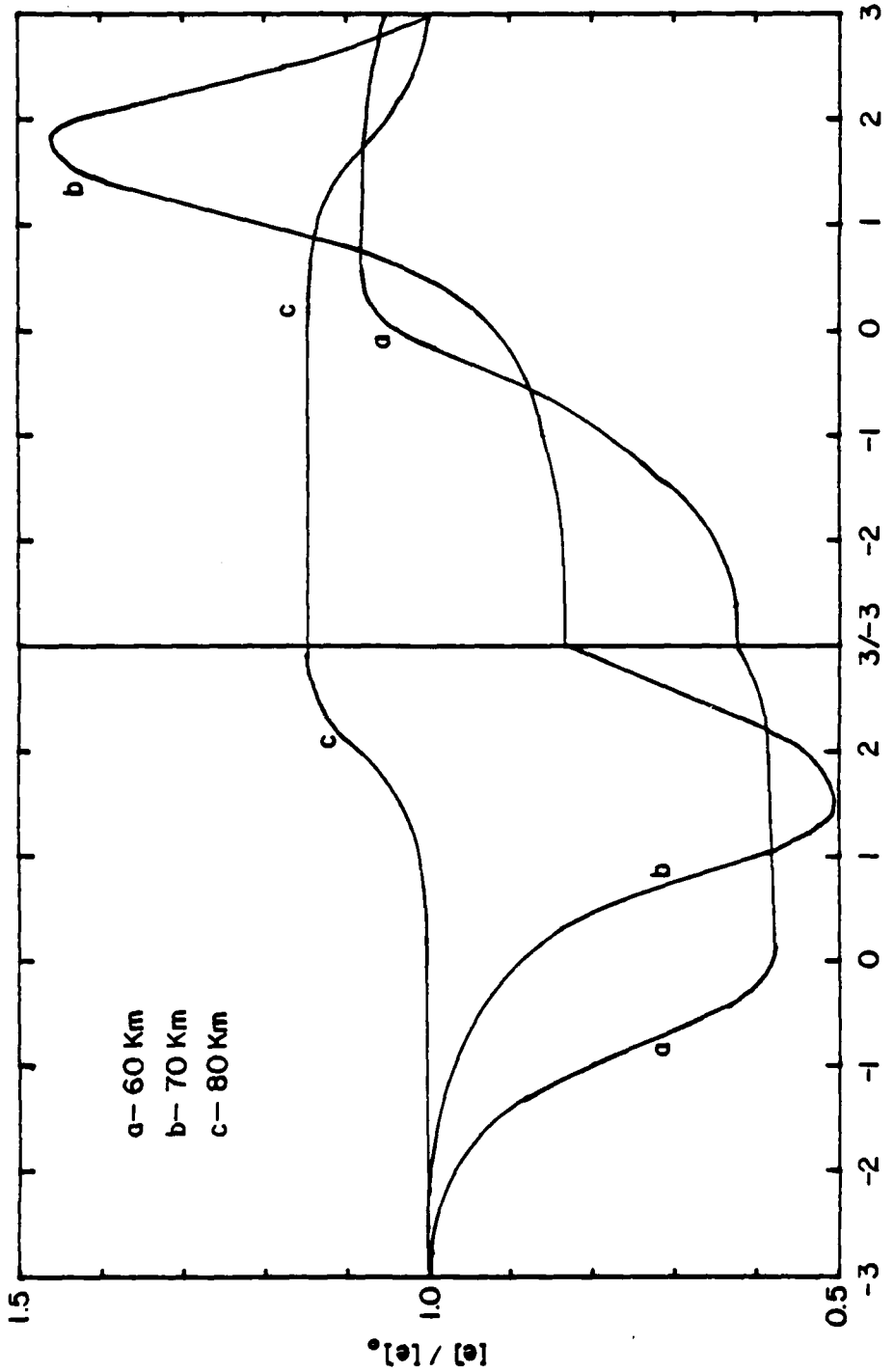

Figure 4.11 Electron density variation during and following a period of CW heating.

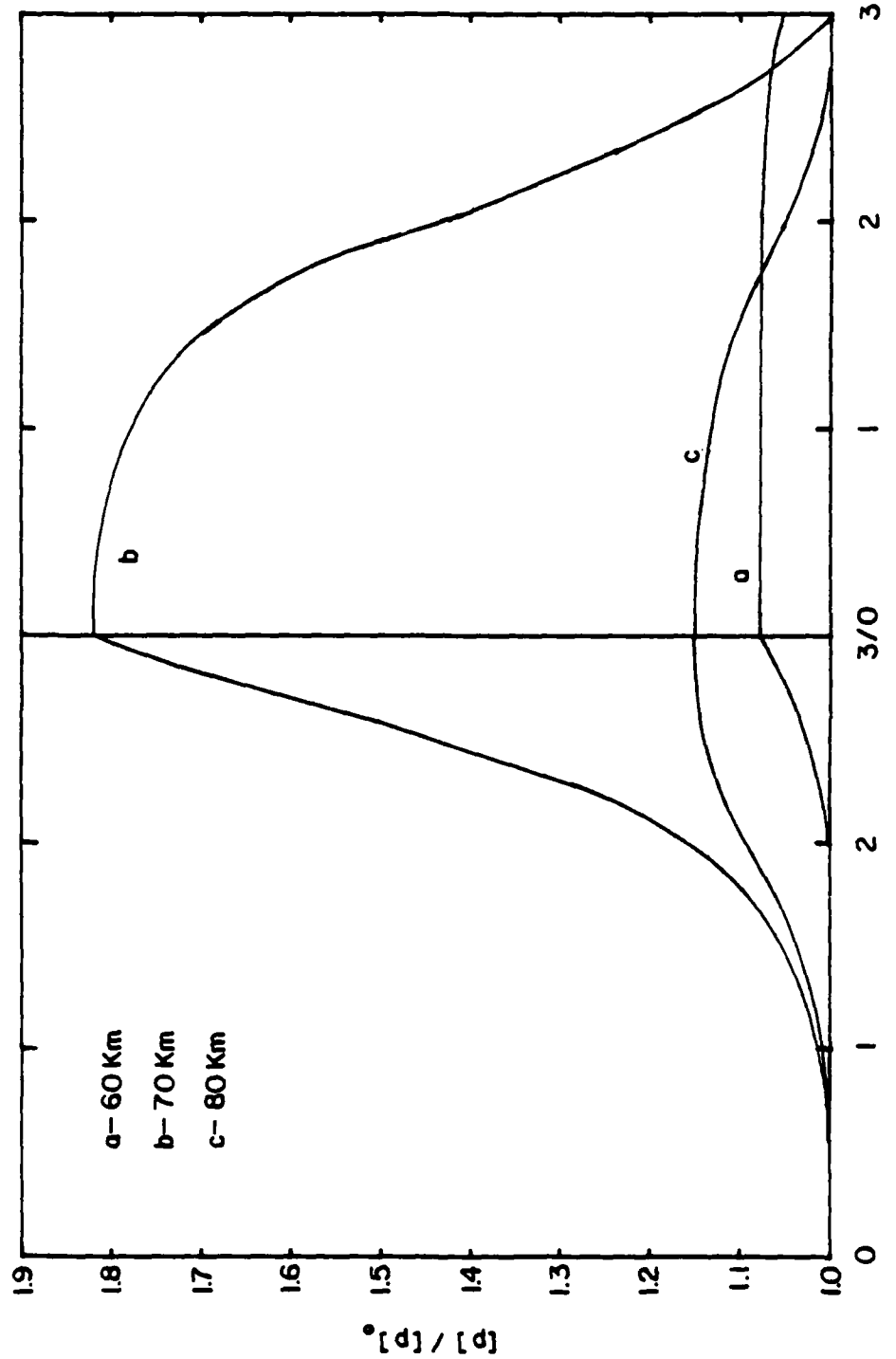

Figure 4.12 Total positive ion density variation during and following a period of CW heating.

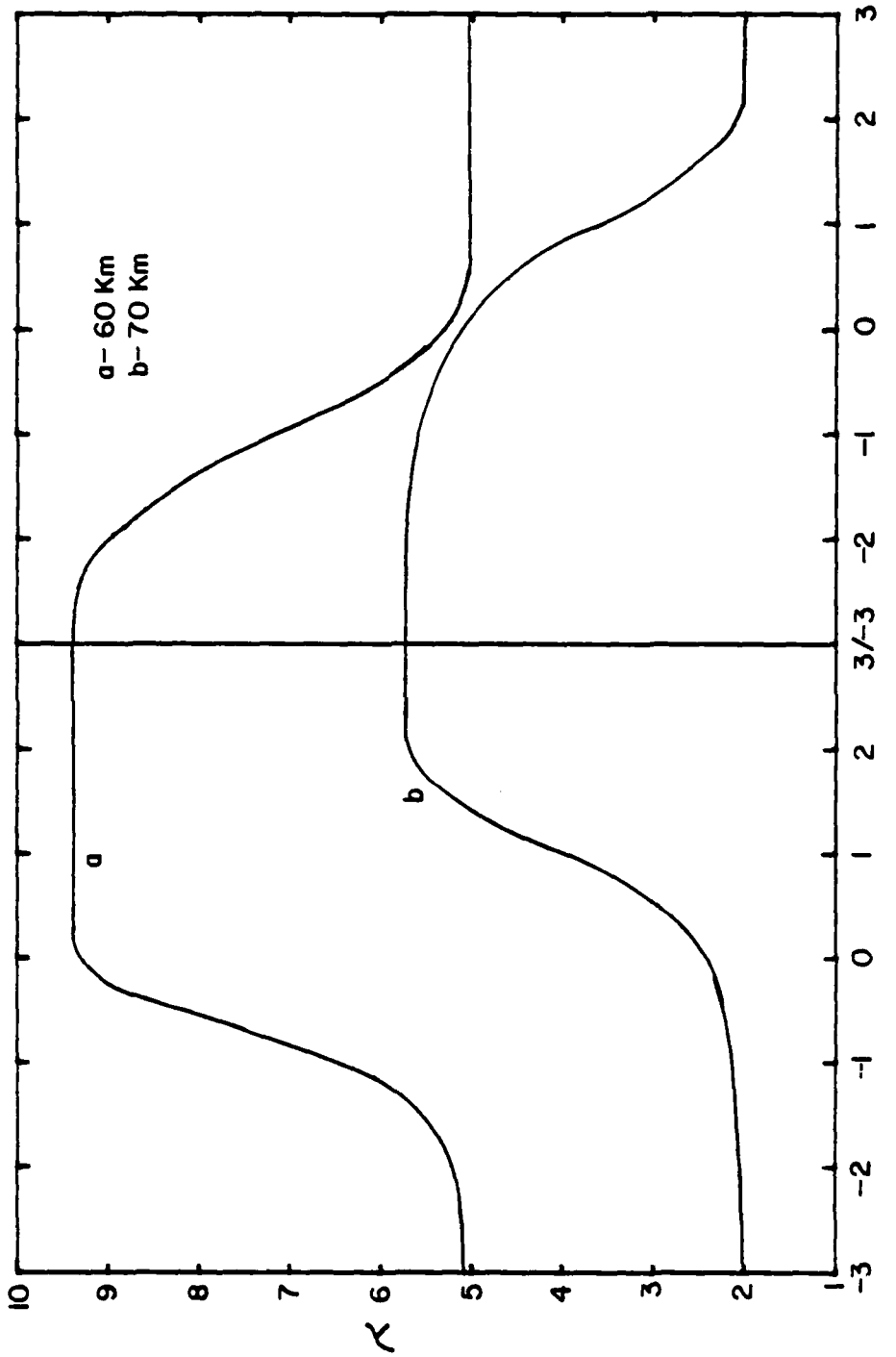

Figure 4.13 Variation of the negative ion to electron ratio during and following a period of CW heating.

turned on, the D-region electron temperature rapidly increases (Figure 4.9), reaching a quasi-steady state in about 1 ms. Maximum heating occurs near 70 km. In response to this temperature enhancement, the electron attachment rate increases from $\beta(T_n)$ to $\beta(T_e)$ while the individual recombination coefficients decrease from $\alpha_{i+}(T_n)$ to $\alpha_{i+}(T_e)$. This, in turn, leads to a variation in the ionic constituents.

The first ion density change that takes place is a rapid increase in $[O_2^-]$ due to the increase in β as shown in Figure 4.10. At 70 km, $[O_2^-]$ peaks after 1 s of heating, then decreases as O_2^- is converted to X^-. The net build-up in negative ions leads to a corresponding decrease in electron density, [e], throughout the lower D-region as shown in Figure 4.11. In the upper D-region, the negative ion to electron ratio, λ, is very small ($\lambda \ll 1$); hence the electron density is unaffected by changes in the negative ion chemistry. During the initial phase of heating (i.e. $t < 10$ s), the total positive ion density $[p] \simeq [Y^+]$, remains constant (Figure 4.12). As [p] gradually begins to increase in response to the decrease in α_{Y+}, $[O_2^-]$, $[X^-]$ and [e] also increase in proportion to [p]. As a consequence, after an initial rapid increase, λ remains essentially constant, as shown in Figure 4.13.

Following termination of CW heating, T_e rapidly decays to its ambient level (Figure 4.9) so that β and the α_{i+} take on their respective ambient values. Thus, $[O_2^-]$, $[X^-]$ and [p] decay back to their ambient levels, each on a progressively longer time scale. A significant feature of this decay process is that as the electron density in

the lower D-region recovers from its depressed level caused by heating, it can overshoot its ambient level as shown in Figure 4.11. The reason for this overshoot phenomenon will become apparent from the following discussion.

4.5 Analysis

A physically meaningful interpretation of the results presented above may be obtained by considering the continuity equations for the chemistry scheme of Figure 4.1. For O_2^- one has

$$\frac{d}{dt}[O_2^-] = \beta [e] - [O_2^-](\bar{X} + \gamma_1 + \alpha_I [p]) \qquad (4.26)$$

$$= \beta([p] - [X^-]) - [O_2^-](a + \beta)$$

where $a = \bar{X} + \gamma_1 + \alpha_I [p]$. After the initiation of CW heating, the electron temperature in the lower D-region quickly attains some quasi-steady state level and then remains essentially constant (Figure 4.9), hence $\beta = \beta(T_e)$ is fixed. Moreover, $[X^-]$ and $[p]$ are slowly varying compared to $[O_2^-]$, hence one can easily solve equation (4.26) and obtain

$$[O_2^-] = [O_2^-]_o e^{-t/\tau_1} + \frac{\beta}{a + \beta}([p] - [X^-])(1 - e^{-t/\tau_1}) \qquad (4.27)$$

where $$\tau_1 = \frac{1}{a + \beta}.$$

Similarly, the continuity equation for $[X^-]$ may be written as

$$\frac{d}{dt}[X^-] = \bar{X}[O_2^-] - [X^-](\gamma_2 + \alpha_I [p])$$

$$= \xi [p] - [X^-](b + \xi) \qquad (4.28)$$

where $$b = \gamma_2 + \alpha_I [p]$$

and $$\xi = \frac{\bar{X} \beta}{a + \beta} .$$

Again, [p] is slowly varying compared to $[\bar{X}]$ and one may readily show that

$$[\bar{X}] = [\bar{X}]_o e^{-t/\tau_2} + \frac{\xi}{b + \xi} [p] (1 - e^{-t/\tau_2}) \qquad (4.29)$$

where $$\tau_2 = \frac{1}{b + \xi} .$$

The time constants τ_1 and τ_2 are plotted in Figure 4.14 along with the heating time constant, τ_H, and the time constant for positive ion changes, τ_R, which will be defined presently. It is apparent from this figure that the time scales for ion chemistry modifications are much larger than that for electron temperature changes; hence, one can correctly set $\partial n_e/\partial t = 0$ in the energy balance equation when considering transient electron temperature variations associated with turning the heating transmitter off and on.

Combining equations (4.27) and (4.29) with equation (4.7), one finds that for $t > \tau_2 > \tau$,

$$\frac{[p]}{[e]} = (1 + \beta/a) (1 + \xi/b) \qquad (4.30)$$

Thus, [p]/[e] is determined by the ratios β/a and ξ/b. Typical values of a, b, β, ξ and other parameters based upon the semi-empirical study of Rowe et al. (1974) are given in Table 4.2. The values are for ambient conditions. During heating β and ξ are increased by some unknown factor. The quantities a and b are in general functions of [p]. However, during the initial stage of heating (i.e. $t \leq \tau_2$), $[p] = [p]_o$,

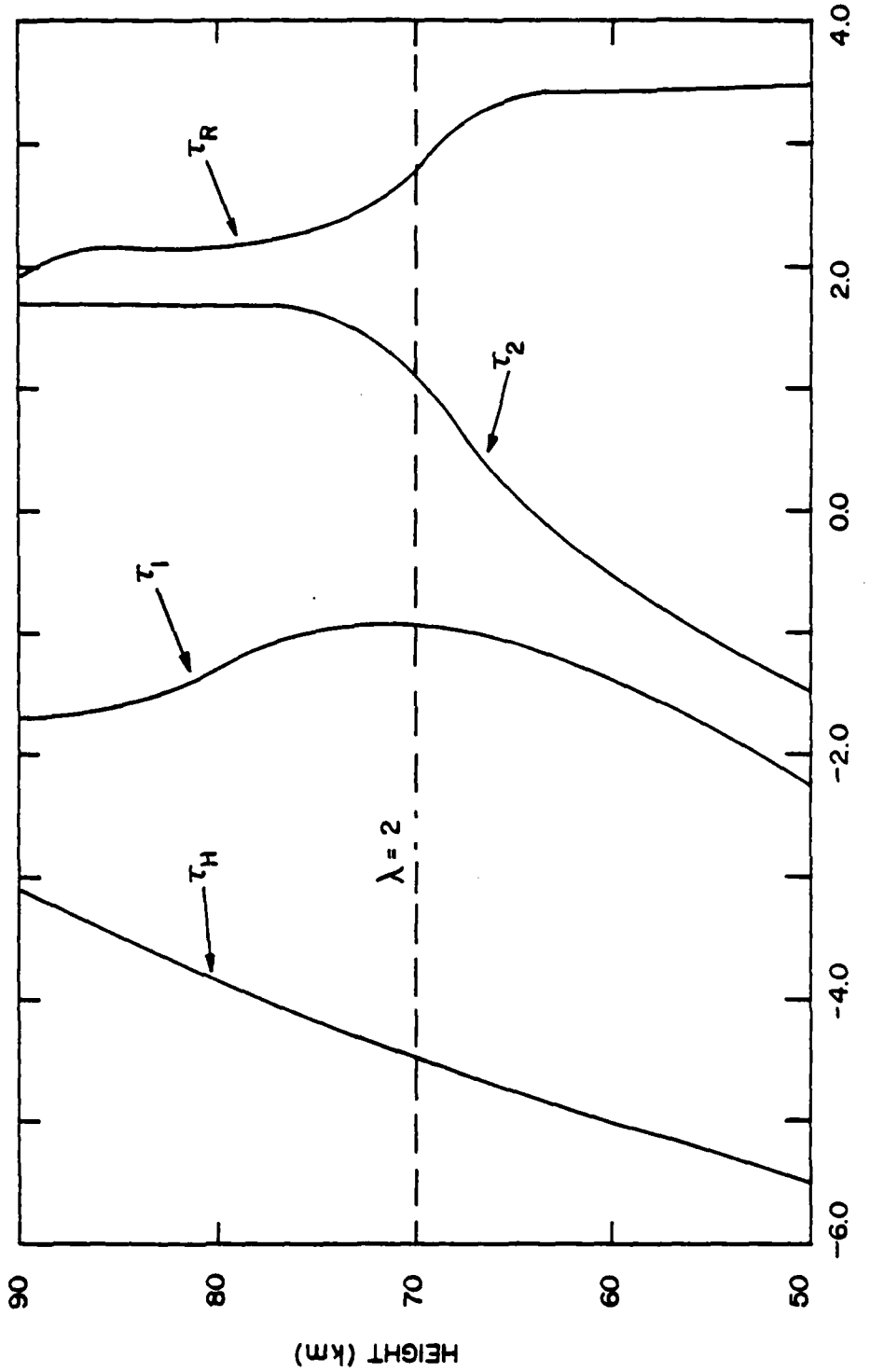

Figure 4.14 D-region time constants as a function of height.

hence, a and b are constant. During the long term variation of [p] (i.e. $t > \tau_2$), a and b will remain constant provided $\alpha_I [p]$ is small compared to γ_2 and $\bar{X} + \gamma_1$. If one takes $\alpha_I [p] \lesssim 10^{-3}$ s^{-1} for normal daytime conditions in the lower D-region and $\bar{X}$, γ_1,γ_2 as given in Table 4.2, then $\alpha_I [p] << X + \gamma_1$ and γ_2. During disturbed ionospheric conditions such as solar flares and PCA's, this condition may not be satisfied (e.g. Mitra, 1975b). With a and b constant and neglecting any long term variation in β and ξ, one has by equation (4.30) $[p]/[e]$ = constant for $t > \tau_2$. It follows that $\lambda = [p]/[e] - 1$ is also constant over this time scale in agreement with Figure 4.13.

Applying this result to the continuity equation for [p] one has

$$\frac{d}{dt}[p] = Q - (\alpha_{eff} + \alpha_I \lambda)[p][e] \qquad (4.31)$$

$$= Q - \bar{\alpha}[p]^2$$

where $$Q = Q'_{O_2^+} + Q'_{NO^+}$$

and $$\bar{\alpha} = \alpha_I + (\alpha_{eff} - \alpha_I)/\{(1 + \beta/a)(1 + \xi/b)\}$$

Upon solving equation (4.31), one finds that

$$[p] = \sqrt{Q/\bar{\alpha}}\,(1 - A)/(1 + A) \qquad (4.32)$$

where $$A = \{\sqrt{Q/\bar{\alpha}} - [p]_o)/(\sqrt{Q/\bar{\alpha}} + [p]_o)\}\, e^{-t/\tau_R}$$

and $$\tau_R = \frac{1}{2\sqrt{Q\,\bar{\alpha}}} .$$

Thus, for a fixed Q, the magnitude and time scale for changes in [p] induced by CW heating are controlled by $\bar{\alpha}$.

The analytic formulation given above is also applicable during the return of the plasma to ambient conditions following termination of heating provided one replaces $[O_2^-]_o$, $[X^-]_o$, and $[p]_o$ by their respective values at the time of heating termination and one sets β and the α_{i+} to their respective ambient values. Thus, the ambient steady state positive ion density is given by

$$[p]_o = \sqrt{Q/\bar{\alpha}\ (T_n)} \tag{4.33}$$

and one finds from (4.32) that the maximum change in p due to CW heating is

$$\frac{[p]}{[p]_o}\ \text{max} = \sqrt{\frac{\bar{\alpha}\ (T_n)}{\bar{\alpha}\ (T_e)}} \tag{4.34}$$

and is attained for $t>>\tau_R$. Referring to Figure 4.14, one can see that $t>>\tau_R$ is much larger in the lower D-region than in the upper D-region, hence, [p] responds much more slowly to heating at the lower heights. For example, in Figure 4.12, [p] is still increasing after 10^3 s of heating at 70 km, is just beginning to increase at 60 km, but has reached its maximum level at 80 km.

As noted earlier, the possibility exists that Q may depend on T_e and/or E. For this case, one can write

$$\frac{[p]}{[p]_o}\ \text{max} = \sqrt{\frac{Q(T_e,\ E)\bar{\alpha}\ (T_n)}{Q(T_n)\ \bar{\alpha}\ (T_e)}} \tag{4.35}$$

Thus, the positive ion concentration can be enhanced during HF heating by decreased recombination or increased production.

The predicted electron density variation during and following

CW heating (Figure 4.11) may be described by the simple formula

$$\frac{[e]}{[e]_o} = f(T_e)\,\frac{[p]}{[p]_o} \tag{4.36}$$

where for $t>3\tau_2$,

$$f(T_e) = \frac{a+\beta(T_n)}{a+\beta(T_e)}\;\frac{b+\xi(T_n)}{b+\xi(T_e)} = \frac{\tau_1(T_e)}{\tau_1(T_n)}\;\frac{\tau_2(T_e)}{\tau_2(T_n)} \tag{4.37}$$

During the initial phase of heating ($t<<\tau_R$) one has $[p] = [p]_o$; hence, the electron density decreases to a level $f(T_e)\,[e]_o$ on a time scale τ_2. As $[p]$ gradually begins to increase, $[e]$ begins to recover from its depressed level on the time scale τ_R. When heating is terminated, β takes on its ambient value, which results in a prompt decrease in the negative ion density on time scale τ_2. On this time scale, the positive ion density remains fixed at its heated level, $[p]_H$. Thus $[e]$ promptly rises to a level $[e]/[e]_o = [p]_H/[p]_o$, resulting in the overshoot phenomena illsutrated in Figure 4.11. Finally on time scale τ_R, $[e]$ decays with $[p]$ to its ambient level.

Two special forms of equation (4.36) are worth noting. First, if $b<<\xi(T_n)$, one has $f(T_e) = \beta(T_n)/\beta(T_e)$, so that the prompt decrease in e during heating is inversely proportional to β. This condition may be satisfied in the lower D-region if γ_2 is small (i.e. $\gamma_2 \lesssim 0.1 s^{-1}$ at 60 km). If γ_2 is large (i.e. $\gamma_2 \gtrsim 4\ s^{-1}$) the change in β due to heating may be obscured so that $f(T_e) \approx 1$. Secondly, if $a>>\beta(T_e)$ and $b>>\xi(T_e)$, then $\bar{\alpha} = \alpha_{eff}$ and $f(T_e) = 1$ so that

$$\frac{[e]}{[e]_o} = \frac{[p]}{[p]_o} = \sqrt{\frac{\alpha_{eff}\,(T_n)}{\alpha_{eff}\,(T_e)}},\quad t>>\tau_R \tag{4.38}$$

as in the work of Holway and Meltz (1973) for the upper D-region.

From the above analysis it is clear that experimental observation of electron density changes during HF heating could give one valuable information about the size of key ion chemistry parameters. From long time scale observations of [e] during and following HF heating, one can determine $[p]max/[p]_o$, $\tau_R(T_e)$ and $\tau_R(T_n)$ which would give one an estimate of $\bar{\alpha}(T_n)$, $\bar{\alpha}(T_e)$ and Q. Observations of the prompt changes in [e] would allow one to determine $f(T_e)$, τ_1 and τ_2. Determination of $f(T_e)$ could give one an indication of the relative size of γ_2.

CHAPTER V

HF HEATING INDUCED ATTENUATION OF DIAGNOSTIC WAVES

5.1 Vertical Incidence Pulse Absorption

Measurements of radio wave absorption by the vertical incidence pulse sounding technique (A1 method) have been used routinely by numerous experimenters for studies of the short and long term variability of the ionopshere (e.g. Gnanalingam and Kane, 1973; Ganguly, 1974). The A1 absorption technique consists of measuring the amplitudes of vertically reflected, pulsed radio waves (diagnostic waves) originating from a ground based HF sounder. The absorption experienced by a diagnostic wave as it propagates over the two-way path from ground level to the wave reflection height, h_r, and back again is given in decibels by (Rishbeth and Garriott, 1969)

$$L = 8.686 \frac{2\omega_D}{c} \int_{h_o}^{h_r} \chi_D(h') \, dh' \qquad (5.1)$$

where ω_D is the angular frequency of the diagnostic wave and χ_D is the corresponding absorption index. Since χ_D depends directly on the electron density and electron-neutral collision frequency, variations in L are interpreted in terms of a change in these parameters.

The A1 technique can also be employed as a straightforward means of monitoring plasma modification resulting from high power radio wave heating of the ionosphere. In this case, one measures the change in amplitude of the reflected diagnostic pulses as the heating transmitter is turned on and off. The ratio of the amplitude of the received diagnostic wave during high power heating to that which would

have been received with no heating is given by

$$\Delta L = 8.686 \frac{2\omega}{c} D \int_{h}^{h_r} [\chi_D(h', T_e) - \chi_D(h', T_n)]\, dh' \qquad (5.2)$$

Measurements of this type were performed at the Platteville HF heating facility during the early seventies and were summarized by Utlaut and Violette (1974). The A1 measurements were made on a 2.667 MHz diagnostic wave and showed about a 6 dB increase in absorption as the plasma was heated at frequencies between 3 and 6 MHz with an effective radiated power of about 100 MW. The diagnostic wave absorption was observed to increase promptly (< 40 ms) after turn on of the heating transmitter, but the time required for the absorption to return to its unheated level following a long period (10 min.) of CW heating was very slow (~ 10 min.). The prompt increase in absorption is attributed to the change in the electron-neutral collision frequency as the electrons are quickly heated by the high power wave field, while the long term recovery is most likely due to an electron density modification arising from the electron temperature dependence of various ion chemistry reactions as discussed in Chapter IV.

In this chapter, the electron temperature and density models developed in the previous chapters are used to compute the short and long term variations in A1 absorption due to HF heating. These theoretical results are compared with the Platteville data and more recent A1 absorption measurements at Arecibo by Tomko et al. (1981).

It should be noted that equations (5.1-2) apply only to the non-deviative component of the absorption experienced by the diagnostic

wave. In general, the wave is also subjected to deviative absorption associated with the bending of the wave near its reflection height. The reflection heights for HF waves are in the E and F layers near the level where the wave and plasma frequency are equal (i.e. $\omega_e = \omega$). The present analysis focuses on plasma modifications below the wave reflection height and hence, only nondeviative absorption is considered.

5.2 Collision Frequency Effects

Figure 5.1 illustrates the change in absorption as defined by equation (5.2) on a 2.4 MHz diagnostic wave due to enhancement of the electron-neutral collision frequency by HF heating as a function of the heating frequency. Curves are shown for X-mode heating (solid) and O-mode heating (dashed) at 100 MW ERP and for both polarizations of the diagnostic wave (as labeled). The shape of the attenuation versus heating frequency curves for X and O mode diagnostics are similar although in general, the X-mode diagnostic is absorbed more than the O-mode for a fixed heating frequency. Likewise, X and O-mode heating for fixed diagnostic polarization result in similar attenuation versus heating frequency curves, although the peak absorption is shifted in frequency between heating modes due to the birefrigent nature of the ionosphere.

The general shape of the attenuation versus heating frequency curve may be explained using the simple quasi-longitudinal approximation for the absorption index of the Appleton-Hartree theory (Budden, 1966). With this approximation, one has

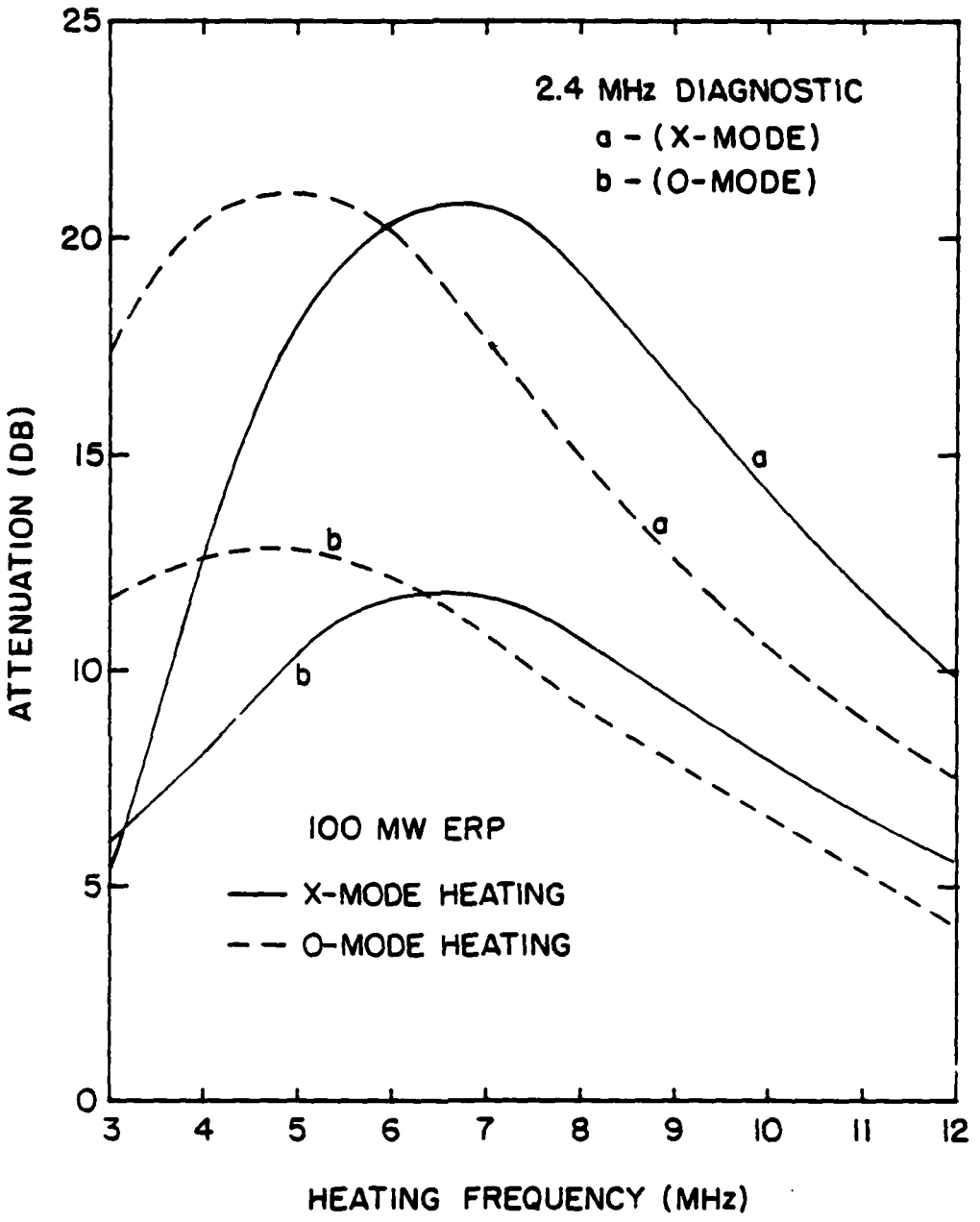

Figure 5.1 Heating induced attenuation at 2.4 MHz as a function of heating frequency.

$$L_{O,X} = \frac{8.686}{c} \int_{h_o}^{h_r} \frac{\omega_e^2 (h') \nu_{en} (h')}{[\omega_{O,X}^2 + \nu_{en}^2 (h')]} dh' \qquad (5.3)$$

where $\omega_{O,X} = \omega_D \pm \omega_G \cos\theta$ (see (2.106)). Figure 5.2 illustrates the height dependence of ω_e and ν_{en} for ambient conditions, and the effective frequencies ω_O and ω_X for a 2.4 MHz diagnostic wave, and Arecibo geomagnetic conditions.

Let $\nu_O = \nu_{en}(T_n)$, $\nu_H = \nu_{en}(T_e)$ and $\Delta\nu = \nu_H - \nu_O$. In the lower D-region, there are a range of heights $h_o < h < h_1$ (region I) such that $\omega_{O,X} < \nu_H$. The change in absorption due to heating over this range of heights is given by

$$L_{O,X} = \frac{-8.686}{c} \int_{h_O}^{h_1} \frac{\omega_e^2 \Delta\nu}{\nu_O \nu_H} dh' \qquad (5.4)$$

independent of the diagnostic frequency or polarization. In the upper D-region, there are a range of heights (region II) $h_1 < h < h_r$ such that $\omega_{O,X} > \nu_H$ and one has

$$\Delta L_{O,X} = \frac{8.686}{c\, \omega_{O,X}^2} \int_{h_1}^{h_r} \omega_e^2 \Delta\nu \, dh' \qquad (5.5)$$

The quantity defined by equation (5.4) represents negative attenuation or enhancement of the diagnostic signal and opposes the effect of the absorption term defined by equation (5.5).

Figure 5.3 shows the change in absorption due to heating as a function of height for heating at 3 MHz X-mode and 6 MHz O-mode at 100 MW ERP and for both diagnostic polarizations. The enhancement

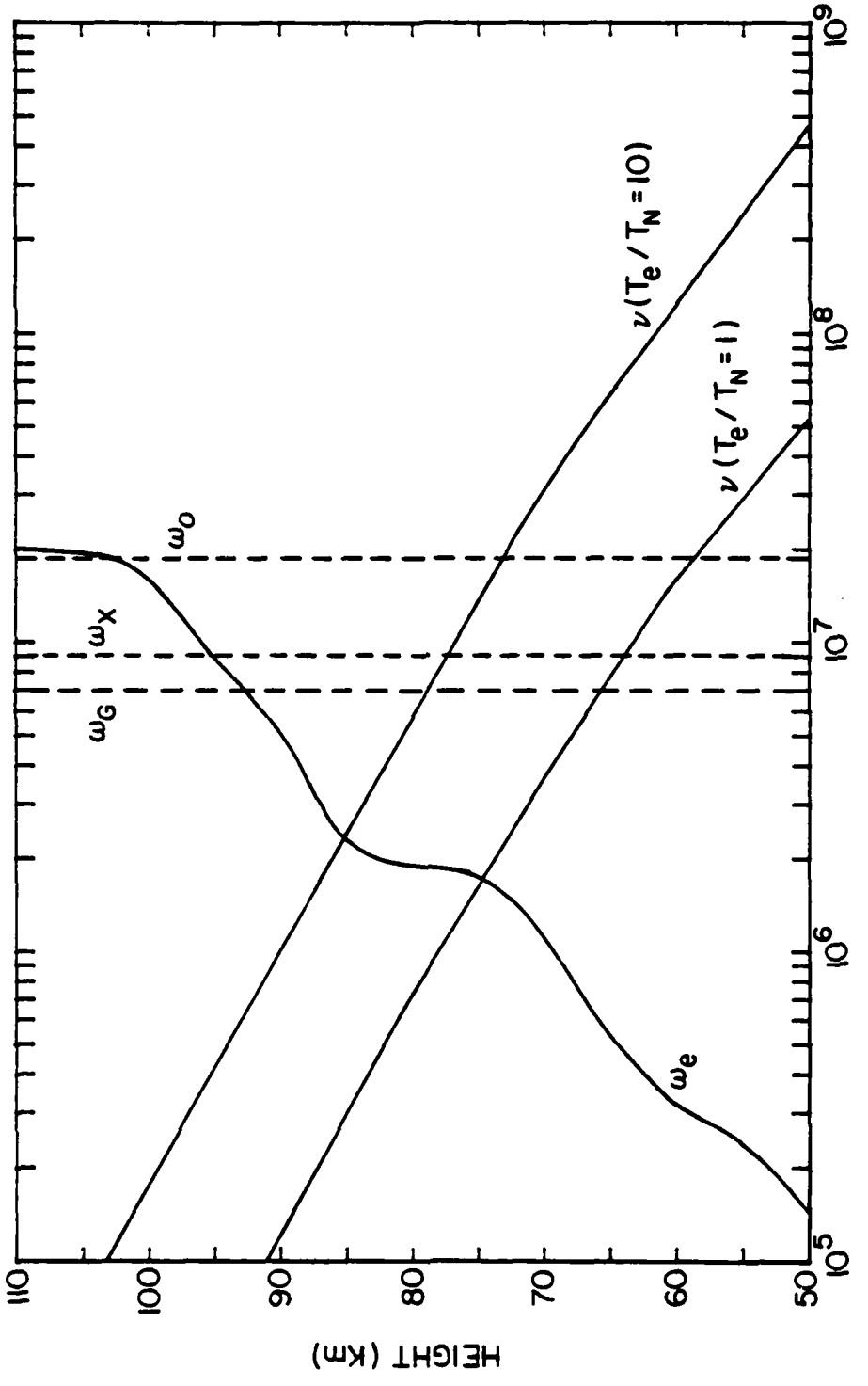

Figure 5.2 Plasma frequency and collision frequency models.

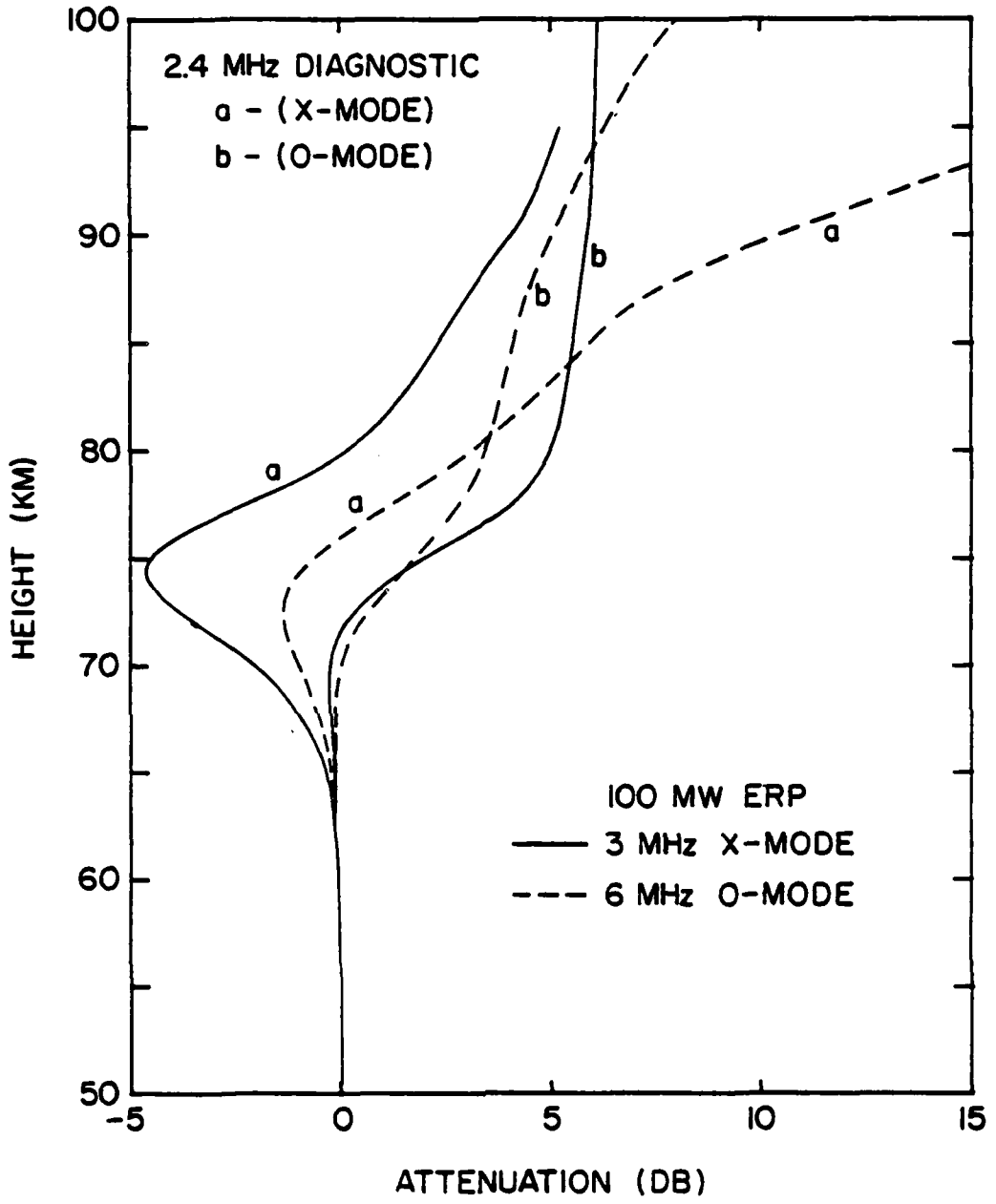

Figure 5.3 Heating induced attenuation at 2.4 MHz as a function of height.

region for X-mode diagnostic is clearly defined and corresponds to the region of maximum electron temperature change (see Figure 3.6). The O-mode diagnostic does not show a notable enhancement since the $\omega_O = \nu_H$ level is considerably lower than the $\omega_X = \nu_H$ level which thus narrows the range of integration in equation (5.4). For the lower end of the range of heating frequencies considered here, $\Delta\nu$ is large in region I and equation (5.4) is competitive with equation (5.5). As one moves to higher heating frequencies, $\Delta\nu$ in region I decreases while increasing in region II, thus the enhancement term diminishes and equation (5.5) is dominant. If only rotational cooling is considered, one can easily show from equation (3.19) that for the higher heating frequencies

$$\Delta\nu = C\, n_{air}\, T_e^{3/2}\, S/(f \pm f_G \cos\theta)^2 \qquad (5.6)$$

where C is a constant and n_{air} is the number density of air. Thus, $\Delta L_{O,X}$ decreases approximately as $1/f^2$.

Comparison of the theoretical results presented in Figure 5.1 with the empirical results reported by Utlaut and Violette (1974) shows limited agreement. For heating at 3.15 MHz X-mode and 6.21 MHz O-mode with an effective radiated power of 100 MW, the observed attenuation on a 2.667 MHz X-mode diagnostic was about 6 dB for both heating frequencies. The theoretical value for an X-mode diagnostic and a heating frequency of 3.15 MHz X-mode is also about 6 dB; however, the theoretical value for 6.21 MHz, O-mode heating, 20 dB, is much larger than the observed value. This discrepancy may be due in

part to the solar zenith angle variation at the electron density. The theoretical values are for $\chi_s = 30^o$ which is more appropriately compared to the 3.15 MHz data which was taken at noontime than the 6.21 MHz data which was taken late in the day (1400 - 1800 LT). The variation of ΔL with solar zenith angle is considered in the following section. The discrepancy between the experimental and theoretical values at 6.21 MHz may also be due to uncertainties in the electron energy loss rates. Figure 5.4 illustrates the effect of a factor of two increase in the rotational cooling rate. One notes that the theoretical heating induced absorption for 6.21 MHz O-mode heating is substantially reduced with respect to the corresponding value without the rate change (Figure 5.1), while the value of ΔL for 3.15 MHz X-mode heating is not significantly altered.

5.3 Electron Density Effects

In this section, the effect of the electron density distribution on the heating induced change in diagnostic wave absorption is considered. Since the absorbing properties of the ionosphere are electron density dependent, any change in n_e, whether natural, such as the diurnal variation with solar zenith angle (see Appendix B), or heating induced, can alter the diagnostic wave attenuation. This is apparent from the simple model for $L_{O,X}$ given in the previous section. Writing out the electron density dependence of $\Delta L_{O,X}$ explicitly, one has from

(5.3)

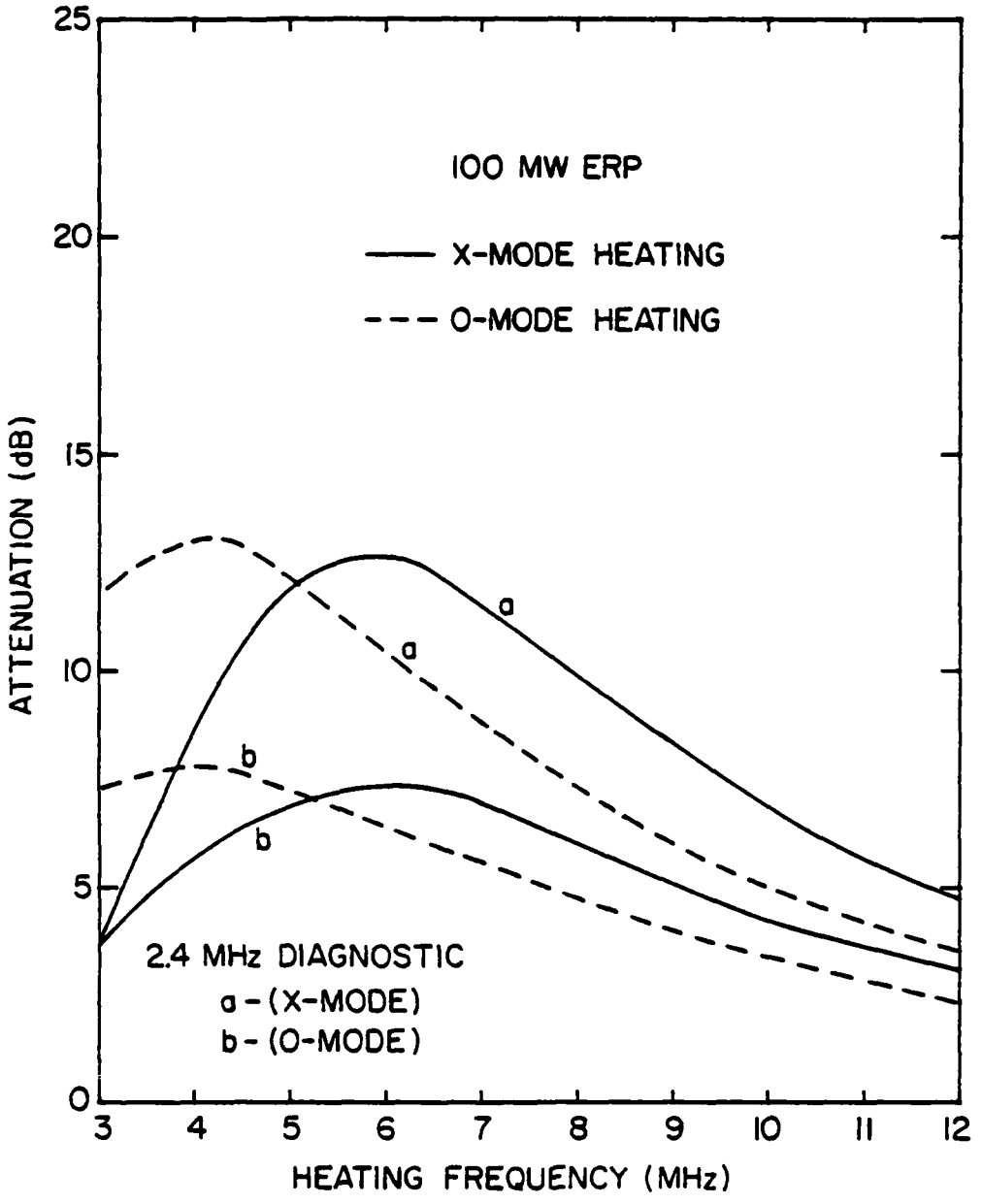

Figure 5.4 Heating induced attenuation at 2.4 MHz as a function of heating frequency with the rotational cooling rate increased by a factor of 2.

$$\Delta L_{O,X} = A \int_{h_o}^{h_r} n_{eo} \left(\frac{\nu_H}{\omega_{O,X}^2 + \nu_H^2} - \frac{\nu_O}{\omega_{O,X}^2 + \nu_O^2} \right) dh' + A \int_{h_o}^{h_r} \frac{\Delta n_e \ \nu_H}{\omega_{O,X}^2 + \nu_H^2} \ dh' \qquad (5.7)$$

where A is a positive constant and

n_{eo} - ambient (unheated) electron density,

Δn_e - change in electron density due to heating,

with ν_H and ν_O being the heated and ambient collision frequencies as defined previously. The first term on the right hand side of (5.7) describes the prompt (i.e. $t \approx \tau_H$) changes in $\Delta L_{O,X}$ due to the heating induced collision frequency enhancement, while the second term describes the long term (i.e. $t \gtrsim \tau_l$) variation in $\Delta L_{O,X}$ due to electron density modifications. The former term depends on the ambient electron density which will vary diurnally as the electron production rate, Q_e, decreases with increasing solar zenith angle.

Figure 5.5 illustrates the change in absorption, ΔL_o, for a 2.4 MHz O-mode diagnostic wave during a period of 10^3 s of heating at 3.175 MHz, X-mode, 120 MW ERP, and during the subsequent cooling of the plasma following heating termination. Curves are given for two different values of the solar zenith angle ($\chi_s = 30^o$ and 80^o) and two different choices of the electron temperature dependence of α_{y+} (b = 0.008 and 0.5; see Section 4.2). All values of ΔL_o were computed from the general equation (5.2) using the Sen-Wyller formula (2.106) for the absorption index. However, the major features of the time

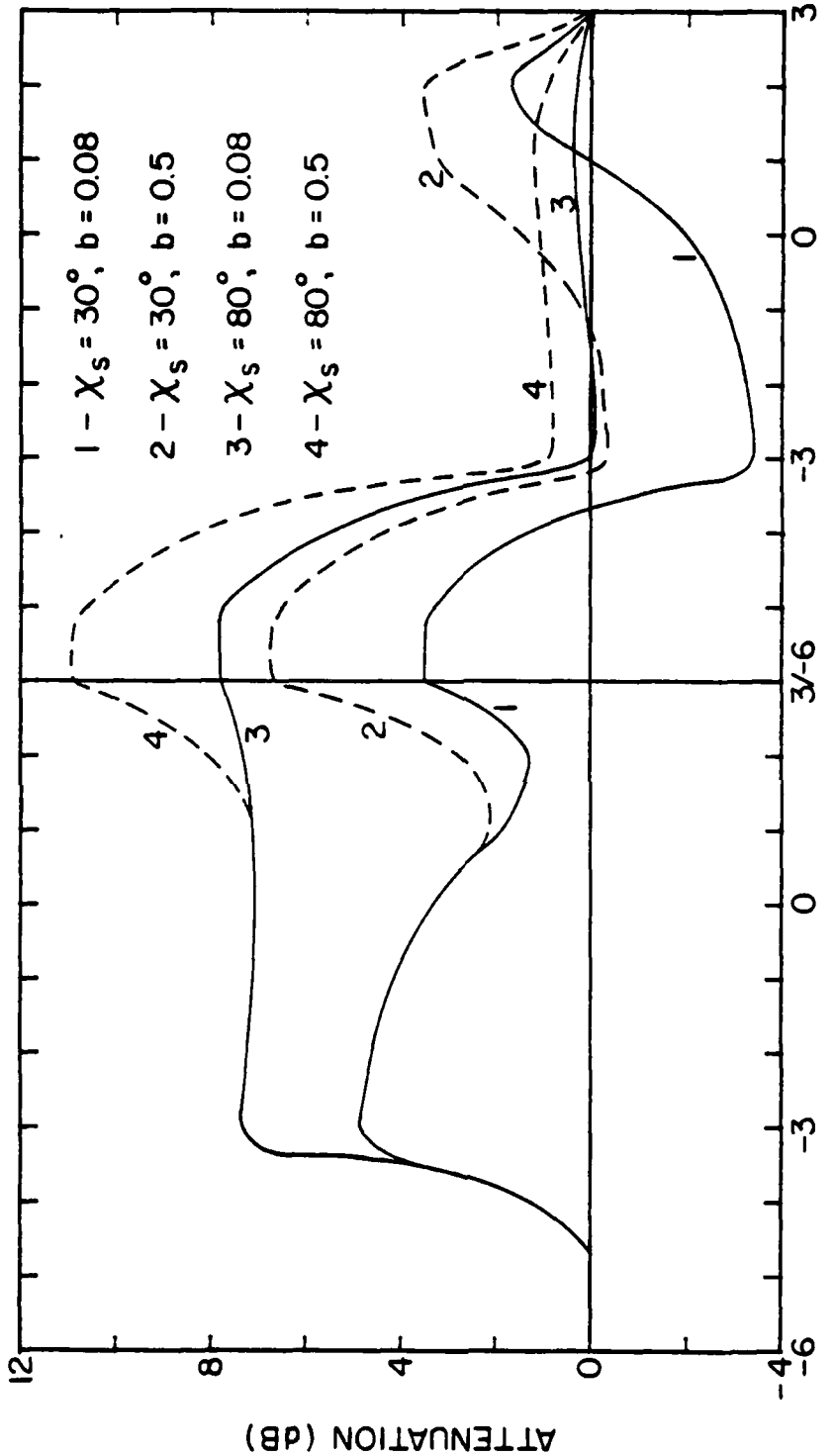

Figure 5.5 Heating induced attenuation at 2.4 MHz as a function of time during and following a period of CW heating.

variation of ΔL_o can be adequately described by (5.7).

Considering first the prompt effect due to collision frequency enhancement (i.e. t = 10^{-3} s in Figure 5.5) one notes that ΔL_o for $\chi_s = 80^o$ is about 3 dB greater than that for $\chi_s = 30^o$. At first sight, this result appears to conflict with equation (5.7) since n_{eo} ($\chi_s = 30^o$) > n_{eo}($\chi_s = 80^o$); however, one must not forget that any change in n_{eo} will alter T_e through the absorption index for the heating wave (see (3.19)). Figure 5.6 illustrates how T_e varies with $n_{eo}(\chi_s)$. Near midday, the electron density in the middle of the D-region is relatively large and the heating wave is rapidly attenuated as it propagates through this region, leading to a peak value of T_e near 70 km. As χ_s increases, n_e decreases, causing less absorption of the heating wave. Consequently, more wave energy is available for heating the upper ionosphere and the T_e peak shifts upwards in height. From the analysis given in the previous section, one notes that there is more heating in the wave attenuation region (i.e. region II, $\omega_o > \nu_H$) for $\chi_s = 80^o$ than for $\chi_s = 30^o$, while the heating in the wave enhancement region (i.e. region I, $\omega_o < \nu_H$) remains about the same. Thus, ΔL_o increases with χ_s because the larger $\Delta\nu$ in region II overcompensates for the decrease in n_{eo}.

The long term variation in ΔL_o shown in Figure 5.5 follows the electron density variations described in Section 4.4. For $\chi_s = 30^o$, there is significant heating in the lower D-region where electron attachment is important, hence there is a sharp decrease in n_e as shown in Figure 4.11 on a time scale of a few seconds. In this case, Δn_e

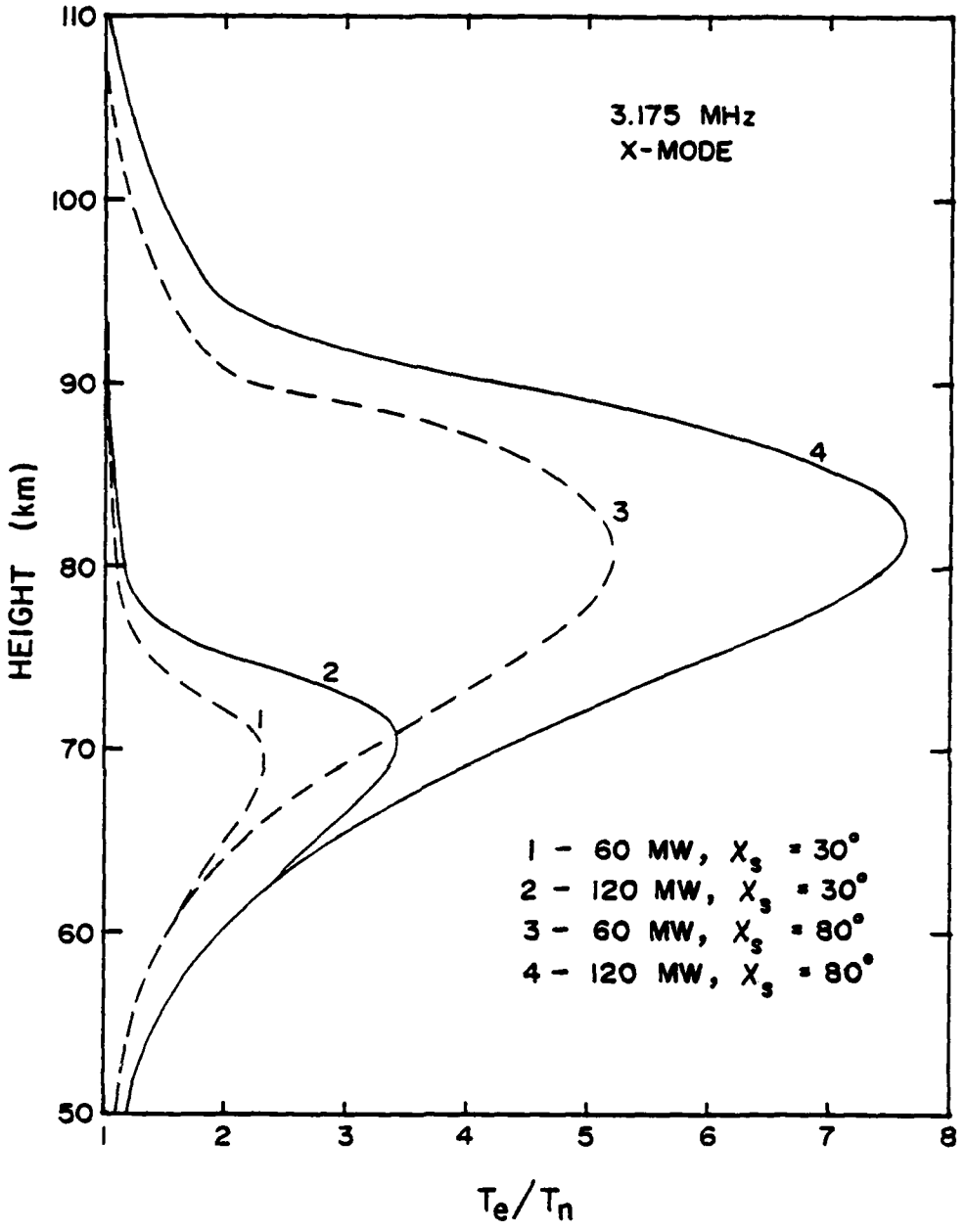

Figure 5.6 Electron temperature profiles for two solar zenith angles at two levels of heating.

is negative, thus from equation (5.7), ΔL_o decreases. On longer time scales, n_e in the lower D-region recovers from its depressed value on a time scale of 10^2 s due to decreased electron recombination with hydrated ions, and n_e also increases in the upper D-region due to the same mechanism. As a result, Figure 5.5 shows a long term increase in ΔL_o. As one expects, the long term change in ΔL_o becomes more pronounced as the temperature coefficient for the Y^+ ions, b, is increased. For $\chi_s = 80^o$, most of the heating is in the upper D-region, hence the electron attachment effects are small and ΔL_o shows only a long term increase due to the n_e enhancement associated with decreased dissociative recombination.

After the heating is terminated, ΔL_o shows a prompt decrease due to the return of ν_{en} to its ambient value (*first term in* (5.7)). On long time scales, ΔL_o for $\chi_s = 30^o$ exhibits the effect of electron density overshoot (see Figure 4.11), while for $\chi_s = 80^o$, only a long term recovery in ΔL_o is apparent, due to recombination effects.

5.4 Al Absorption Experiment

This section describes the results of Al absorption measurements made during the Fall, 1980, ionospheric modifications program at the new high power HF transmitting facility of the National Astronomy and Ionosphere Center on the island of Puerto Rico. The Al absorption measurements were made using a portable 2.4 MHz ionospheric sounding system developed at Penn State.

The NAIC HF heating facility is located on the northeast coast of Puerto Rico near the town of Islote, about 50 miles west of San Juan.

The facility has four 200 KW transmitters which drive a 4 x 8 array of non-planar log periodic antennas operating in the backfire mode (Trask, 1979). The maximum directive gain of this array is expected to exceed 23 dBi over the 3 to 12 MHz range, giving an effective radiated power of over 160 MW. The half power beam width of the array is about 10 degrees.

The Penn State A1 sounding system was located 5 km southwest of the HF heating facility at Higuillales. This site was chosen because it is close enough to the heating facility that the vertical sounding intersects the main beam of the heater in the D-region, it is in mountainous terrain, thereby providing good shielding of the receiving equipment from the heater ground wave, and it is the only available site where direct communications with both the heating facility and the main NAIC facility, Arecibo Observatory, were available. A block diagram of the sounding system is given in Figure 5.7. The sounder consists of a 2.4 MHz transmitter with a peak power output of 5 KW which drives an inverted V dipole antenna. The transmitter is pulsed at a rate of 300 pulses/s and the pulse width is about 330 μs. The receiving system is a modified version of that developed by Sulzer (1973). The receiver has a gain of about 10^5 and a bandwidth of about 60 KHz (a compromise between narrow band for improved signal to noise ratio and a short rise time ($\sim$ 3 μs) for accurate location of the detected echo. The receiver contains automatic gain control circuity developed by Sulzer (1979) to keep the detected receiver output constant for wave interaction measurements. The response time of the AGC

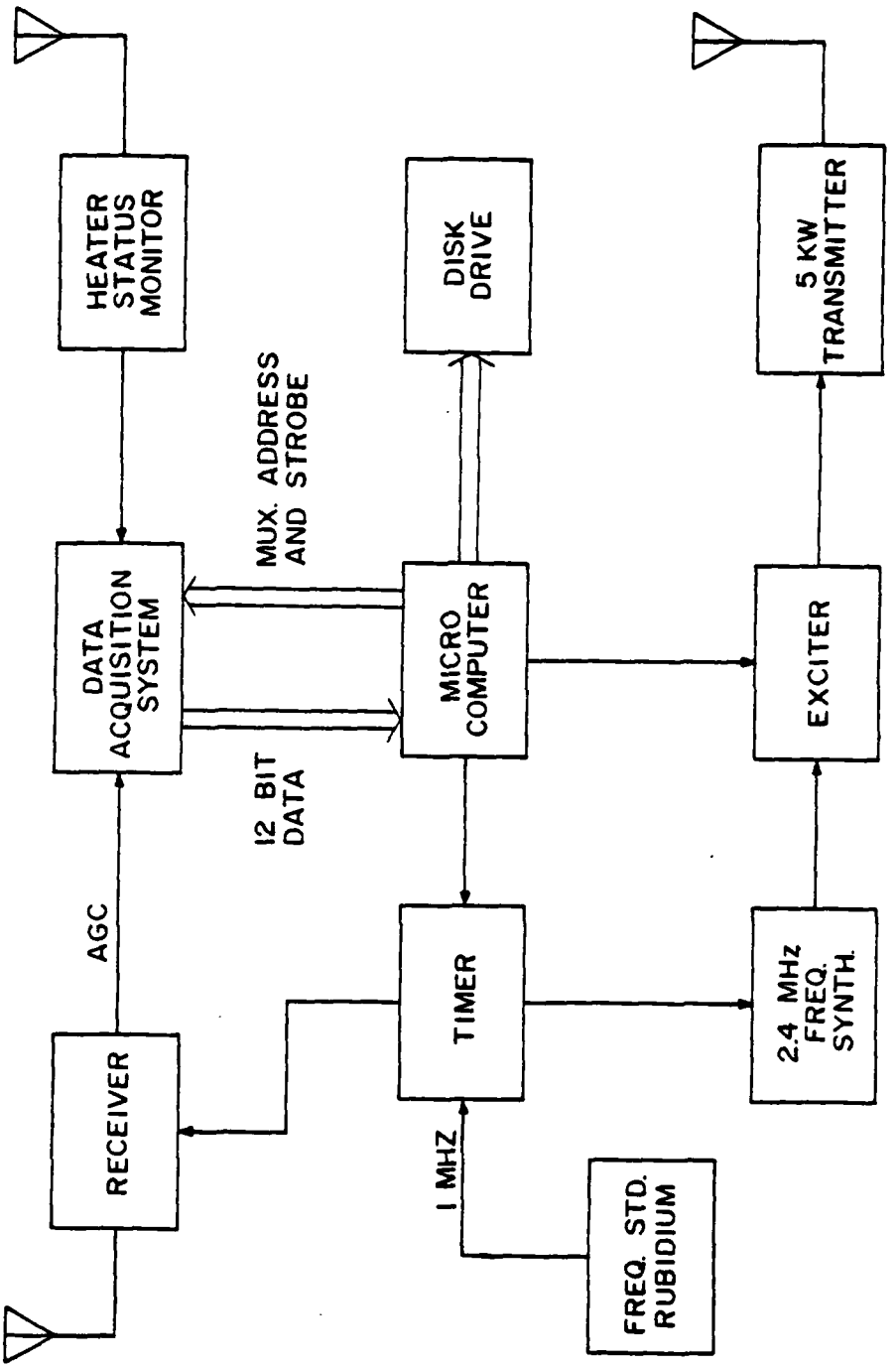

Figure 5.7 2.4 MHz ionospheric sounding system.

system is about 0.05 s. The AGC system generates a voltage which is proportional to the logarithm of the RF input voltage and thus serves as an indicator of diagnostic wave absorption. The voltage transfer characteristics for this system are shown in Figure 5.8. The AGC voltage was sampled using a 12 bit A/D converter with a resolution of 5 mV. Data collection and experiment control were provided by a microcomputer and the digitized AGC voltages were stored on 5" floppy disks. The status of the heating transmitter (ON or OFF) was simultaneously sampled and recorded.

Table 5.1 gives a quick summary of the experimental conditions under which 2.4 MHz absorption was measured. On 8/29, all four heating transmitters were operational at 75 KW on 3.175 MHz. Based on the model calculations of Trask (1979) the antenna gain at this frequency is about 23 dB (allowing 3 dB for losses). The effective radiated power for this day was thus estimated to be about 60 MW. On all of the other dates listed in Table 5.1, failures in one or more of the heating transmitters and their associated feedlines restricted the heating capability of the Islote HF facility to two transmitters operating at 75 KW or less and driving half of the 32 element array. The effective radiated power on these dates was $\lesssim$ 15 MW. At this reduced level of heating, no correlated variation in Al absorption with heater status (i.e. OFF or ON) was observed. Accordingly, the data presented here are the 60 MW results from 8/29.

Figures 5.9 and 5.10 illustrate the observed variation in Al absorption at 2.4 MHz due to CW heating at 3.175 MHz and 60 MW ERP.

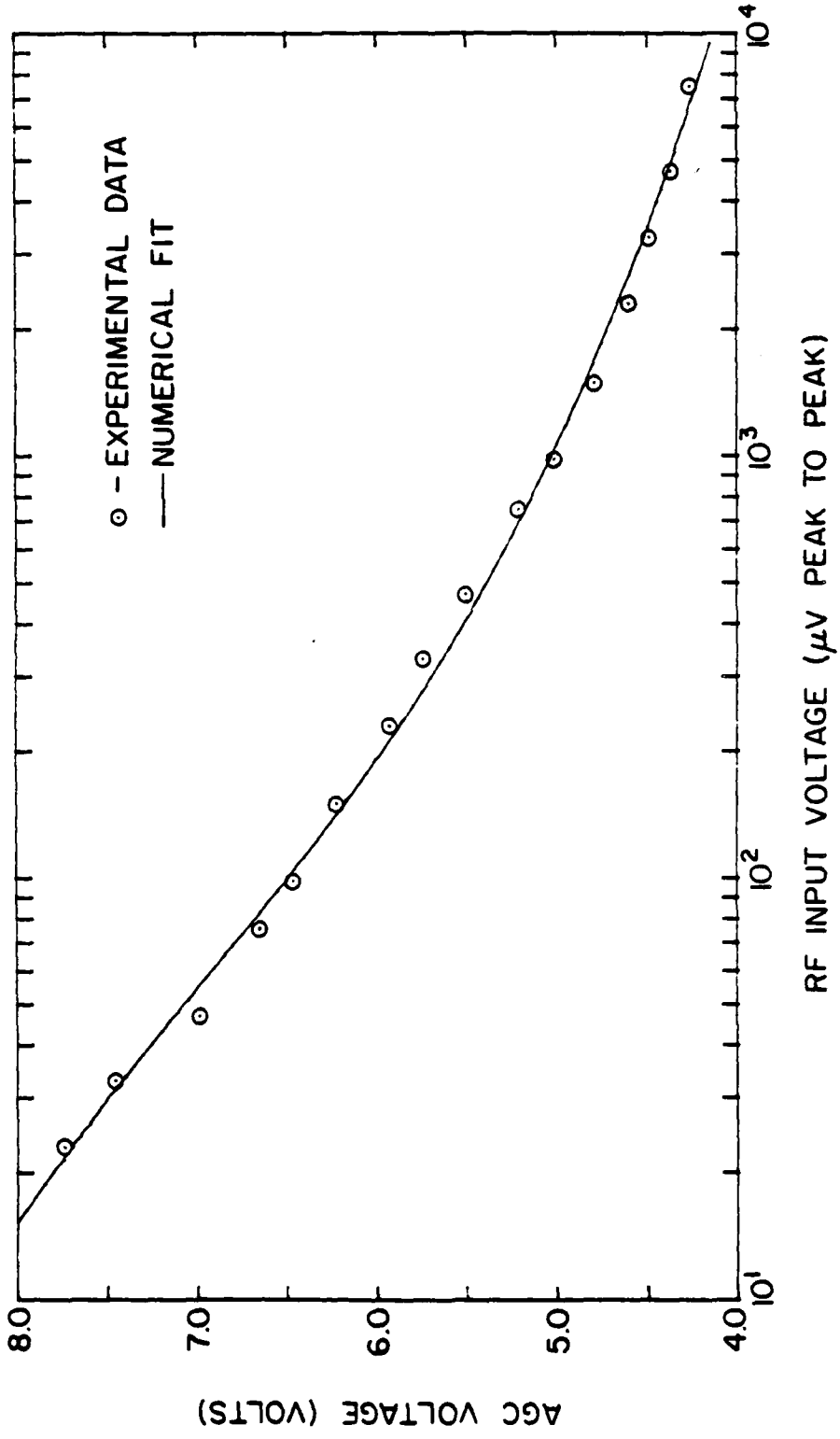

Figure 5.8 Voltage transfer characteristic of 2.4 MHz receiver.

Table 5.1 Summary of absorption measurements

DATE	LOCAL TIME	SOLAR ZENITH ANGLE	HEATING FREQUENCY	HEATING WAVE POLARIZATION	HEATING TRANSMITTER POWER	EFFECTIVE RADIATED POWER (ESTIMATED)	AGC SAMPLE SPACING
8/29	18:05-19:35	86-106°	3.175 MHz	L-CR	75 KW x 4	60 MW	0.48 s
8/30	16:10-19:00	60-100°	3.175 MHz	Varied	<75 KW x 2	<15 MW	0.48 s
8/31	7:46-10:11	66-29°	3.175 MHz	LN	<75 KW x 2	<15 MW	0.48 s
9/4	7:12-10:46	72-75°	3.175 MHz	L-CR	75 KW x 2	15 MW	0.22 s

NOTE: L-CR = left circular polarization

LN = linear polarization

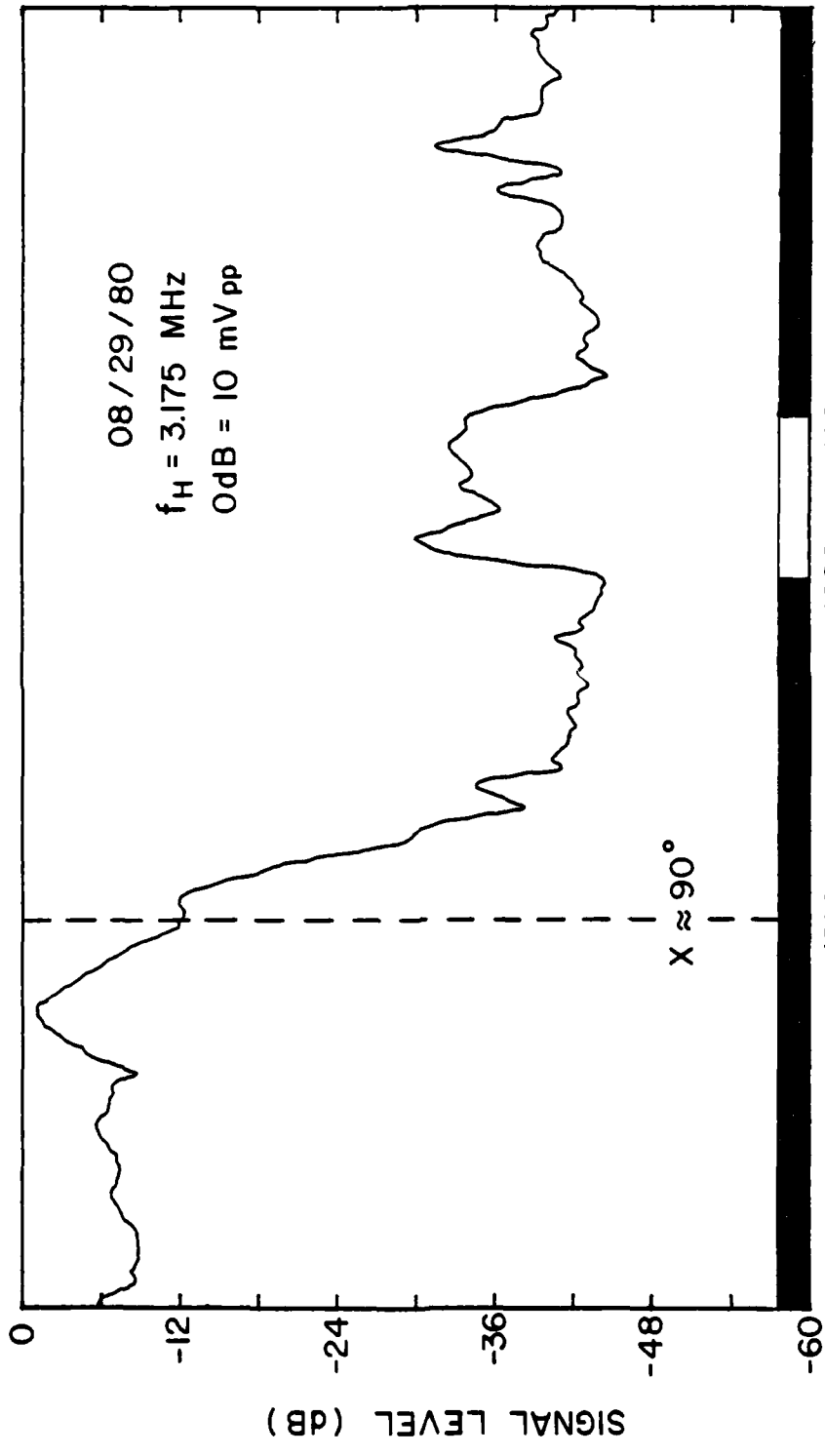

Figure 5.9 2.4 MHz absorption at sunset during a period of CW heating.

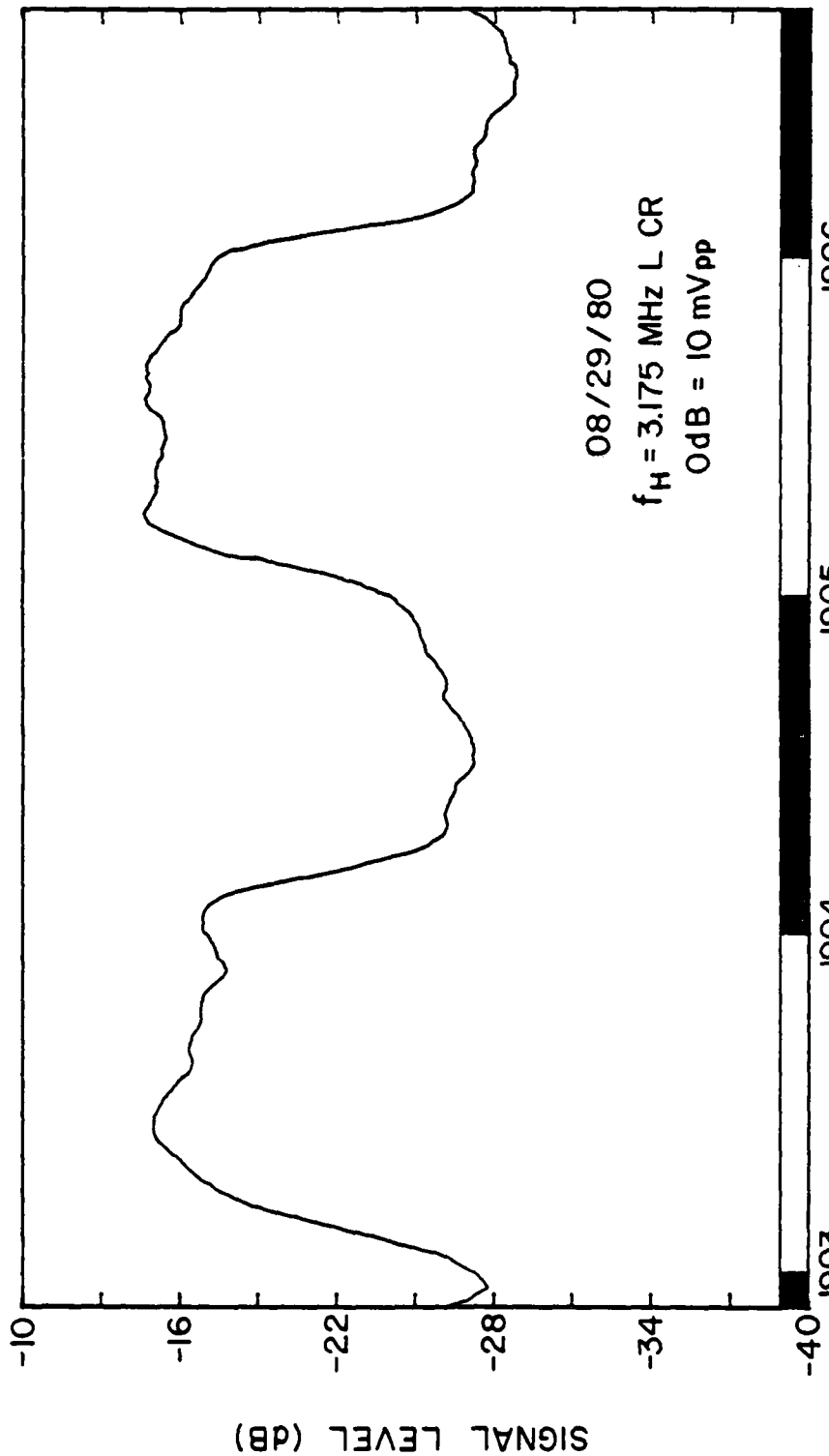

Figure 5.10 2.4 MHz absorption during a period of 1 minute heater on/off cycles.

The 2.4 MHz signal level at the input to the receiver is plotted in decibels relative to 10 mV_{pp} as a function of time. Typical strong daytime echos from an unheated ionosphere are about 10 mV_{pp}, while the ambient noise level is $\lesssim$ 50 μV_{pp}. The data plotted in these figures has been digitally low pass filtered to a bandwidth of 50 mHz to minimize noise and short term variability of the data and thus give a relatively smooth plot. The dark bars at the bottom of each figure indicated periods when the heating transmitter was on while the white areas indicated period of heater off.

Figure 5.9 presents a 23 minute segment of data at the start of the observation period on 8/29. The HF heating transmitter was on at the start of this period and the diagnostic signal level was relatively strong. Sunset occurred shortly after the start of the experiment and is readily apparent as a sharp drop in signal strength starting at about 1814 LT. A similar drop in signal level is observed at sunset during unheated conditions. The heating transmitter was turned off at 1820 for a three-minute period and a rapid increase in signal level was observed. The average signal enhancement during the off period was 8.4 $\pm$ 0.5 dB.

During the period 1856 to 1929 LT the HF heating transmitter was turned off and on at one-minute intervals. Figure 5.10 shows the variation in 2.4 MHz absorption over a segment of this period. The average increase in signal level during the heater off periods was about 9 dB.

5.5 Discussion

With the limited new data given in the previous section and the preliminary Platteville data reported by Utlaut and Violette (1974),

one can form only a very crude picture of the heating induced variation in diagnostic wave absorption for comparison with the theoretical predictions given in Figure 5.5. The nighttime values of ΔL measured at Arecibo (9 dB) are larger than the daytime values obtained at Platteville (6 dB) despite the fact that the effective radiated power at Arecibo (~ 60 MW) was probably less than that at Platteville (~ 100 MW). This is consistent with the diurnal variation of ΔL predicted in Figure 5.5.

The slow (10 min,) recovery of ΔL following a period (10 min.) of CW heating which was observed at Platteville is difficult to explain. The theory predicts a prompt decrease in absorption following heating termination and then a much smaller long term variation due to electron density modifications. The overshoot phenomenon associated with electron attachment partially compensates for the prompt absorption decrease as T_e returns to its ambient level and it gives better agreement with the observed long term recovery of ΔL than one would obtain if only recombination effects were included in the model.

Finally the sunset Arecibo data do not show any significant long term change in absorption over the two-minute on and off periods, which is consistent with the predictions given in Figure 5.5.

Evaluation of the theoretical chemistry model developed in this work is continuing using new absorption measurements recently taken at Platteville (Rush, 1981) and VLF/LF propagation data (Chilton, 1981). Additional measurements at Al absorption will probably be needed to establish a broad empirical base for evaluation and improvement of the model.

CHAPTER VI

NONLINEAR DEMODULATION

6.1 Basic Theory and Experimental Review

This chapter shall discuss the generation of ELF and VLF radiations by HF modification of the ionospheric current system. This phenomena involves the irradiation of the ionospheric plasma by a strong HF wave which is modulated at some frequency, Ω. The periodic plasma heating that results from this wave stimulates the emission of radiation of frequency Ω by the ionopshere; hence this effect is commonly referred to as nonlinear demodulation or ionospheric detection.

The basic physics of the nonlinear demodulation effect is illustrated in Figures 6.1 and 6.2. The electrons within the area of plasma irradiated by the HF beam experience periodic heating at the HF modulation frequency. Since the ionospheric conductivity is electron temperature dependent, the conductivity undergoes a similar periodic variation. Natural ionospheric currents (e.g. dynamo, electrojet, etc.) which pass through the heated region are modulated by the conductivity. Under ambient conditions the density of the ionospheric current is given by

$$\vec{J}_o = \underline{\sigma}_o \vec{E}_G \tag{6.1}$$

where $\vec{E}_G$ is the strength of the geoelectric field which drives the currents and $\underline{\sigma}_o = \underline{\sigma}(T_n)$ is the ambient conductivity tensor. Within the heated region, the current density is

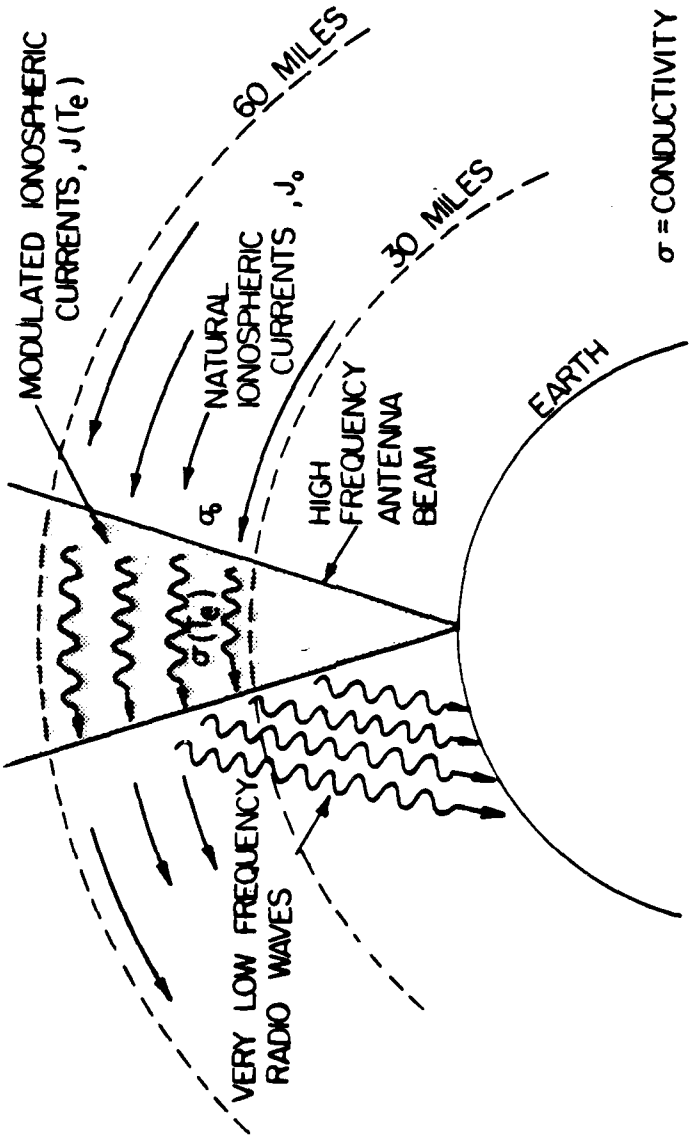

Figure 6.1 Geometry of the nonlinear demodulation experiment.

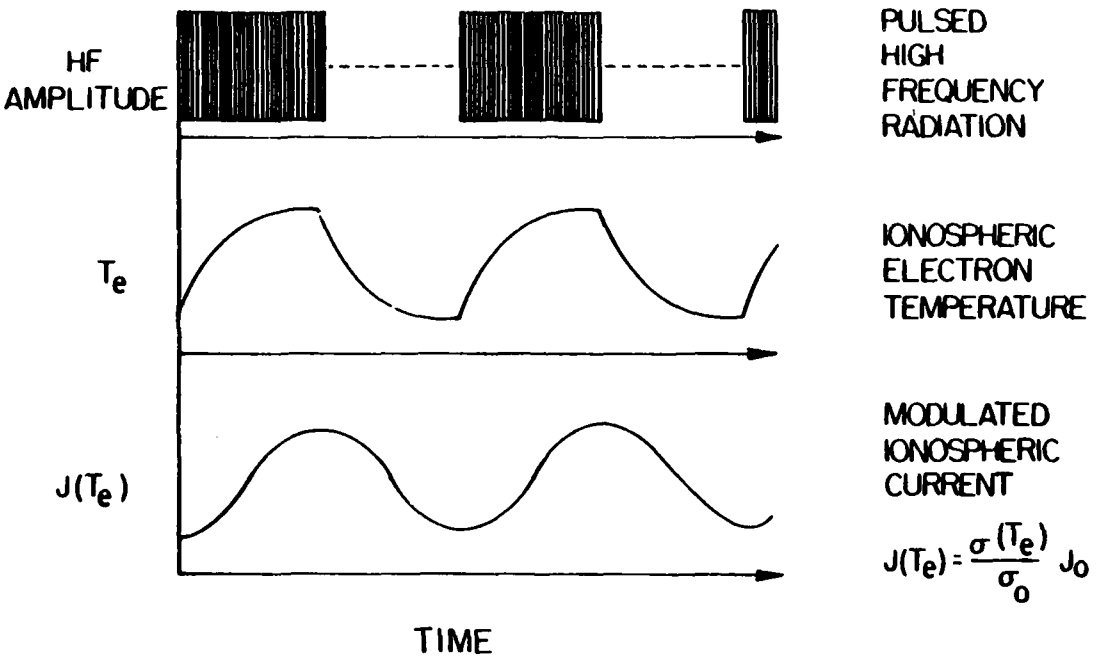

Figure 6.2 ELF/VLF generation by HF heating.

$$\vec{J} = \underline{\sigma}(T_e)\ \vec{E}_G = \vec{J}_o + \Delta\sigma(T_e)\ \vec{E}_G \qquad (6.2)$$

where

$$\Delta\underline{\sigma}(T_e) = \underline{\sigma}(T_e) - \underline{\sigma}_o \ .$$

Thus, HF modulation of the ionospheric conductivity gives rise to a periodic current at the modulation frequency, Ω, of density

$$\vec{J}_\Omega = \Delta\underline{\sigma}(T_e)\ \vec{E}_G \qquad (6.3)$$

This current is a source of Ω-frequency radiation, a type of antenna without wires.

Nonlinear demodulation phenomena of the type described above were observed during the Soviet heating experiments at Gorkii (Getmantsev et al., 1974). During these experiments the polar currents were modulated at frequencies from 1 kHz to 7 kHz using a 5.75 MHz carrier with an effective radiated power of 15 MW. Signals were regularly observed during the daytime at 2.5 kHz and 4 kHz but not at 1 kHz or 7 kHz. The field strength at 2.5 kHz varied from 2×10^{-2} to 25×10^{-2} μV/m. A distinct diurnal variation of the signal was observed with the intensity reaching a maximum at noontime and being generally unobservable at nighttime. Subsequent measurements by Budilin et al. (1977) have shown that the average height of the region of generation of the nonlinear current, $\vec{J}_\Omega$, is about 75 km.

The above results were for magnetically quiet conditions. Getmantsev et al. (1974) also report that measurements performed under magnetically disturbed conditions show that the VLF field is highly variable during these conditions and that the signal strength sometimes

greatly exceeds the intensity of signals detected during magnetically quiet conditions. Nighttime measurements by Kapustin et al. (1977) during geomagnetic disturbances show that the observed VLF signal strength is well correlated with the strength and position of auroral currents as detected by groundbased magnetometers. The VLF signals were absent during magnetically quiet nighttime conditions.

Recently, Turunen et al. (1980) and Stubbe (1980) have reported the observation of VLF/ELF signals due to nonlinear demodulation of MF and HF waves during geomagnetic disturbances in Northern Scandinavia. Stubbe (1980) observes a maximum signal strength at 2.5 kHz.

6.2 HF Modulation of Plasma Conductivities

From the results of Chapter III one can write the electron energy balance equation for plasma heating by a modulated HF wave approximately as (see (3.22))

$$\frac{\partial}{\partial t} T_e = P_e(t) - \frac{1}{\tau_H} (T_e - T_n) \tag{6.4}$$

where the heating production term is a periodic function of the form

$$P_e(t) = \sum_{k=-\infty}^{\infty} P_{ek} \, e^{jk\Omega t} \tag{6.5}$$

The Fourier coefficients of the production term, P_{ek}, are determined by the shape of the modulation envelope on the heating wave. In general, τ_H and the P_{ek} are functions of T_e; however, in the following simplified analysis, they are assumed to be constant.

Solving equation (6.4) for T_e, one has

$$T_e = T_n + \sum_{k=-\infty}^{\infty} \Delta T_{ek} \, e^{jk\Omega t} \tag{6.6}$$

where

$$\Delta T_{ek} = \frac{P_{ek}\,\tau_H}{(1 + jk\Omega\tau_H)}$$

Thus, the electron temperature exhibits a periodic variation at Ω and its harmonics. For $k\Omega<<1/\tau_H$, $|\Delta T_{ek}|$ attains its maximum value $|P_{ek}|\tau_H$, while for $k\Omega>>1/\tau_H$, one has $|\Delta T_{ek}| = |P_{ek}|/k\Omega$. Referring to Figure 4.14, one finds that the ionospheric time constants restrict the values of Ω which can effectively modulate the electron temperature to the ELF/VLF range.

The periodic temperature variations can alter the ionospheric conductivity in two ways. On time scales of the order of τ_H, the collision frequency, $\nu_{en}(T_e)$ is modified, while on longer time scales (i.e. $t>\tau_1$), the electron density will be modified. The manner in which $\underline{\sigma}$ depends on ν_{en} and n_e is best illustrated by considering a special form of equation (2.61). If one assumes that $U(v_e)$ can be replaced by $U(T_e)$ (i.e. $\nu_{en}(v_e)$ replaced by $\nu_{en}(T_e)$), then upon integrating over $d\vec{v}_e$, one has for $\omega=\Omega$ and $\vec{E} = \vec{E}_G$

$$\sigma_T(T_e) = n_e(T_e)\,\frac{e^2}{m_e}\,\frac{\nu_{en}(T_e)}{\omega_G^2 + \nu_{en}^2(T_e)} \tag{6.7}$$

$$\sigma_H(T_e) = n_e(T_e)\,\frac{e^2}{m_e}\,\frac{\omega_G}{\omega_G^2 + \nu_{en}^2(T_e)} \tag{6.8}$$

$$\sigma_L(T_e) = n_e(T_e)\,\frac{e^2}{m_e}\,\frac{1}{\nu_{en}(T_e)} \tag{6.9}$$

The above approximate formulae show that each of the elements of the conductivity tensor has a distinctly different dependence on ν_{en},

while the n_e dependence is the same for all. Electron density modifications to $\underline{\sigma}$ will only be important when $\Omega<1/\tau_1$. From Figure 4.14 one finds that $\Omega<100$ rad/s is required for significant electron density modifications to occur. For $1/\tau_1 < \Omega < 1/\tau_H$, only collision frequency effects are important.

Figure 6.3 shows the D-region conductivity distribution for ambient and heated conditions when $n_e = n_e(T_n)$, $\Omega/2\pi$ = 1 kHz, ω = 5 MHz, X-mode at 100 MW ERP. The collision frequency ν_{en} varies approximately as T_e/T_n (e.g. Banks and Kockarts, 1973), thus one has $\sigma_H(T_e) < \sigma_H(T_n)$ and $\sigma_L(T_e) < \sigma_L(T_n)$ but $\sigma_T(T_e) > \sigma_T(T_e)$ for $\omega_G >> \nu_{en}(T_e)$ while $\sigma_T(T_e) < \sigma_T(T_B)$ for $\omega_G << \nu_{en}(T_e)$.

6.3 The Wireless Antenna

The principal ionospheric current system is the dynamo system. which is driven by the local induced electric field resulting from the movement of the ionospheric plasma across the lines of the geomagnetic field under the action of solar and lunar tidal forces. The induced field is typically of the order of 1 mV/m (Rishbeth and Garriott, 1969). At high latitudes, a second current system, the polar system, becomes important. Unlike the dynamo currents, the polar currents are driven by electric fields arising in the magnetosphere (Ratcliffe, 1972). Both the dynamo and polar currents have peak densities in the E-region at about 110 km. The ionospheric currents can vary considerably during geomagnetic distrubances, particularly in polar regions, and they can also be altered by local sources such as thunderclouds (Park and Dejnakarintra, 1973). Finally, it should be noted that recent rocket

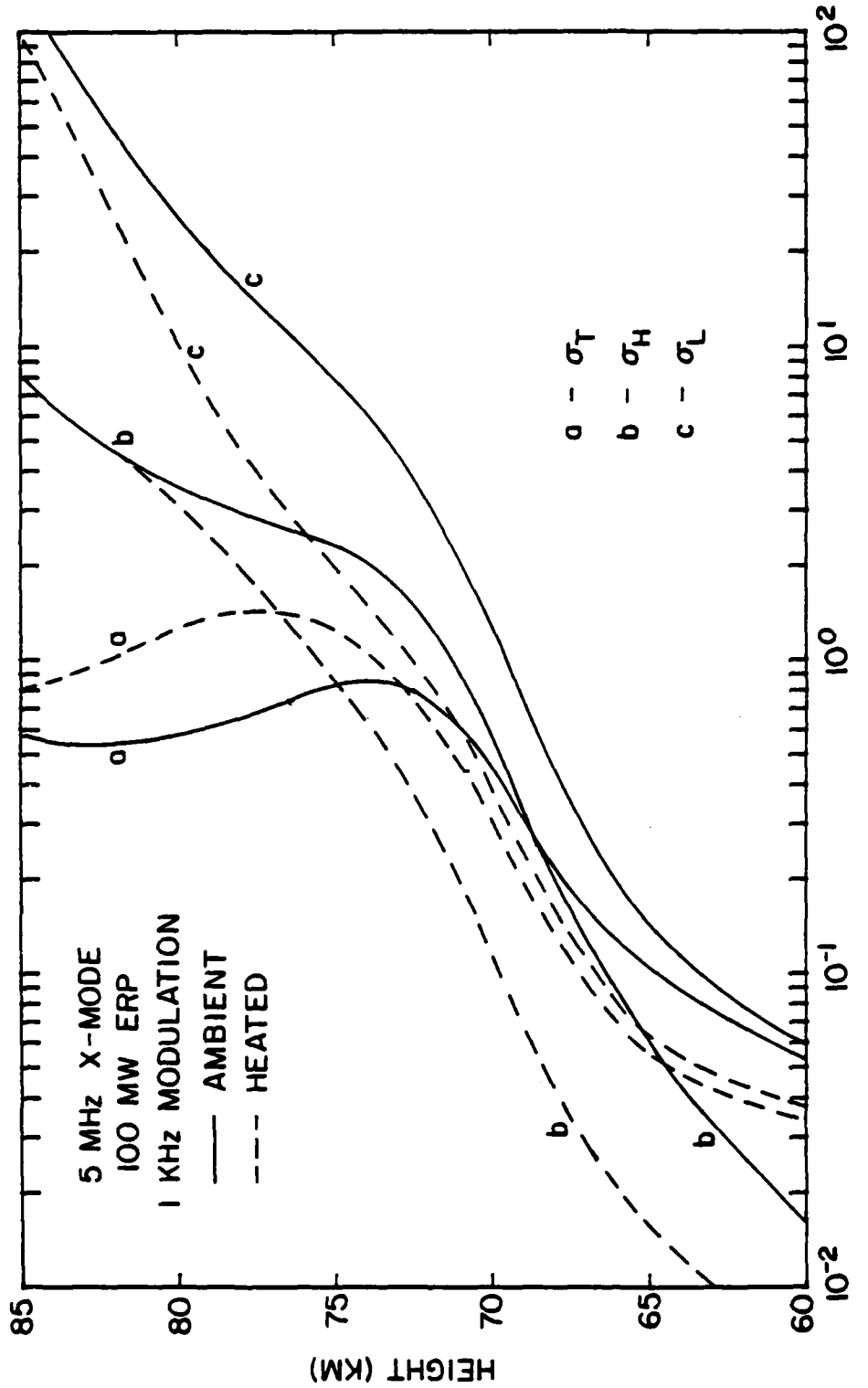

Figure 6.3 D-region conductivity profiles.

observations suggest that vertical electric fields of 1 V/m or more may exist at times in the D-region (Kocheev et al., 1976; Tyutin, 1976; Hale and Croskey, 1979). If they exist, these intense fields could be major current sources.

As shown earlier, the natural ionospheric currents can be modified by local conductivity variations induced by modulated HF heating, giving rise to a periodic current of density $\vec{J}_\Omega$. This periodic current is a source of radiation at the modulation frequency, Ω, and its harmonics:

$$\vec{J}_\Omega(\vec{r}, t) = \sum_{k=-\infty}^{\infty} \vec{J}_{k\Omega}(\vec{r})\, e^{jk\Omega t} \tag{6.10}$$

The electromagnetic field arising from the k-th harmonic component of $\vec{J}_\Omega$ is specified by the vector potential (e.g. Jordan and Balmain, 1968)

$$\vec{A}_k(\vec{r}, t) = \frac{\mu_o}{4\pi} \int \vec{J}_{k\Omega}(\vec{r}')\, \frac{e^{-jKR}}{R}\, d\vec{r}'\, e^{jk\Omega t} \tag{6.11}$$

where $R = |\vec{r} - \vec{r}'|$. The range of integration in (6.11) extends over the entire volume of plasma which is heated by the HF wave. This radiating volume defines the spatial extent of the so-called wireless antenna. If one assumes that the spatial extent of the radiating volume is small compared to a wavelength (i.e. $|\vec{r}'| << k\Omega/c$) then the vector potential for the wireless antenna is essentially that of a Hertzian dipole (e.g. Jordan and Balmain, 1968):

$$\vec{A}_k(\vec{r}, t) = \frac{\mu_o}{4\pi r} \int \vec{J}_{k\Omega}(r')\, \vec{dr}'\, \exp\left\langle jk\Omega\left(t - \frac{r}{c}\right)\right\rangle \tag{6.12}$$

Theoretical studies of the radiation emitted by the wireless antenna by Willis and Davis (1973) and Stubbe and Kopka (1977) have used this

approximation. The above formula also assumes that the wireless antenna is surrounded by free space. In actuality, of course, the antenna is immersed in a plasma, hence trapping and ducting effects may play a key role in determining the vector potential at a given point.

6.4 The Arecibo HF Demodulation Experiment

On December 2 and 3, 1980, experiments were performed at the Arecibo Observatory using the Islote HF Heating Facility which sought to generate ELF/VLF radiation by modulating the ionospheric current system. The ionosphere was heated by radiation from two transmitters operating at 75 KW each on a carrier frequency of 3.175 MHz, left circular polarization. The effective radiated power was estimated to be about 30 MW. The carrier was pulse modulated with a 50% duty cycle at frequencies of from 500 Hz to 10 kHz and the resultant ELF/VLF radiation was monitored using the receiving system shown in Figure 6.4. The receiving antenna consists of 350 turns of No. 14 wire wound on a plywood form one meter in diameter. It is similar to that used by Dinger et al. (1980) to measure 1 - 4 kHz ambient electromagnetic noise. The signals induced in the loop are amplified, filtered and then coherently detected using a PAR 129 A lock-in amplifier. Coherence is maintained by driving the frequency synthesizers for the lock-in reference and HF modulation signals with identical 1 MHz rubidium frequency standards. The inphase and quadrature components of the detected radiation were sampled by a microcomputer controlled data acquisition system and were later converted into amplitude and phase data. The lock-in amplifier was set for a 30 second integration time, which corresponds to a system bandwidth of

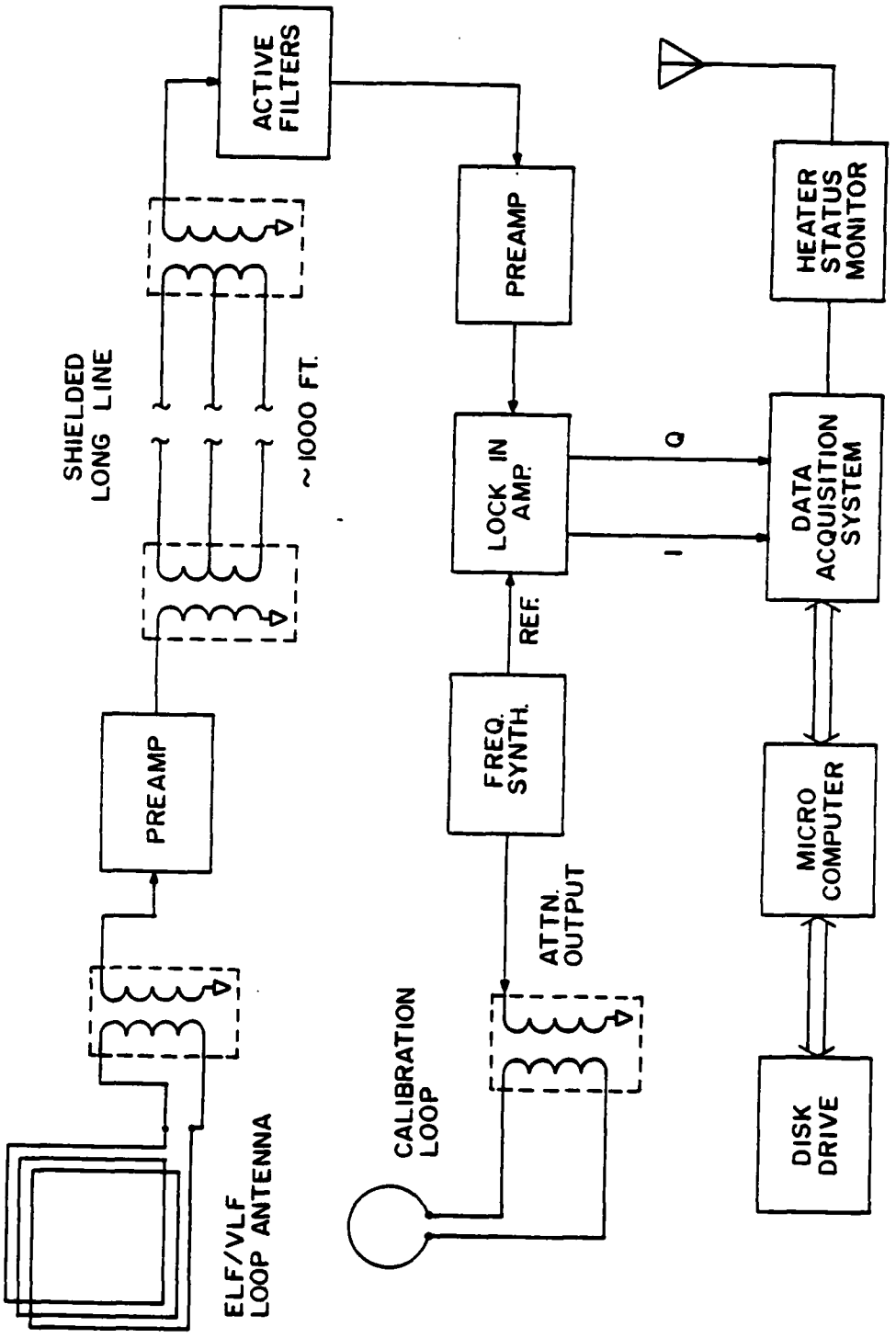

Figure 6.4 ELF/VLF receiving system.

8 millihertz. The experiment was generally conducted by operating the HF transmitter at a fixed pulse rate for 2 minutes, and then the HF was turned off for 2 minutes. This cycle was repeated several times, and then the pulse rate was changed to a different frequency. The exact modulation frequencies were 0.5, 1, 2, 2.5, 4, 5 and 10 kHz. Strong signals which were well correlated with the HF status (OFF or ON) were detected at 4 and 5 kHz. The signals detected at the other frequencies were much weaker and were not well correlated with the HF status. Figures 6.5 through 6.9 show some of the results which were obtained at 4 and 5 kHz. The status of the HF heating transmitter is indicated at the bottom of each graph with the dark areas indicating that the HF was on and the white areas denoting HF off.

Figures 6.5 and 6.6 show the detected amplitude and phase at 4 and 5 kHz respectively during nighttime conditions. The amplitude of the detected radiation is clearly correlated with the HF status. Amplitude values are given in volts at the output of the lock-in amplifier. The receiving system was not calibrated during this preliminary experiment; hence, the field strength corresponding to a given output voltage is not known. The detected signal is, however, clearly much greater than the background noise level (i.e. HF off). The phase characteristics of the radiation are well defined during HF on and become random during HF off.

Figures 6.7 through 6.9 illustrate the diurnal features of the detected radiation at 5 kHz. At nighttime (Figure 6.7), the detected signal level was as large as 12 volts. During the morning the detected signal level was typically 3 to 4 volts (Figure 6.8), while by mid-afternoon (Figure 6.9), the signal level was less than 1 volt.

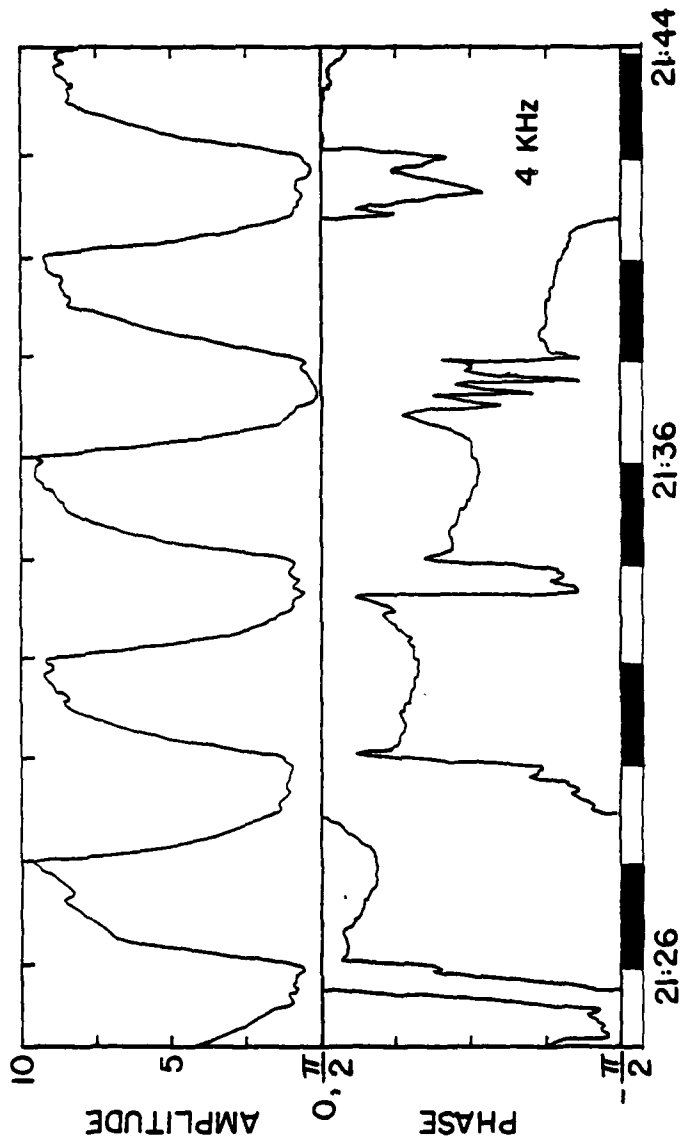

Figure 6.5 Amplitude and phase of detected VLF radiation as a function of time.

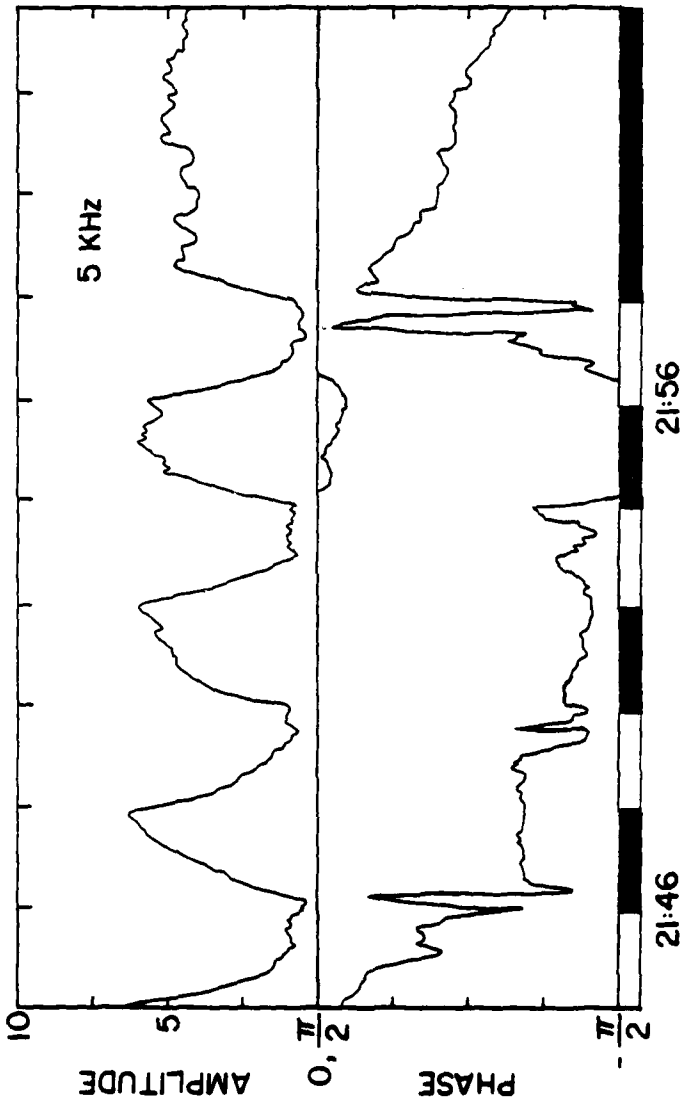

Figure 6.6 Amplitude and phase of detected VLF radiation as a function of time.

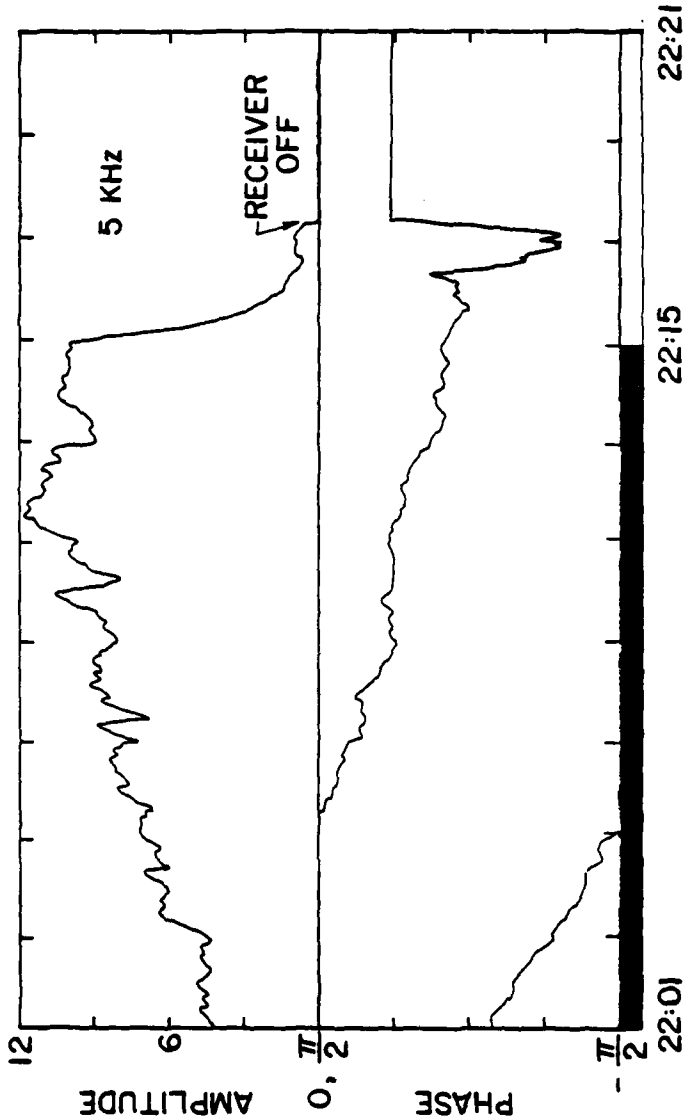

Figure 6.7 Amplitude and phase of detected VLF radiation as a function of time.

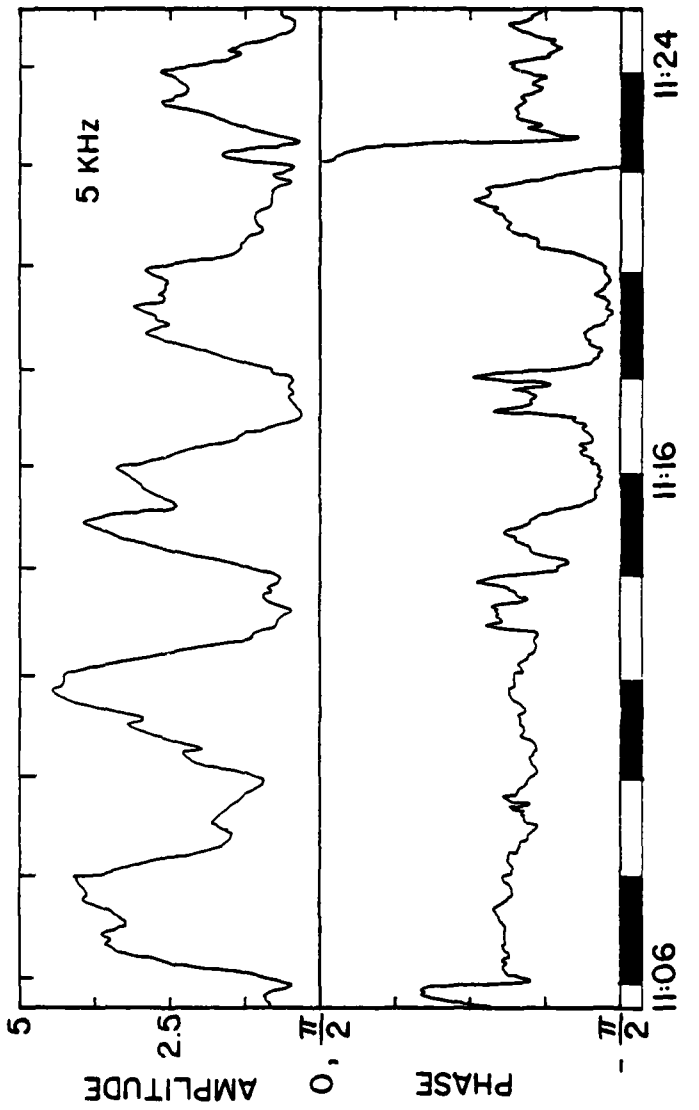

Figure 6.8 Amplitude and phase of detected VLF radiation as a function of time.

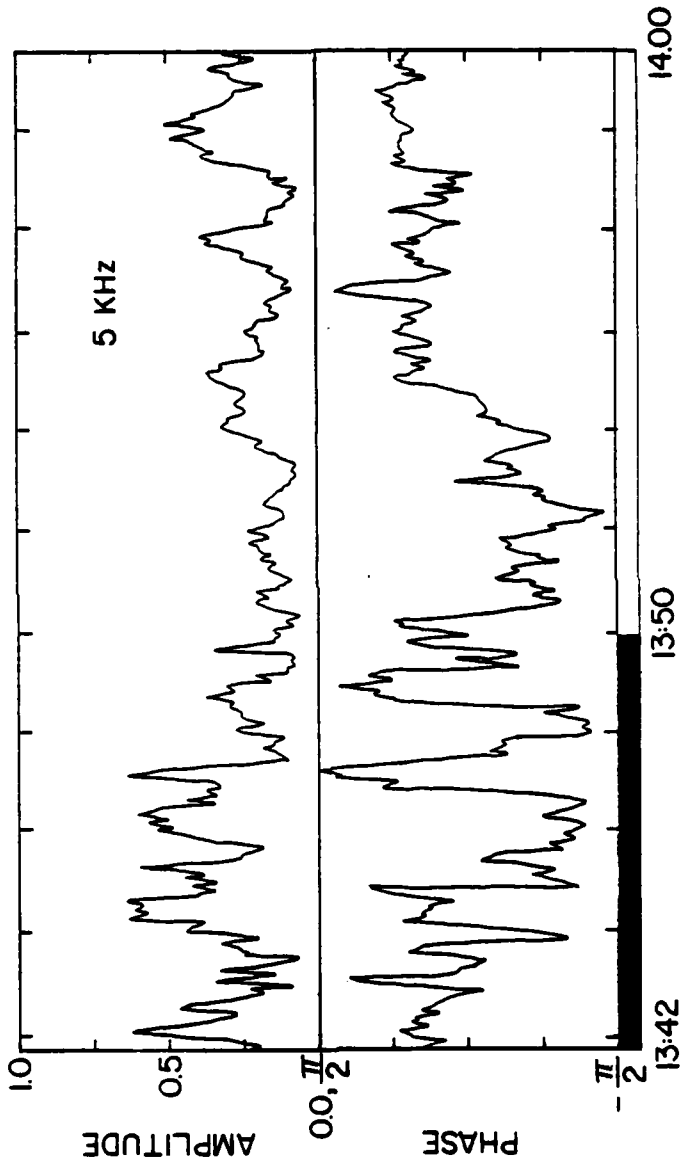

Figure 6.9 Amplitude and phase of detected VLF radiation as a function of time.

6.5 Discussion

The observed correlation between the detected signal voltage and the HF status could arise from several sources other than nonlinear demodulation effects in the ionosphere. The most likely candidate among these false effects is nonlinear demodulation of the HF ground wave or the HF sky wave in the receiving system. The observed diurnal fading of the detected signal suggests that its source is not the HF groundwave, since the groundwave is independent of ionospheric variations. Moreover, no change in detected signal strength was observed when the loop was rotated. On the other hand, the HF sky wave would exhibit diurnal features and could thus cause the observed effect.

During 24-30 March, 1981, tests were conducted at Arecibo to determine whether the observed signals were real ionospheric VLF signals or false VLF signals arising from HF demodulation in the receiving system. The December experiment was repeated and strong signals were again detected. During a period when the detected signals were very stable, the bandwidth of one of the active filters was adjusted so that the modulation frequency was out of the passband. Thus, any real VLF would be rejected while the level of modulated HF leakage would remain essentially the same. The detected signal voltage vanished in the noise when the filter was adjusted off frequency, indicating that HF leakage through the filter was not being demodulated by nonlinear processes in the preamps or the lock-in amplifier to any significant extent.

During the March experiments, strong signals were detected at all frequencies from 500 Hz to 10 KHz. When the data were corrected for the gain-frequency characteristics of the receiving loop, it was found that

the detected signal strength decreases with increasing modulation frequency. This is exactly what one would expect from theoretical consideration since the change in collision frequency (or electron temperature) decreases with increasing modulation frequency (see equation (6.6)). A similar result is predicted when electron density modifications due to decreased dissociative recombination are included (Stubbe and Kopka, 1977). It should be noted, however, that if the primary source region for the ELF is near 75 km as suggested by Budilin et al. (1977), then electron attachment effects could decrease the radiated field strength over some range of ELF modulation frequencies.

During the March experiments, the receiving system was calibrated following the procedure described by Jeans et al. (1961) using a single turn loop as an ELF/VLF reference source (see Figure 6.4). Preliminary analysis of the calibration data suggests that the strength of the electric field incident upon the receiving loop during modulated HF heating could be as large as 20 μV/m at 5 KHz.

Finally, it is interesting to note that the observed diurnal variation of the detected VLF radiation at Arecibo is the opposite of that reported by Getmantsev et al. (1974) for polar conditions. At Arecibo the strength of the detected signal is strongest at nighttime and decreases as noon approaches, while at Gorkii, the signal strength peaked at noon and decreased toward nightfall.

CHAPTER VII

CLOSURE

7.1 Summary

This study has focused on plasma modifications and nonlinear electromagnetic effects arising from the interaction of a powerful radio wave with the weakly ionized plasma of the lower ionosphere. The source of the radio wave is assumed to be a ground based HF transmitter with an effective radiated power of the order of 100 MW.

The principal effect of the radio wave-plasma interaction is a local enhancement of the electron temperature due to the absorption of energy from the wave by the plasma electrons. Theoretical calculations presented in this work show that the time scale for electron temperature enhancements ranges from a few microseconds in the lower D-region to several milliseconds at the base of the E-layer and that the steady state electron temperature may be a factor of five or more above the ambient plasma temperature. The magnitude of the electron temperature enhancement is strongly dependent on the density of the plasma electrons and the rate of electron energy transfer to neutral particles as well as on the frequency and power density of the radio wave.

For a fixed radiated power and wave frequency, the radio wave power density available to heat the plasma electrons at a given height is determined by the amount of absorption experienced by the wave as it propagates to that height from ground level. As the plasma electrons are heated by the radio wave, the attenuation experienced by the wave is altered since the absorption properties of the plasma are electron energy dependent. Consequently, the leading edge of a radio wave pulse

from a powerful transmitter can cause additional absorption on the remainder of the pulse by its heating action on the plasma. This self-absorption effect takes place primarily in the middle of the D-region and can severely limit the power density available at higher heights. It is shown that the amount of self-absorption experienced by a wave as it propagates through the D-region increases as the radiated power level is increased, and that a saturation effect may take place in which any increase in radiated power beyond some threshold level is completely offset by increased self-absorption resulting in no net increase in power density above the D-layer. It is thus apparent that one must take D-region self-absorption effects into account when analyzing the results of E and F region HF heating experiments, and when one attempts to estimate the level of ionospheric heating due to microwave radiations by frequency scaling HF heating data, as is done in ionospheric impact studies of the solar power satellite, as well as when one studies D-region HF heating.

Since the reaction rates for chemical processes in which electrons participate are electron energy dependent, radio wave heating of the plasma electrons can modify the composition of the plasma. In this study, a simplified D-region ion chemistry scheme has been combined with plausible models for the electron temperature dependence of electron attachment and ion-electron recombination processes in order to study plasma density modifications induced by continuous high power radio wave heating. Enhancement of the electron temperature in the lower ionosphere by radio wave heating causes increased electron attachment and decreased recombination. The increase in attachment produces a rapid decrease

in electron density while enlarging the negative ion concentration on a time scale of several seconds or less. On the other hand, decreased recombination leads to increases in the positive ion and electron densities on time scales of several minutes to an hour. These two effects compete to determine the electron density distribution in the lower ionosphere, with electron attachment effects being most important in the lower D-region while ion-electron recombination effects are dominant in the upper D-region and the E-region.

The radio wave heating induced electron temperature and electron density modifications described above alter the absorption properties and the conductivity of the ionospheric plasma giving rise to two important types of nonlinear electromagnetic phenomena: the cross-modulation effect and the demodulation or detection effect. The cross modulation effect is a two wave interaction in which a strong wave modifies the absorption properties of the plasma by its heating action and thereby alters the amplitude of another wave which propagates through the heated region. Since the level of plasma heating depends on the amplitude of the strong wave field, modulation on the strong wave can be transferred to the other wave via the plasma. In the detection effect, the plasma conductivity is modified in a periodic manner by a strong modulated wave, giving rise to periodic currents in the plasma at the modulation frequency. These periodic currents radiate energy at the modulation frequency; thus, the plasma effectively demodulates the strong wave. Theoretical calculations presented in this work show that large changes in wave absorption and plasma conductivity are to be expected when the effective radiated power of the HF heating transmitter is of the order

of 100 MW.

Two experiments were conducted in order to observe the nonlinear electromagnetic effects resulting from HF heating induced plasma modifications. The first experiment used the vertical incidence pulse absorption technique to measure the change in absorption on a diagnostic wave as the HF heating transmitter was turned on and off (i.e. cross-modulation effect). Data from this experiment clearly show a large (9 dB) increase in wave absorption at 2.4 MHz due to high power (60 MW ERP) HF heating of the ionosphere. This result compares favorably with theoretical predictions. In the second experiment, the HF heating wave was modulated at very low frequencies and a coherent detection scheme was employed to observe any VLF radiation due to ionospheric demodulation of the HF wave. Strong VLF signals were detected during the experiment, and it is believed that this radiation is due to HF heating induced conductivity modulation of the dynamo current system.

7.2 Suggestions for Future Work

At present, the available data on the effects of high power HF heating on the lower ionosphere and on radio wave propagation in this medium are still very limited. There are a few observations of a number of different effects taken at several HF facilities operating at various levels of heating under different geophysical conditions. What is required, at this point, is a systematic study of HF heating effects using several proven diagnostic techniques (e.g. absorption, wave interaction, incoherent backscatter, etc.) with the aim of determining how these effects depend on the power density, frequency and polarization of the heating wave and on changing geophysical conditions. A study of this

type is essential for testing the predictions of HF heating theory and for the proper evaluation and improvement of ionospheric models. From a theoretical standpoint, several improvements and extensions of the results of this study should be undertaken. First, since the chemistry of the D-region is much less complex during naturally disturbed conditions (e.g. solar flares, eclipses and polar cap absorption events) than during the normal daytime, it would be useful for the planning of future HF heating experiments to model radio wave heating effects during these conditions. Secondly, in view of the current interest in the nonlinear demodulation effect and the potential applications of this phenomena to the study of geoelectricity and to submarine communications, a thorough study of the wireless antenna should be undertaken which incorporates the plasma heating and chemistry models developed in this study with empirical and theoretical models of the ionospheric currents, conductivities and fields. Finally, it should be noted that one of the weaknesses of the plasma heating theory presented in this work is that transport effects have been neglected; hence, the importance of these effects should be ascertained.

REFERENCES

Arfken, G., Mathematical Methods for Physicists, Academic Press, New York, 1970.

Banks, P. M., Collision frequencies and energy transfer: electrons, Plant. Space Sci., 14, 1085-1104, 1966.

Banks, P. M. and G. Kockarts, Aeronomy, Academic Press, New York, 1973.

Biondi, M. A., Atmospheric electron-ion and ion-ion recombination processes, Can. J. Chem., 47, 1711-1719, 1969.

Biondi, M. A., Charged-particle recombination processes, in Defense Nuclear Agency Reaction Rate Handbook, DNA 1948H, Revision No. 6, 1975.

Brandstatter, J. J., An Introduction to Waves, Rays and Radiation in Plasma Media, McGraw-Hill, New York, 1963.

Budden, K. G., Effect of electron collisions on the formulas of magneto-ionic theory, Radio Sci., 69D, 191-211, 1965.

Budden, K. G., Radio Waves in the Ionosphere, Cambridge University Press, Cambridge, 1968.

Budilin, L. V., G. G. Getmantsev, P. A. Kapustin, D. S. Kotik, N. A. Mityakov, A. A. Petrovskii, V. O. Rapoport, Yu. A. Sazonov, S. Yu. Smirnov and V. Yu. Trakhtengerts, Localization of height of nonlinear currents responsible for low-frequency radiation in the ionosphere, Izv. Vyssh. Ucheb. Zaved. (Radiofiziki), 20, 83-86, 1977.

Caledonia, G. E., A survey of gas phase negative ion kinetics of inorganic molecules. Electron attachment reactions, Chem. Rev., 75, 333-351, 1975.

Chanin, L. M., A. V. Phelps and M. A. Biondi, Measurements of the attachment of low-energy electrons to oxygen molecules, Phys. Rev., 128, 219-230, 1962.

Chilton, C. J., Wave interaction observations of ionospheric modification in the D-region, NTIA Report 81-66, U.S. Department of Commerce, 1981.

CIRA, COSPAR International Reference Atmosphere, North-Holland, Amsterdam, 1972.

Coco, D. S., An experimental study of electron thermal runaway in the lower ionosphere, M. S. Thesis, Rice University, 1979.

Dinger, R. J., W. D. Meyers and J. R. Davis, Experimental measurements of ambient electromagnetic noise from 1.0 to 4.0 KHz, NRL Report 8413, Naval Research Laboratory, Washington, D.C., 1980.

Dingle, R. B., D. Arndt and S. K. Roy, The integrals C_p and D_p and their tabulation, Appl. Sci. Res., 6B, 155-164, 1957.

Duncan, L. M. and J. Zinn, Ionosphere-microwave interactions for solar power satellite, LA-UR-78-758, Los Alamos Laboratory, 1978.

Farley, D. T., Artificial heating of the electrons in the F region of the ionosphere, J. Geophys. Res., 68, 401-413, 1963.

Fejer, J. A., The interaction of pulsed radio waves in the ionosphere, J. Atmos. Terr. Phys., 1, 322-332, 1955.

Ganguly, S., Nighttime and sunrise variations of absorption, Radio Sci., 9, 1101-1108, 1974.

Getmantsev, G. G., N. A. Zuikov, D. S. Kotik, L. F. Mironenko, N. A. Mityakov, V. O. Rapoport, Yu. A. Sazonov, V. Yu. Trakhtengerts and V. Ya. Eidman, Combination frequencies in the interaction between high-power short-wave radiation and ionospheric plasma, JEPT Lett., 20, 229-232, 1974.

Gerjouy, E. and S. Stein, Rotational excitation of slow electrons, Phys. Rev., 97, 1671-1679,

Ginzburg, V. W., The Propagation of Electromagnetic Waves on Plasmas, 2nd, ed., Pergamon Press, Oxford, 1970.

Ginzburg, V. L. and A. V. Gurevich, Non-linear phenomena in a plasma located in an alternating electromagnetic field, Sov. Phys. Usp., 3, 115-146, 175-194, 1960.

Glaser, P. E., The potential of satellite solar power, Proc. IEEE, 65, 1162-1176, 1977.

Gnanalingam, S. and J. A. Kane, A study of electron density profiles in relation to ionization sources and ground-based radio wave absorption measurements, Part I, Report No. X-625-73-355, Goddard Space Flight Center, 1973.

Gordon, W. E., H. C. Carlson and R. L. Showen, Ionospheric heating at Arecibo: first tests, J. Geophys. Res., 76, 7808-7813, 1971.

Gurevich, A. V., Nonlinear Phenomena in the Ionosphere, Springer-Verlag, New York, 1978.

Gurevich, A. V., G. M. Milikh and I. S. Shlyuger, Rotational strengthening of cross modulation of radio waves in the ionosphere, Izv. Vyssh. Ucheb. Zaved. (Radiofizika), 20, 79-82, 1977a.

Gurevich, A. F., G. M. Milikh and I. S. Shlyuger, Changing ionization of the lower ionosphere due to high power radio waves, Izv. Vyssh. Ucheb. Zaved. (Radiofizika), 20, 1790-1804, 1977b.

Gurevich, A. V. and I. S. Shlyuger, Investigation of nonlinear phenomena when powerful radio pulses propagate in the lower layers of the ionosphere, Izv. Vyssh. Ucheb. Zaved. (Radiofizika), 18, 1237-1260, 1975.

Hale, L. C. and C. L. Croskey, An auroral effect on the fair weather electric field, Nature, 278, 239-241, 1979.

Hara, E. H., Approximations to the semiconductor integrals $C_p(x)$ and $D_p(X)$ for use with the generalized Appleton-Hartree magnetoionic formulas, J. Geophys. Res., 68, 4388-4389, 1963.

Herzberg, G., Spectra of Diatomic Molecules, van Nostrand, Princeton, 1950.

Holstein, T., Energy distribution of electrons in high-frequency gas discharges, Phys. Rev., 70, 367-384, 1946.

Holt, E. H. and R. E. Haskell, Plasma Dynamics, Macmillian, New York, 1965.

Holway, L. H., A. H. Katz and G. Meltz, Ionospheric effects of a high power space-borne microwave beam, Effects of the Ionosphere on Space and Terrestrial systems, ed. J. M. Goodman, Government Printing Office, Washington, D. C., 1980.

Holway, L. H. and G. Meltz, Heating of the lower ionosphere by powerful radio waves, J. Geophys. Res., 78, 8402-8408, 1973.

Huang, C. M., M. Whitaker, M. A. Biondi and R. Johnson, Electron-temperature dependence of recombination of electrons with $H_3O^+ \cdot (H_2O)_n$-series ions, Phys. Rev. A, 18, 64-67, 1978.

Jeans, A. G., H. E. Taggart and J. R. Wait, Calibration of loop antennas at VLF, J. Res. NBS, 65, 189-193, 1961.

Jones, T. B., K. Davies and B. Weider, Observations of D-region modifications at low and very low frequencies, Nature, 238, 33-34, 1972.

Jones, T. B., Modification effects in the ionospheric D-region, AGARD Conf. Proc., 138, 1973.

Jordan, E. C. and K. G. Balmain, Electromagnetic Waves and Radiating Systems, Prentice-Hall, New Jersey, 1968.

Kapustin, I. N., R. A. Pertsovskii, A. N. Vasilev, V. S. Smirnov, O. M. Raspopov, L. E. Soloveva, A. A. Ulyachenko, A. A. Arykov, and N. V. Galakhova, Generation of radiation at combination frequencies in the region of the auroral electric jet, JETP Lett., 25, 228-231, 1977.

Kebarle, P., S. K. Searles, A. Zolla, J. Scarborough and M. Arshadi, The solution of the hydrogen ion by water molecules in the gas phase. Heats and entropies of solvation of individual reactions: $H^+ (H_2O)_{n-1} + H_2O \rightleftarrows H^+ (H_2O)_n$, J. Am. Chem. Soc., 89, 6393-6399, 1967.

Kocheev, A. A., L. N. Smirnykh and A. A. Tyumin, Direct simulataneous measurements of ion concentration, electrical conductivity, and the vertical component of the electric field intensity of the atmosphere at altitudes of 0 - 85 km, Cosmic Res., 14, 139-142, 1976.

Kopka, H., P. Stubbe and R. Zwick, On the ionospheric modification experiment projected at MPI Lindau: practical realizations, AGARD conference on Artificial Modification of Propagation Media, Brussels, 26-30 April, 1976.

Krotova, Z. N., N. D. Krupenya, and V. A. Ryzhov, Self-action effects of radio waves in the D-layer, Izv. Vyssh. Ucheb. Zaved. (Radiofizika), 20, 72-78, 1977.

Leu, M. T., M. A. Biondi and R. Johnson, Measurements of the recombination of electrons with $H_3O^+ \cdot (H_2O)_n$ - series ions, Phys. Rev. A, 7, 292-298, 1973.

Lombardini, P. P. Alteration of the electron density of the lower ionosphere with ground-based transmitters, Radio Sci., 69D, 83-94, 1965.

McDaniel, E. W., Collision Phenomena in Ionized Gases, Wiley, New York, 1964.

Meltz, G., L. H. Holway and N. M. Tomljanovich, Ionospheric heating by powerful radio waves, Radio Sci., 9, 1049-1063, 1974.

Meltz, G. and R. E. LeLevier, Heating the F region by deviative absorption of radio waves, J. Geophys. Res., 75, 6406-6416, 1970.

Mentzoni, M. H. and R. V. Row, Rotational excitation and electron relaxation in nitrogen, Phys. Rev., 130, 2312-2316, 1963.

Mitra, A. P., Chemistry of the earth's atmosphere and its implications in radio communication and environemntal hazards, Proc. Indian Nat. Sci. Academy, 41A, 537-578, 1975a.

Mitra, A. P., D-region in disturbed conditions including flares and energetic particles, J. Atmos. Terr. Phys., 37, 895-913, 1975.

Mitra, A. P. Minor constituents and climate: some major input parameters, Report RSD-102, National Physical Laboratory, New Delhi, 1979.

Mitra, A. P. and J. N. Rowe, Ionospheric effects of solar flares - VI. Changes in D-region ion chemistry during solar flares, J. Atmos. Terr. Phys., 34, 795-806, 1972.

Mul, P. M. and J. W. McGowan, Merged electron-ion beam experiments III. Temperature dependence of dissociative recombination for atmospheric ions NO^+, O_2^+ and N_2^+, J. Phys. B: Atom. Molec. Phys., 12, 1591-1601, 1979.

Pack, J. L. and A. V. Phelps, Electron attachment and detachment, I. Pure O_2 at low energy, J. Chem. Phys., 44, 1870-1883, 1966.

Park, C. G. and M. Dejnakarintra, Penetration of thundercloud electric fields into the ionosphere and magnetosphere. 1. Middle and subauroral latitudes, J. Geophys. Res., 78, 6623-6633, 1973.

Perkins, F. W. and R. G. Roble, Ionospheric heating by radio waves: predictions for Arecibo and the satellite power station, J. Geophys. Res., 83, 1611-1624, 1978.

Ralston, A. and H. S. Wift, Mathematical Methods for Digital Computers, Wiley, New York, 1960.

Ratcliff, J. A., An Introduction to the Ionosphere and Magnetosphere, Cambridge University Press, Cambridge, G.B., 1972.

Rishbeth, H. and O. K. Garriott, Introduction to Ionospheric Physics, Academic Press, New York, 1969.

Rowe, J. N., Model studies of the lower ionosphere, PSU-IRL-SCI-406, The Pennsylvania State University, 1972.

Rowe, J. N., A. P. Mitra, A. J. Ferraro and H. S. Lee, An experimental and theoretical study of the D-region, II. A semi-empirical model for mid-latitude D-region, J. Atmos. Terr. Phys., 36, 755-785, 1974.

Rush, C. M., Recent developments in artifical ionospheric heating, The Effect of the Ionosphere on Radiowave Systems, ed. J. M. Goodman, Government Printing Office, Washington, D.C. 1981.

Schunk, R. W. and A. F. Nagy, Electron temperatures in the F region of the ionosphere: theory and observations, Rev. Geophys. Space Phys., 16, 355-399, 1978.

Sen, H. K. and A. A. Wyller, On the generalization of the Appleton-Hartree magnetoionic formulas, J. Geophys. Res., 65, 3931-3950, 1960.

Showen, R. L., Artificial heating of the lower ionosphere, J. Geophys. Res., 77, 1923-1933, 1972.

Spence, D. and G. J. Schulz, Three-body attachment in O_2 using electron beams, Phys. Rev. A, 5, 724-732, 1972.

Stubbe, P., The heating project at Tromsø, CCOG Handbook. Circular Letter No. 7, ed. W. Stoffregen, Sweden, 1980.

Stubbe, P. and H. Kopka, Modulation of the polar electrojet by powerful HF waves, J. Geophys. Res., 82, 2319-2325, 1977.

Stubbe, P. and W. S. Varnum, Electron energy transfer rates in the ionosphere, Planet. Space Sci., 20, 1121-1126, 1972.

Sulzer, M. P., A portable receiving system for use in the wave interaction experiment at Arecibo Observatory, PSU-IRL-IR-30, The Pennsylvania State University, 1973.

Sulzer, M. P., The detection of atmospheric gravity waves by means of the wave interaction experiments, PSU-IRL-SCI-461, The Pennsylvania State University, 1979.

Sulzer, M., A. Tomko, A. J. Ferraro and H. S. Lee, Complementary cross modulation: a new technique for ionospheric modification studies, J. Geophys. Res., 81, 4754-4756, 1976.

Thomas, L., The composition of the mesosphere and the lower thermosphere, Phil. Trans. R. Soc. Lond. A, 296, 243-260, 1980.

Tomko, A. A., High power radio wave modification of the lower ionosphere, PSU-IRL-IR-63, The Pennsylvania State University, 1978.

Tomko, A. A., A. J. Ferraro, H. S. Lee and A. P. Mitra, A theoretical model of D-region ion chemistry modifications during high power radio wave heating, J. Atmos. Terr. Phys., 42, 275-285, 1980.

Tomko, A. A., A. J. Ferraro and H. S. Lee, Vertical incidence pulse absorption measurements during high power radio wave heating of the D-region, The Effect of the Ionosphere on Radiowave Systems, ed. J. M. Goodman, Government Printing Office, Washington, D.C. 1981.

Trask, C., A high gain vertical beam antenna array using orthogonal non-planar log-periodic structures in a backfire configuration, M.S. Thesis, The Pennsylvania State University, 1979.

Truby, F. K., Low temperature measurements of the three-body electron-attachment coefficient in O_2, Phys. Rev. A, 6, 671-676, 1972.

Turunen, T., P. S. Cannon and M. J. Rycroft, ELF radio signals in the auroral ionosphere generated by non-linear demodulation of LF and MF transmissions, Nature, 286, 375-377, 1980.

Tyutin, A. A., Mesospheric maximum of the electric-field strength, Cosmic Res., 14, 132-133, 1976.

Utlaut, W. F., An ionospheric modification experiment using very high power, high frequency transmission, J. Geophys. Res., 75, 6402-6495, 1970.

Utlaut, W. F., Ionospheric modification induced by high-power HF transmitters - A potential for extended range VHF-UHF communications and plasma physics research, Proc. IEEE, 63, 1022-1043, 1975.

Utlaut, W. F. and E. J. Violette, A summary of vertical incidence radio observations of ionospheric modification, Radio Sci., 9, 895-903, 1974.

Velinov, P., On ionization in the ionospheric D-region by galactic cosmic rays, J. Atmos. Terr. Phys., 30, 1891-1905, 1968.

Walker, J. C. G., Active experimentation with the ionospheric plasma, Rev. Geophys., 17, 534-544, 1979.

Willis, J. W. and J. R. Davis, Radio frequency heating effects on electron density in the lower E-region, J. Geophys. Res., 78, 5710-5717, 1973.

Yeh, K. C. and C. H. Liu, Theory of Ionospheric Waves, Academic Press, New York, 1972.

APPENDIX A

THE ELECTRON ATTACHMENT COEFFICIENT

The three body attachment coefficient for the reaction $e + O_2 + O_2 \rightarrow O_2^- + O_2$ has been modeled as

$$K_a(T_e, T_n) = K_{ao}(T_n)\, T_e^{-0.65} \exp\left\{ -\frac{a_1}{T_e}(T_n) - \left(\frac{a_2(T_n)}{T_e}\right)^2 - \left(\frac{a_3(T_n)}{T_e}\right)^3 \right\}$$

where

$$K_{ao}(T_n) = 1.1617 \times 10^3 - 3.4665\, T_n + 3.2825 \times 10^{-3}\, T_n^2$$

$$a_1(T_n) = 7.8193 \times 10^2 - 3.2964\, T_n$$

$$a_2(T_n) = -1.9159 \times 10^2 + 3.7646\, T_n - 4.5446 \times 10^{-3}\, T_n^2$$

$$a_3(T_n) = -7.5834 \times 10^1 + 1.2277 \times 10^{-2}\, T_n - 7.6427 \times 10^{-3}\, T_n^2 + 1.7856 \times 10^{-5}\, T_n^3$$

The constraints used to construct this model are:

1. the electron temperature variation of the attachment coefficient for T_n = 77 and 300°K given by Chanin et al. (1962),
2. the values of the attachment coefficient for thermal equilibrium conditions ($T_e = T_n$) given by Truby (1972),
3. location of the peak value of K_a at 700°K ($\langle u \rangle$ = 0.09 eV),
4. the neutral temperature dependence of the 0.09 eV peak given by Spence and Schulz (1972)

The temperature variation of the model is illustrated in Figure 4.4.

APPENDIX B

ELECTRON DENSITY MODELS

The following table gives a set of ambient electron density models for different values of the solar zenith angle. The models were computed from the Mitra-Rowe six ion scheme using the electron production rate formulae given by Rowe (1972).

Table B.1 Electron density models

h (km)	$\chi_s = 30^o$ n_e	$\chi_s = 60^o$ n_e	$\chi_s = 70^o$ n_e	$\chi_s = 80^o$ n_e
50	5.65×10^0	5.34×10^0	3.28×10^0	2.27×10^0
60	5.75×10^1	3.70×10^1	2.36×10^1	1.03×10^1
70	5.82×10^2	2.36×10^2	9.85×10^1	3.70×10^1
80	1.53×10^3	1.17×10^3	5.63×10^2	2.83×10^2
90	1.48×10^4	4.55×10^3	1.69×10^3	1.16×10^3
100	1.76×10^5	8.45×10^4	4.71×10^4	1.26×10^4
110	1.91×10^5	1.46×10^5	1.42×10^5	8.15×10^4

NOTE: χ_s = solar zenith angle. Electron densities in cm^{-3}.

Distribution List for Pennsylvania State University

Contract No. N00014-81-K-0276

August 1981

ONR Branch Office

Office of Naval Research
495 Summer Street
Boston, MA 02210
1 cy

ACO

ONR Resident Representative
Carnegie-Mellon University
Room 407 Margaret Morrison Building
Pittsburgh, PA 15213
1 cy

Department of Defense

Director
Defense Advanced Research Projects Agency
1400 Wilson Boulevard
Arlington, VA 22209
1 cy ATTN: T10
1 cy ATTN: STO
1 cy ATTN: NRMO

Director
Defense Communications Agency
8th Street and South Courthouse Road
Arlington, VA 22204
3 cys ATTN: MEECN Office

Defense Documentation Center
Cameron Station
Alexandria, VA 22314
12 cys ATTN: TC

Director
Defense Nuclear Agency
Washington, DC 20305
1 cy ATTN: STTL
1 cy ATTN: DDST
3 cys ATTN: RAAE
1 cy ATTN: RAEV

Joint Chiefs of Staff
Department of Defense
Washington, DC 20301
1 cy ATTN: J-6

Director
National Security Agency
Fort George G. Meade, MD 20755
2 cys ATTN: Technical Library

Under Secretary of Defense (Research and Engineering)
Department of Defense
Washington, DC 20301
2 cys ATTN: DDS&SS

Deputy Assistant Secretary of Defense (C^3)
Department of Defense
Washington, DC 20301
2 cys ATTN: Dr. Quinn

Department of Commerce

U. S. Department of Commerce
Office of Telecommunications
Institute for Telecommunication Sciences
National Telecommunications and Information
Administration
Boulder, Colorado 80303
2 cys ATTN: W.F. Utlaut

Department of the Army

Commander/Director
Atmospheric Sciences Laboratory
U. S. Army Electronics Command
White Sands Missile Range, NM 88002
1 cy ATTN: DRSEL-BL-SY-S
F. E. Niles

Director
U. S. Army Ballistic Research Laboratories
Aberdeen Proving Grounds, MD 21005
1 cy ATTN: George E. Keller

Commander
U. S. Army Foreign Sciences and Technology Center
220 7th Street, N.E.
Charlottesville, VA 22901
1 cy ATTN: Robert Jones

Department of the Navy

Chief of Naval Operations
Department of the Navy
Washington, DC 20350
1 cy ATTN: NOP 985
1 cy ATTN: NOP 094H

Chief of Naval Research
Department of the Navy
800 North Quincy Street
Arlington, VA 22217
1 cy ATTN: Code 464, R. G. Joiner
1 cy ATTN: Code 427, H. Mullaney

Commander
Naval Electronic Systems Command
Department of the Navy
Washington, DC 20360
1 cy ATTN: PME-117
1 cy ATTN: PME-117T
1 cy ATTN: PME 117-21
1 cy ATTN: PME 110-112
1 cy ATTN: PME 117-22

Director
Naval Ocean Systems Center
Electromagnetic Propagation Division
271 Catalina Boulevard
San Diego, CA 92152
1 cy ATTN: Code 2200, W. F. Moler
1 cy ATTN: Code 2200, J. Richter
1 cy ATTN: Code 2200, John Bickel

Director
Naval Research Laboratory
4555 Overlook Avenue, S. W.
Washington, DC 20375
1 cy ATTN: Code 7700, Timothy P. Coffey
1 cy ATTN: Code 7709, Wahab Ali
2 cys ATTN: Code 7750, John Davis
1 cy ATTN: Code 2627

Commander
Naval Surface Weapons Center (White Oak)
Silver Spring, MD 20910
1 cy ATTN: Technical Library

Director
Naval Underwater Systems Center
New London Lab
New London, CT 06320
2 cys ATTN: Peter Banister

Office of Naval Research Western Regional Office
1030 East Green Street
Pasadena, CA 91106
1 cy

Department of the Air Force

Commander
Air Force Geophysical Laboratory, AFSC
L. G. Hanscom Air Force Base, MA 01731
1 cy ATTN: LKB, W. Swider
1 cy ATTN: LKB, K. Champion

Director
Air Force Technical Applications Center
Patrick Air Force Base, FL 32920
1 cy ATTN: TD
1 cy ATTN: HQ 1035th TCHOG/TFS

Department of Defense Contractors

General Electric Company
TEMPO - Center for Advanced Studies
816 State Street
Santa Barbara, CA 93102
1 cy ATTN: Warren S. Knapp
1 cy ATTN: DASIAC

Lockheed Missiles and Space Company
3251 Hanover Street
Palo Alto, CA 94304
1 cy ATTN: J. B. Reagan
1 cy ATTN: W. Imhof
1 cy ATTN: Martin Walt

Mission Research Corporation
735 State Street
Santa Barbara, CA 93101
1 cy ATTN: M. Scheibe
1 cy ATTN: D. Sowle

Pacific-Sierra Research Corporation
1456 Cloverfield Boulevard
Santa Monica, CA 90404
1 cy ATTN: E. C. Field

Pennsylvania State University
Ionospheric Research Laboratory
College of Engineering
318 Electrical Engineering - East Wing
University Park, PA 16802
1 cy ATTN: John S. Nisbet
1 cy ATTN: Les Hale
1 cy ATTN: A. J. Ferraro
1 cy ATTN: H. S. Lee

R & D Associates
4640 Admiralty Way
Marina Del Rey, CA 90291
1 cy ATTN: R. Lelevier
1 cy ATTN: F. Gilmore
1 cy ATTN: R. Turco

The Rand Corporation
1700 Main Street
Santa Monica, CA 90406
1 cy ATTN: Cullen Crain

Professor Chalmers F. Sechrist
155 Electrical Engineering Building
University of Illinois
Urbana, IL 61801
1 cy ATTN: C. Sechrist

Stanford Research Institute
333 Ravenswood Avenue
Menlo Park, CA 94025
1 cy ATTN: Allen M. Peterson
1 cy ATTN: Ray L. Leadabrand

Stanford University
Radio Science Lab
Stanford, CA 94305
1 cy ATTN: A. C. Frazer-Smith
1 cy ATTN: R. Hellimell
1 cy ATTN: C. Park

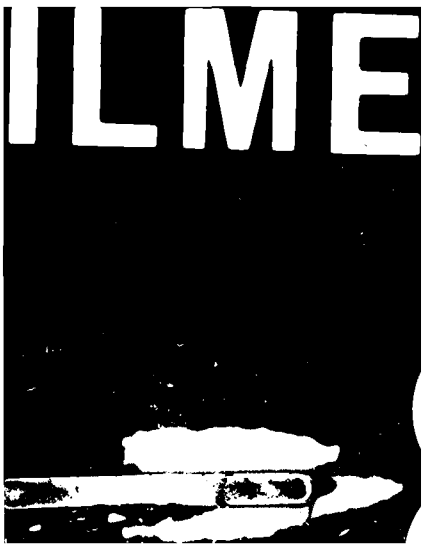
ILME